

**DOT/FAA/AR-02/62**

Office of Aviation Research  
Washington, D.C. 20591

# **Crash Simulation of Vertical Drop Tests of Two Boeing 737 Fuselage Sections**

August 2002

Final Report

This document is available to the U.S. public  
through the National Technical Information  
Service (NTIS), Springfield, Virginia 22161.



U.S. Department of Transportation  
**Federal Aviation Administration**

**20021115 018**

## NOTICE

This document is disseminated under the sponsorship of the U.S. Department of Transportation in the interest of information exchange. The United States Government assumes no liability for the contents or use thereof. The United States Government does not endorse products or manufacturers. Trade or manufacturer's names appear herein solely because they are considered essential to the objective of this report. This document does not constitute FAA certification policy. Consult your local FAA aircraft certification office as to its use.

This report is available at the Federal Aviation Administration William J. Hughes Technical Center's Full-Text Technical Reports page: [actlibrary.tc.faa.gov](http://actlibrary.tc.faa.gov) in Adobe Acrobat portable document format (PDF).

1. Report No. DOT/FAA/AR-02/62		2. Government Accession No.		3. Recipient's Catalog No.	
4. Title and Subtitle CRASH SIMULATION OF VERTICAL DROP TESTS OF TWO BOEING 737 FUSELAGE SECTIONS				5. Report Date August 2002	
				6. Performing Organization Code	
7. Author(s) Karen E. Jackson and Edwin L. Fasanella				8. Performing Organization Report No.	
9. Performing Organization Name and Address U.S. Army Research Laboratory Vehicle Technology Directorate NASA Langley Research Center Hampton, VA				10. Work Unit No. (TRAIS)	
				11. Contract or Grant No.	
12. Sponsoring Agency Name and Address U.S. Department of Transportation Federal Aviation Administration Office of Aviation Research Washington, DC 20591				13. Type of Report and Period Covered Final Report	
				14. Sponsoring Agency Code ANM-102	
15. Supplementary Notes The FAA William J. Hughes Technical Center Task Monitor was Dr. Tong Vu and the Crash Worthiness Program Manager was Gary Frings.					
16. Abstract A 30-ft/s vertical drop test of a 10-ft-long fuselage section of a Boeing 737 (B737) aircraft was conducted in October of 1999 at the Federal Aviation Administration (FAA) William J. Hughes Technical Center, Atlantic City International Airport, NJ. This test was performed to evaluate the structural integrity of a conformable auxiliary fuel tank mounted beneath the fuselage floor and to determine its effect on the structural response of the airframe. A second drop test of a similar B737 fuselage section was conducted in November of 2000 in which two different overhead stowage bins were evaluated. These tests present an invaluable opportunity to evaluate the capabilities of computational tools for crash simulation through analytical and experimental correlation. To perform this evaluation, a full-scale three-dimensional finite element model of the fuselage section was developed. A crash simulation was conducted using the explicit, nonlinear transient dynamic code, MSC.Dytran™. For the initial simulation, structural deformation and floor-level acceleration responses were generated and correlated with experimental data obtained during the drop test of the B737 fuselage section with the auxiliary fuel tank. The focus of the follow-on simulation was to develop pretest predictions of the fuselage and overhead bin responses for correlation with data from the vertical drop test of the second B737 fuselage section. An assessment of the accuracy of the pretest predictions was made and model improvements were suggested. Several of the model improvements were implemented and the effects of the changes on model accuracy were evaluated. This report describes the development of the finite element model, the correlation between simulation predictions and test data from the 1999 vertical drop test, modifications to the model to represent the second test configuration, the correlation between the pretest predictions and data from the 2000 vertical drop test, and an evaluation of the influence of suggested improvements on model accuracy. In addition, a discussion of test data evaluation and filtering procedures is provided in appendix A of this report.					
17. Key Words Vertical drop test, Crashworthiness, Crash simulation, Auxiliary fuel tank, Overhead stowage bins, Analytical modeling			18. Distribution Statement This document is available to the public through the National Technical Information Service (NTIS) Springfield, Virginia 22161.		
19. Security Classif. (of this report) Unclassified		20. Security Classif. (of this page) Unclassified		21. No. of Pages 96	22. Price

## ACKNOWLEDGEMENTS

This research was performed under an Interagency Agreement (IAA) DTFA03-98-X-90031 between the U.S. Army Research Laboratory (ARL), Vehicle Technology Directorate (VTD) and the Federal Aviation Administration William J. Hughes Technical Center. The contributions and technical support provided by Gary Frings, Tong Vu, and Allan Abramowitz are gratefully acknowledged.

## TABLE OF CONTENTS

	Page
EXECUTIVE SUMMARY	xi
INTRODUCTION	1
EXPERIMENTAL PROGRAM	2
Vertical Drop Test of a B737 Fuselage Section With an Auxiliary Fuel Tank	3
Vertical Drop Test of a B737 Fuselage Section With Overhead Bins and Luggage	8
B737 FUSELAGE SECTION MODEL DEVELOPMENT	10
ANALYTICAL CORRELATION WITH EXPERIMENTAL DATA FROM THE B737 VERTICAL DROP TEST WITH AN AUXILIARY FUEL TANK	13
Comparison of Simulation Predictions and Experimental Data	13
Assessment of Model Accuracy	18
MODIFICATIONS TO THE B737 MODEL TO REPRESENT THE SECOND DROP TEST CONFIGURATION	19
Model of the Heath Tecna Overhead Bin	21
Model of the Hitco Overhead Bin	25
B737 Fuselage Section Model Execution	27
ANALYTICAL CORRELATION WITH EXPERIMENTAL DATA FROM THE B737 VERTICAL DROP TEST WITH OVERHEAD BINS AND LUGGAGE	30
Comparison of Pretest Predictions and Experimental Data	30
Seat Track Locations	30
Fuselage Sidewall Locations	33
Heath Tecna Bin	36
Hitco Bin	37
Floor Corners	41
Assessment of Model Accuracy	42
EVALUATION OF POSTTEST MODEL IMPROVEMENTS	46
Contact Surface Modifications	46
Adjustments to the Contact Force Penalty Factor	46
Frictional Contact	47

Modifications to Model Features	49
Reduction in Yield Stress	49
Corrected Mass Properties	52
Modifications to Gain a More Accurate Physical Representation of the Problem	53
Incorporation of a Platform Model	53
Incorporation of a Luggage Model	58
Corrections to the Cargo Door and Associated Stiffened Structure	64
Combined Luggage and Cargo Door Modifications	69
CONCLUDING REMARKS	74
REFERENCES	75
APPENDIX A—FILTERING AND DATA QUALITY EVALUATION	

#### LIST OF FIGURES

Figure		Page
1	Pretest Photograph of the B737 Fuselage Section With Auxiliary Fuel Tank	3
2	Photograph of the Conformable Auxiliary Fuel Tank	4
3	B737 Fuselage Section Floor Plan View	4
4	Photograph of the Cargo Door Located on the Lower Right Side of the Fuselage Section, Located at FS 440 to FS 490, Approximately	5
5	Pretest Photograph	6
6	Posttest Photograph of B737 Fuselage Section	7
7	Floor-Level Velocity Versus Time Responses	7
8	Pretest Photograph of the B727 Fuselage Section With Overhead Bins and Luggage	8
9	Posttest Photograph of the B737 Fuselage Section With Overhead Bins and Luggage	9
10	Floor-Level Velocity Versus Time Responses	10
11	Model of the B737 Fuselage Section With an Auxiliary Fuel Tank	11

12	Components of the MSC.Dytran Model of the B737 Fuselage Section	12
13	Contact Force of the Tank Into the Cargo (0.01 s) and Passenger (0.05 s) Floor	13
14	Tank Intrusion Into the Floor Beams at FS 460 and 480 at Time 0.07 s	14
15	Posttest Rear View of Test Article Compared With the Analysis	14
16	Front Views of the Drop Test Compared With Analysis	15
17	Left and Right Side Measured Floor Velocity at FS 420 Compared With Analysis	16
18	Left and Right Side Measured Floor Acceleration Compared With Analysis	17
19	Comparison of the Acceleration on the Floor at the Right Rear Seat (Right Rear Leg) Between Experiment and Analysis	17
20	Comparison of the Acceleration on the Floor at the Right Front Seat (Left Rear Leg) Between Experiment and Analysis	18
21	Comparison of the Acceleration on the Floor at the Left Front Seat (Left Rear Leg) Between Experiment and Analysis	18
22	Front View of the Model of the B737 Fuselage Section With Overhead Bins	20
23	Heath Tecna Bin Photograph and Component Designations	21
24	Finite Element Model of the Heath Tecna Bin	22
25	Components of the Finite Element Model of the Heath Tecna Bin	23
26	Load Versus Displacement Response of a Heath Tecna Vertical Support Strut Assembly	24
27	Photograph and Component Designations for the Hitco Bin	25
28	Finite Element Model of the Hitco Bin	26
29	Components of the Finite Element Model of the Hitco Bin	27
30	Predicted and Experimental Left Seat Track Acceleration Responses	31
31	Predicted and Experimental Right Seat Track Acceleration Responses	32
32	Predicted and Experimental Velocity Time Histories of the Outer Seat Tracks at FS 418	33
33	Typical Locations of the Nodes Used to Predict the Upper and Lower Sidewall Responses	33

34	Predicted and Experimental Left Sidewall Acceleration Responses	34
35	Predicted and Experimental Right Sidewall Acceleration Responses	35
36	Predicted and Experimental Vertical Acceleration Responses of the Heath Tecna Bin	36
37	Predicted and Experimental Axial Force Responses of the Vertical Support Struts HT-1 and HT-3 of the Heath Tecna Bin	36
38	Predicted and Experimental Vertical Acceleration Responses of the Hitco Bin	37
39	Predicted and Experimental Axial Force Time Histories of Hitco Bin Link H-1	38
40	Predicted and Experimental Axial Force Time Histories of Hitco Bin Link H-2	38
41	Predicted and Experimental Axial Force Time Histories of Hitco Bin Link H-3	38
42	Predicted and Experimental Axial Force Time Histories of Hitco Bin Link H-4	39
43	Predicted and Experimental Axial Force Time Histories of Hitco Bin Link H-5	39
44	Predicted and Experimental Axial Force Time Histories of Hitco Bin Link H-6	39
45	Predicted and Experimental Axial Force Time Histories of Hitco Bin Link H-7	40
46	Predicted and Experimental Axial Force Time Histories of Hitco Bin Link H-8	40
47	Predicted and Experimental Axial Force Time Histories of Hitco Bin Link H-9	40
48	Predicted and Experimental Axial Force Time Histories of Hitco Bin Link H-10	41
49	Predicted and Experimental Axial Force Time Histories of Hitco Bin Link H-11	41
50	Predicted Vertical Displacement Responses of the Left Front and Rear Corners of the Floor	42
51	Predicted Vertical Displacement Responses of the Right Front and Rear Corners of the Floor	42
52	Posttest Photograph of the B737 Fuselage Section With Overhead Bins	43
53	Photograph Showing the Various Linkages and Connections of the Hitco Bin	44
54	Front Views of the Deformed Model and Film-Capture Photographs	45
55	Effect of Contact Force Penalty Factor (FACT) on Left Seat Track Acceleration Responses	47

56	Effect of Contact Force Penalty Factor (FACT) on Right Seat Track Acceleration Responses	47
57	Effect of Friction on Left Seat Track Acceleration Responses	48
58	Effect of Friction on Right Seat Track Acceleration Responses	48
59	Deformation Patterns of the Reduced Yield and Pretest Models and Test Results	49
60	Measured Vertical Acceleration Responses Plotted With the Pretest and Reduced Yield Model Predictions for the Left Side Seat Track at Four Locations	50
61	Measured Vertical Acceleration Responses Plotted With the Pretest and Reduced Yield Model Predictions for the Right Side Seat Track at Four Locations	51
62	Left Seat Track Acceleration Responses Compared With Pretest and Reduced Mass Model Predictions	52
63	Right Seat Track Acceleration Responses Compared With Pretest and Reduced Mass Model Predictions	53
64	Schematic Drawing of the Drop Test Platform and Instrumentation Layout	54
65	Photograph of the Drop Test Platform	55
66	Three-Quarter View of the Integrated B737 Fuselage Section and Platform Model	55
67	Comparison of Experimental and Analytical Force Responses for Six Platform Load Cells	56
68	Acceleration Responses of the Left Inner and Outer Seat Tracks at FS 452 Plotted With the Pretest Predictions and the Responses Obtained From the Integrated Platform and B737 Fuselage Section Model	57
69	Acceleration Responses of the Right Inner and Outer Seat Tracks at FS 452 Plotted With the Pretest Predictions and the Responses Obtained From the Integrated Platform and B737 Fuselage Section Model	58
70	B737 Fuselage Model With Luggage	58
71	Luggage Crush Test Results	59
72	Comparisons of the Deformation Patterns of the Luggage and Pretest Models With Experiment	61
73	Measured Vertical Acceleration Responses Plotted With the Pretest and Luggage Model Predictions for the Left Side Seat Track at Four Locations	62

74	Measured Vertical Acceleration Responses Plotted With the Pretest and Luggage Model Predictions for the Right Side Seat Track at Four Locations	63
75	Comparison of Experimental Velocity Responses of the Left and Right Outer Seat Tracks at FS 418 With Pretest and Luggage Model Predictions	64
76	Revised Model of the Cargo Door and Surrounding Structure	65
77	Measured Vertical Acceleration Responses Plotted With the Pretest and Cargo Door Model Predictions for the Left Side Seat Track at Four Locations	66
78	Measured Vertical Acceleration Responses Plotted With the Pretest and Cargo Door Model Predictions for the Right Side Seat Track at Four Locations	67
79	Comparisons of the Deformation Patterns of the Cargo Door and Pretest Models With Experiment	68
80	Comparison of Experimental Velocity Responses of the Left and Right Outer Seat Tracks at FS 418 With Pretest and Cargo Door Model Predictions	69
81	Comparisons of the Deformation Patterns of the Combined Luggage and Cargo Door and Pretest Models With Experiment	70
82	Comparison of Experimental Velocity Responses of the Left and Right Outer Seat Tracks at FS 418 With Pretest and Combined Luggage and Cargo Door Model Predictions	71
83	Measured Vertical Acceleration Responses Plotted With the Pretest and the Combined Luggage and Cargo Door Model Predictions for the Left Side Seat Track at Four Locations	72
84	Measured Vertical Acceleration Responses Plotted With the Pretest and the Combined Luggage and Cargo Door Model Predictions for the Right Side Seat Track at Four Locations	73

#### LIST OF TABLES

Table		Page
1	Material Properties Used in MSC.Dytran Model of the B737 Fuselage Section With an Auxiliary Fuel Tank	12
2	Material Properties Used in the MSC.Dytran Model of the B737 Fuselage Section With Overhead Bins and Luggage	24
3	Weight Comparison of the Model and Test Article	28

## EXECUTIVE SUMMARY

A 30-ft/s vertical drop test of a 10-ft-long fuselage section of a Boeing 737 (B737) aircraft was conducted in October of 1999 at the Federal Aviation Administration William J. Hughes Technical Center, Atlantic City International Airport, NJ. This test was performed to evaluate the structural integrity of a conformable auxiliary fuel tank mounted beneath the fuselage floor and to determine its effect on the structural response of the airframe. A second drop test of a similar B737 fuselage section was conducted in November of 2000 in which two different overhead stowage bins were evaluated. These tests present an invaluable opportunity to evaluate the capabilities of computational tools for crash simulation through analytical and experimental correlation. To perform this evaluation, a full-scale three-dimensional finite element model of the fuselage section was developed. A crash simulation was conducted using the explicit, nonlinear transient dynamic code, MSC.Dytran™. For the initial simulation, structural deformation and floor-level acceleration responses were generated and correlated with experimental data obtained during the drop test of the B737 fuselage section with the auxiliary fuel tank. The focus of the follow-on simulation was to develop pretest predictions of the fuselage and overhead bin responses for correlation with data from the vertical drop test of the second B737 fuselage section. An assessment of the accuracy of the pretest predictions was made and model improvements were suggested. Several of the model improvements were implemented and the effects of the changes on model accuracy were evaluated. This report describes the development of the finite element model, the correlation between simulation predictions and test data from the 1999 vertical drop test, modifications to the model to represent the second test configuration, the correlation between the pretest predictions and data from the 2000 vertical drop test, and an evaluation of the influence of suggested improvements on model accuracy. In addition, a discussion of test data evaluation and filtering procedures is provided in appendix A of this report.

## INTRODUCTION

An important aspect of crashworthiness research is the demonstration and validation of computational tools for accurate simulation of airframe structural response to crash impacts. In fact, the validation of numerical simulations was identified as one of five key technology shortfalls during the Workshop on Computational Methods for Crashworthiness [1] that was held at NASA Langley Research Center in 1992. Analytical codes have the potential to greatly facilitate the crashworthy design process, to help certify seats and aircraft to dynamic crash loads, to predict seat and occupant response to impact with the probability of injury, and to evaluate numerous crash scenarios not economically feasible with full-scale crash testing.

The U.S. Army has been active in supporting the development and utilization of crash modeling and simulation codes for many decades. More than 30 years ago, the U.S. Army sponsored initial development of a kinematic crash analysis code, KRASH [2], by the Lockheed-California Company. Kinematic codes employ a semiempirical modeling approach using lumped masses, beams, and nonlinear springs to represent the airframe structure. These codes rely heavily on test data for definition of spring properties to characterize the crushing behavior of the subfloor, landing gear, and other energy absorbing components. Typical kinematic models are generally composed of less than 100 elements. Simplification of the complex structure of an aircraft to less than 100 elements requires significant engineering judgement and numerous approximations. Good correlation between the analytical and experimental data is usually obtained for global parameters, such as engine or landing gear responses. In addition, these kinematic simulations enable quick computations and are well suited for early design simulations where structural details are not defined. However, these codes would be unable to predict localized responses, e.g., the stress level in an airframe component at a particular time during a crash event. A recent trend has been to perform a hybrid simulation in which detailed finite element analyses are used to determine the structural response of energy absorbing components, such as the subfloor. This information is then used to define spring properties in the kinematic simulation.

Currently, engineering workstation computation power is sufficient to allow use of a new generation of crash analysis codes to simulate the nonlinear, transient dynamic response of airframe structures in detail. These finite element codes, such as LS-DYNA [3], MSC.Dytran™ [4], and PAM-CRASH [5], use an explicit solver that eliminates the need to repetitively decompose large global stiffness matrices as is required for implicit codes. Explicit codes require an extremely small time step, typically less than a microsecond, whose duration is controlled by the smallest element in the model. Thus, impact simulations of large models having a pulse duration on the order of 30-40 milliseconds can require several central processing unit (CPU) hours to solve on an engineering workstation. These codes are presently being used extensively to model automobile crashes. To build confidence in the application of these finite element codes to aircraft structures, it is important to demonstrate their computational capabilities through analytical and experimental correlation.

The FAA has conducted 30-ft/s vertical drop tests of two 10-ft-long B737 fuselage sections, one with an auxiliary fuel tank mounted beneath the floor [6] and one with two different overhead bins and luggage [7]. These tests provide an invaluable opportunity to evaluate the capabilities of computational tools for crash simulation through analytical and experimental correlation. To

perform this evaluation, a full-scale three-dimensional finite element model of the fuselage section was developed using MSC.Dytran [4]. MSC.Dytran is a general-purpose finite element code for simulating highly nonlinear transient response of solids, structures, and fluids. The code uses an explicit time integration technique and has the capability of simulating fluid-structure interactions, which may be required to solve certain crash analysis problems such as water impact simulations. The Lagrangian solver (structural component of the MSC.Dytran code) is based on the public domain DYNA3D code [8], which was developed at the Lawrence Livermore National Laboratory. The code also includes an Eulerian solver to represent fluids that is based on the PISCES [9] code. The MSC.Dytran code interface has been written to make the input of the code as compatible as possible with MSC.Nastran [10], a general-purpose finite element code that is commonly used in the aerospace industry for structural analysis. The MSC.Patran [11] pre- and postprocessing software was used with the MSC.Dytran Preference to build the finite element models and to postprocess the results. The compatibility between MSC.Dytran, MSC.Patran, and MSC.Nastran is an added benefit that may eliminate the need for developing a separate airframe model specifically for performing a crash analysis.

The initial finite element model was developed to represent the B737 fuselage section with the conformable auxiliary fuel tank. A crash simulation was executed and predictions of the structural deformation and floor-level acceleration responses were correlated with test data obtained from the 30-ft/s drop test. A follow-on simulation was conducted to generate pretest predictions of the fuselage and overhead bin responses during the second vertical drop test. An assessment of the accuracy of the pretest predictions was made and model improvements were suggested. Several of the suggested improvements have been implemented and the effects of the changes on model accuracy evaluated. This report describes the development of the finite element model, the correlation between simulation predictions and test data from the 1999 vertical drop test, modifications to the model to represent the second test configuration, the correlation between the pretest predictions and data from the 2000 vertical drop test, and an evaluation of the influence of suggested improvements on model accuracy. In addition, a discussion of test data evaluation and filtering procedures is provided in appendix A of this report.

## EXPERIMENTAL PROGRAM

The Crashworthiness Program at the FAA William J. Hughes Technical Center obtained two fuselage sections of a narrow-body transport category B737 airplane. This airplane is subject to Part 25 of the Federal Aviation Regulations. The interior paneling was removed from both fuselage sections, exposing the internal skeletal structure. In October of 1999, the FAA conducted a vertical drop test of a 10-ft-long B737 fuselage section with a conformable auxiliary fuel tank mounted beneath the floor. The purpose of the test was to evaluate the structural integrity of the auxiliary fuel tank, its fuel containment characteristics, and its effect on the structural response of the fuselage section. A 30-ft/s vertical drop test of the second fuselage section was conducted in November of 2000. For this test, the fuselage section was outfitted with two different overhead stowage bins. Instead of the auxiliary fuel tank, luggage was placed beneath the floor in the cargo hold. This test was conducted to evaluate the structural response of the overhead bins during a severe, but potentially survivable, impact. Brief summaries of the two vertical drop tests are provided in the following subsections.

VERTICAL DROP TEST OF A B737 FUSELAGE SECTION WITH AN AUXILIARY FUEL TANK.

A pretest photograph of the B737 fuselage section with the conformable auxiliary fuel tank is shown in figure 1. The vertical drop test of this fuselage section was conducted at the FAA's Dynamic Drop Test Facility in October of 1999 [6]. The test article is a 10-foot section of a Boeing 737-200 airplane from fuselage station (FS) 400 to 500A (520). The fuselage was configured with six triple-occupant passenger seats. The middle position of each seat contained an instrumented Hybrid II anthropomorphic dummy and the remaining seats contained noninstrumented mannequins, each weighing approximately 165 lbs

The conformable auxiliary fuel tank was filled with 404 gallons of water and was mounted beneath the floor of the fuselage section. A photograph of the fuel tank is shown in figure 2, and its location in the fuselage section is illustrated in the schematic floor plan shown in figure 3. The fuel tank weighed 3,740 lbs and the fully instrumented fuselage section weighed 8,780 lbs. The outer floor beams at each end of the test section were reinforced to minimize the open-end effects. Several features of the fuselage configuration are important to note for the model development due to the fact that they affect model symmetry and overall stiffness. The section contained a cargo door and associated stiffened structure located on the lower right side of the fuselage, as shown in figure 4. Also, as shown in figure 3, it is important to note that the fuel tank, which accounts for approximately half of the total weight of the fuselage section, was not centered beneath the floor but was located closer to the rear of the fuselage section.

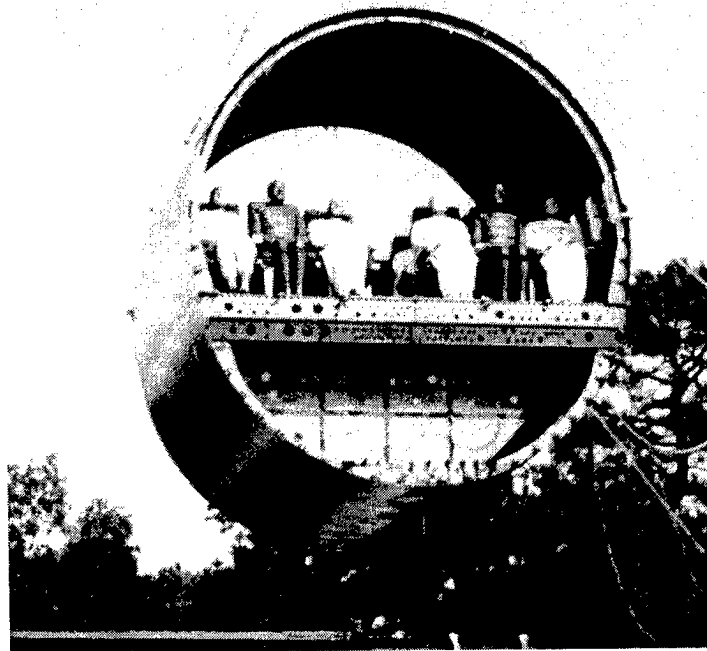


FIGURE 1. PRETEST PHOTOGRAPH OF THE B737 FUSELAGE SECTION WITH AUXILIARY FUEL TANK

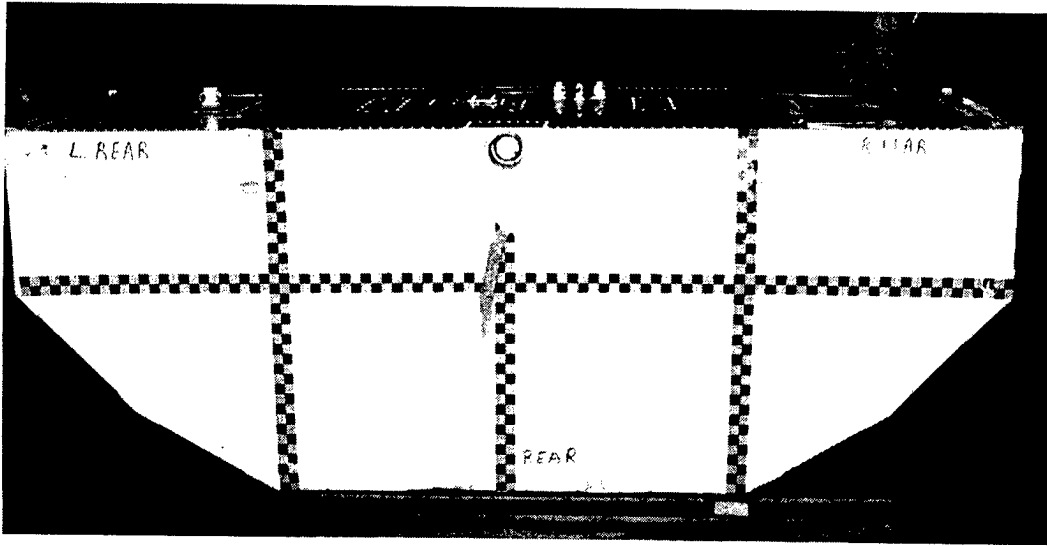


FIGURE 2. PHOTOGRAPH OF THE CONFORMABLE AUXILIARY FUEL TANK

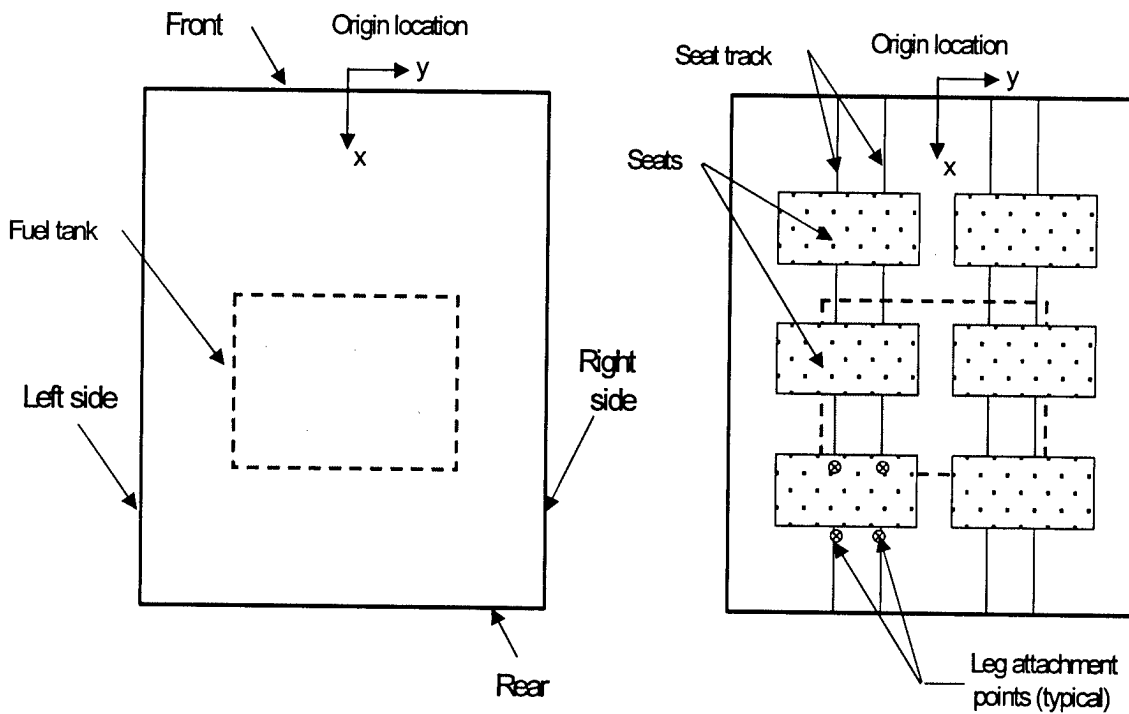


FIGURE 3. B737 FUSELAGE SECTION FLOOR PLAN VIEW (Drawing not to scale)

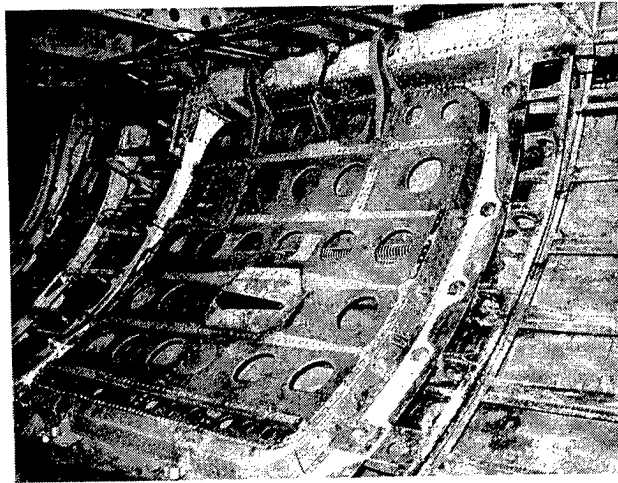


FIGURE 4. PHOTOGRAPH OF THE CARGO DOOR LOCATED ON THE LOWER RIGHT SIDE OF THE FUSELAGE SECTION, LOCATED AT FS 440 TO FS 490, APPROXIMATELY

The fuselage section was instrumented with accelerometers placed on the seat rails and sidewalls. In addition, accelerometers were mounted along the rooftop and at various circumferential positions on the fuselage frames. The six anthropomorphic dummies were instrumented with lumbar accelerometers and load cells. The fuel tank was also instrumented with accelerometers. The impact surface at the Dynamic Drop Test Facility consists of a wooden platform supported by a series of heavy steel I-beams, as shown in figure 5. The platform was instrumented with 12 accelerometers, 12 string potentiometers, and 12 load cells placed under the platform. Approximately 120 channels of data were collected at 10,000 samples/second during the impact test using a digital data acquisition system.

The fuselage section was raised through its center-of-gravity to a height of 14 ft using four cables attached to brackets located on the upper sides of the fuselage section. A photograph of the fuselage section raised to the correct drop height prior to release is shown in figure 5. The section was dropped vertically to achieve a 30-ft/s velocity at impact. Plots of the unfiltered data were generated for each channel, and any anomalies such as over-ranged data, polarity errors, and zero offsets were noted. Any data with serious anomalies were excluded from correlation with the crash simulation. Floor-level acceleration data in the vertical direction were integrated to obtain the vertical velocity change. Any channel in which the integrated velocity change was not comparable with the impact velocity plus rebound was not used for correlation with the analysis. In general, the floor-level acceleration traces contained high-amplitude, high-frequency oscillations. Consequently, prior to correlation with the analytical data, selected raw acceleration traces were filtered using a 48-Hz, four-pole Butterworth low-pass digital filter to remove the high frequency ringing from the underlying crash pulse. The filtering was performed forward in time, then backward in time to eliminate any phase shift in time. It is also noted that accelerometers located on the floor above the fuel tank were not used for analytical correlation, as some acceleration peaks exceeded the maximum range set for the data acquisition instrumentation. These accelerometers were installed for timing purposes only. A detailed discussion of test data evaluation and filtering procedures is provided in appendix A.

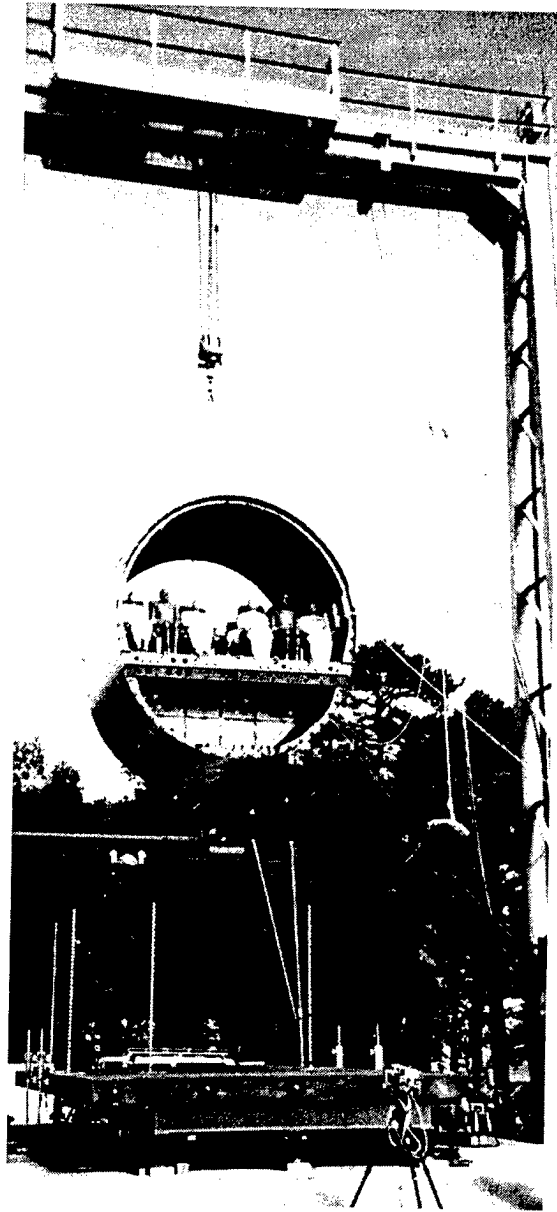


FIGURE 5. PRETEST PHOTOGRAPH

A posttest photograph of the fuselage section is shown in figure 6. Damage consisted of severe yielding and fracture of the lower fuselage frames and wrinkling of the skin on the lower left side of the fuselage section. The deformation of the lower fuselage was asymmetric about the centerline due to the presence of the cargo door and its associated stiffened structure located on the lower right-hand side of the fuselage. On the left-hand side, additional fuselage frames fractured. Similar damage was not observed on the right-hand side of the fuselage. The auxiliary fuel tank was punctured from below, causing water leakage posttest. In addition, failure of the seat tracks and major structural damage to the seats were observed, especially on the right-hand side of the fuselage floor [6].

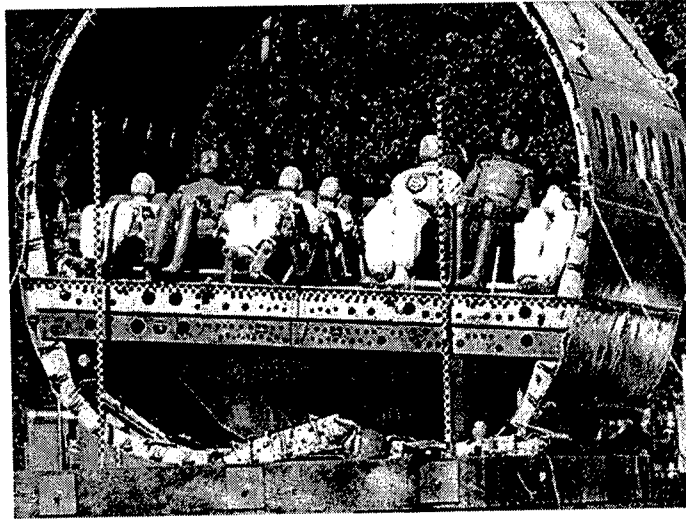


FIGURE 6. POSTTEST PHOTOGRAPH OF B737 FUSELAGE SECTION

Important factors in the fuselage configuration are the asymmetries due to the door located on the lower right side of the fuselage and due to the off-center location of the fuel tank. To illustrate the importance of the asymmetry caused by the door, two acceleration traces obtained from accelerometers located at FS 420, one on the right side and one on the left side of the floor, were integrated to obtain the velocity change versus time, as shown in figure 7. The accelerometers are located close to the forward edge of the floor, with the right side accelerometer positioned above the door. As shown in figure 7, the velocity on the right side of the fuselage floor is being removed much more quickly than the velocity on the left side of the fuselage. The velocity response of the right side accelerometer has stopped by 0.07 seconds, while the left side accelerometer did not come to rest until 0.12 seconds. These results illustrate the effect of the door and its associated stiffened structure on the fuselage response.

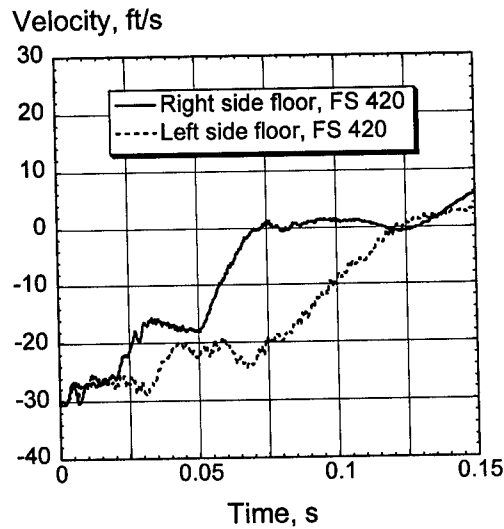


FIGURE 7. FLOOR-LEVEL VELOCITY VERSUS TIME RESPONSES

VERTICAL DROP TEST OF A B737 FUSELAGE SECTION WITH OVERHEAD BINS AND LUGGAGE.

A second vertical drop test of a B737 fuselage section was conducted at the FAA Technical Center in November of 2000 [7]. The test article is a 10-foot section of a Boeing 737-100 airplane from fuselage stations (FS) 380 to 500. Even though there are minor differences in the type of B737 aircraft and fuselage stations, this airframe is structurally similar to the one tested with the conformable auxiliary fuel tank. For this test, the fuselage section was outfitted with two different overhead stowage bins. Instead of the auxiliary fuel tank, 3,229 lbs of luggage were packed in the cargo hold to represent a maximum takeoff weight condition. The objective of this test was to evaluate the response of the overhead stowage bins in a narrow-body transport fuselage section when subjected to a severe, but survivable, impact condition. A pretest photograph of the fuselage section is shown in figure 8.

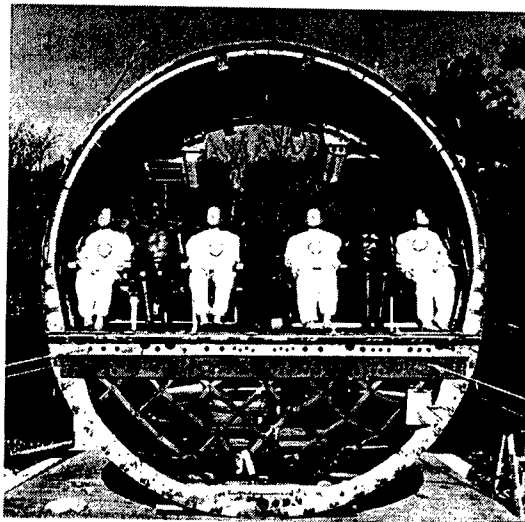


FIGURE 8. PRETEST PHOTOGRAPH OF THE B727 FUSELAGE SECTION WITH OVERHEAD BINS AND LUGGAGE

The test article was outfitted with two commercial overhead stowage bins mounted in the passenger cabin. A 60-inch Hitco bin was mounted on the left side of the cabin between FS 429 and FS 489. A 60-inch Heath Tecna bin was mounted on the right side of the cabin between FS 426 and FS 486. The overhead bins were loaded by installing 200 lbs of wood in the Hitco bin and 120 lbs of wood in the Heath Tecna bin, corresponding to the maximum weights specified for each bin. The plywood was installed in the bins to achieve a uniformly distributed mass loading. The bins were instrumented with five accelerometers. Triaxial accelerometers were mounted to the bottom of each bin and two vertical accelerometers were mounted to the center of the ends of each bin. In addition, the support linkages and brackets were heavily instrumented with strain gages that were calibrated to provide axial load data.

The passenger cabin was outfitted with six triple-occupant passenger seats, as in the previous test. An instrumented Hybrid II anthropomorphic dummy was placed in the center position of each seat, while the remaining seats contained noninstrumented mannequins. The outer floor beams at each end of the test section were reinforced to minimize the open-end effects. In

general, the test configuration was similar to the previous test, with the exception of the overhead bins and luggage. Another difference between the two test configurations was that two large camera mounts, each weighing 70 lbs, were attached to the upper fuselage frames. Two cameras, each weighing 22 lbs, were secured to the mounts to record the response of the overhead bins. The total weight of the fully instrumented B737 fuselage section was 8,870 lbs.

The fuselage section was instrumented with vertical and triaxial accelerometers placed on the inner and outer seat rails and vertical accelerometers mounted to the upper and lower sidewalls. The six anthropomorphic dummies were instrumented with lumbar accelerometers and load cells. In addition, the impact platform at the Dynamic Drop Test Facility was instrumented with 12 accelerometers, 12 load cells, and 12 string potentiometers located beneath the platform. In a similar fashion as the previous test, the fuselage section was raised through its center-of-gravity to a height of 14 ft, then was dropped vertically to achieve a 30-ft/s velocity at impact. Approximately 140 channels of data were collected at 10,000 samples/second during the impact test using a digital data acquisition system. Quality checks were performed on the test data, as described previously.

A posttest photograph of the fuselage section is shown in figure 9. The location and type of damage experienced by the second fuselage section was similar to that incurred during the 1999 test. The damage consisted of yielding and fracture of the lower fuselage frames and wrinkling of the skin on the lower left side of the fuselage section. The deformation of the lower fuselage was asymmetric about the centerline due to the presence of the door and its associated stiffened structure located on the lower right-hand side of the fuselage. On the left-hand side, a second damage site developed with fracture of the fuselage frames. Similar to the first test, all seats on the right side of the fuselage floor failed during the second test. However, no failure of the overhead bin support brackets or linkages occurred. Due to the presence of the luggage, the deformation pattern of the lower fuselage frames was more uniform than that seen in the previous test.

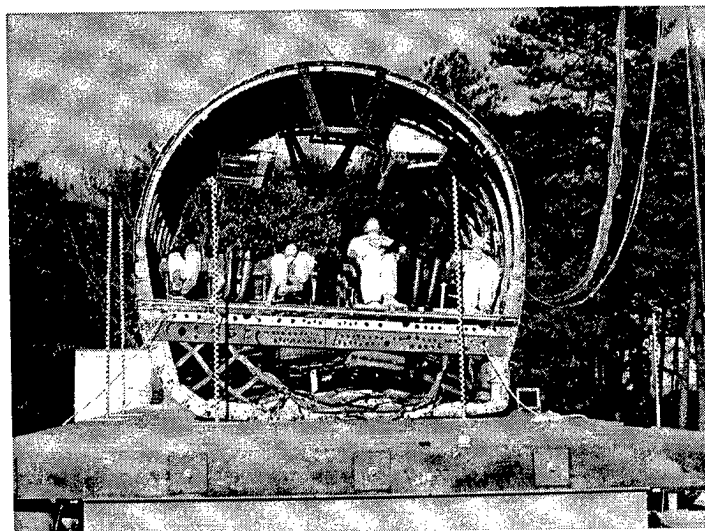


FIGURE 9. POSTTEST PHOTOGRAPH OF THE B737 FUSELAGE SECTION WITH OVERHEAD BINS AND LUGGAGE

For the second fuselage configuration, only the asymmetry, due to the door, is present, i.e., without the fuel tank the midplane asymmetry is removed. To determine the effect of the door for this second drop test, the acceleration traces obtained from two accelerometers located on the right and left outer seat tracks at FS 418 were integrated to obtain the velocity time histories shown in figure 10. This plot indicates that until about 0.06 second, the two responses are nearly the same. After that time, the velocity on the right side is being removed somewhat more quickly than on the left side. However, the difference is much less dramatic than that of the previous test, as shown in figure 7. The velocity responses of the right and left outer seat track accelerometers have stopped by 0.11 and 0.12 second, respectively. These results indicate that the influence of the door on the fuselage response has been mitigated by the presence of the luggage in the cargo hold.

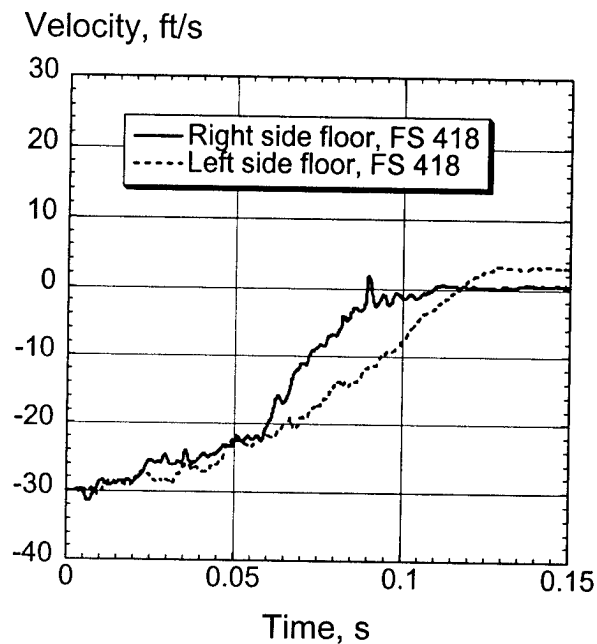


FIGURE 10. FLOOR-LEVEL VELOCITY VERSUS TIME RESPONSES

#### B737 FUSELAGE SECTION MODEL DEVELOPMENT

The model geometry was developed from detailed geometric measurements made of the second test article, since engineering or technical drawings of the fuselage section were not available. Several assumptions were made to keep the geometry as simple as possible. For example, many of the cutouts, joints, fasteners, and doublers were ignored. Development of the model was performed using the preprocessing software package, MSC.Patran [11]. A geometric model of the fuselage section was developed containing the important structural features of the airframe. The geometric model was discretized and element and material properties were assigned. The complete finite element model of the B737 fuselage section with the auxiliary fuel tank is shown in figure 11.

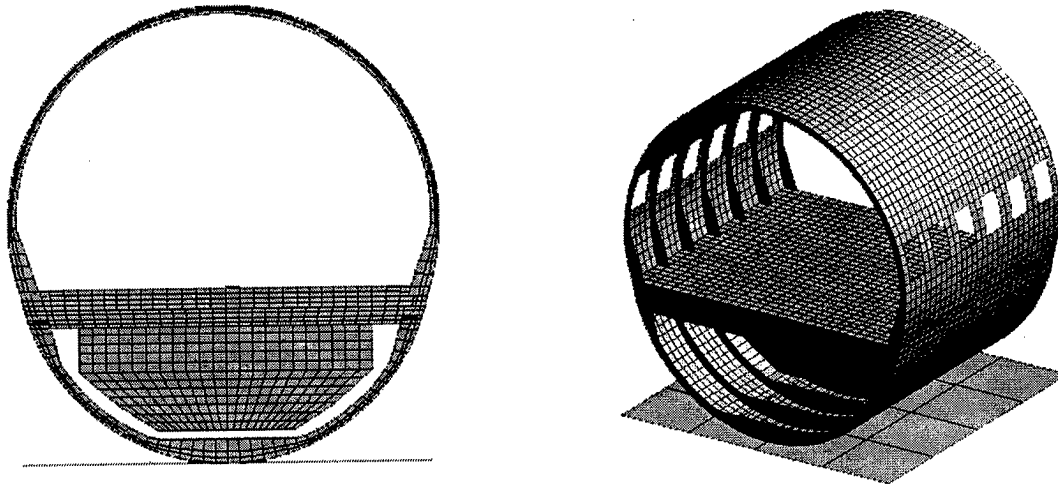


FIGURE 11. MODEL OF THE B737 FUSELAGE SECTION WITH AN AUXILIARY FUEL TANK

The MSC.Dytran model consists of approximately 9,600 nodes and 13,000 elements, including 9,000 shell and 4,000 beam elements, to represent the outer skin, fuselage frames, floor, longitudinal stringers, the fore and aft floor reinforcements, and the auxiliary fuel tank with attachments. In addition, the cargo door on the lower right side of the fuselage section was modeled, including its associated stiffened structure. Cutouts in the fuselage skin were used to represent the windows on both sides of the section and the stiffened structure surrounding the windows was modeled using beam elements. The outer surface of the fuel tank was modeled using shell elements, and the thickness assigned to these elements was adjusted such that the total weight of the tank was 370 lbs, matching the experimental weight. Concentrated masses were placed inside the fuel tank to represent the mass and inertia of 404 gallons of water. A flat impact surface was added to the model. Each edge node on the impact surface was fixed; i.e., the nodes were constrained from translational and rotational motion. Some of the individual components of the model are shown in figure 12, including the outer skin, fuselage frames, and auxiliary fuel tank. It should be noted that the beam elements are difficult to distinguish from the shell elements in the figure because they are represented as straight lines.

A master-surface to slave-node contact was defined between the impact surface and the nodes forming the lower portion of the fuselage section. A second contact surface was defined between the fuel tank and the nodes forming the fuselage structure surrounding the tank. This contact was needed to prevent the fuselage section nodes and elements from passing through the fuel tank as they deformed during the impact.

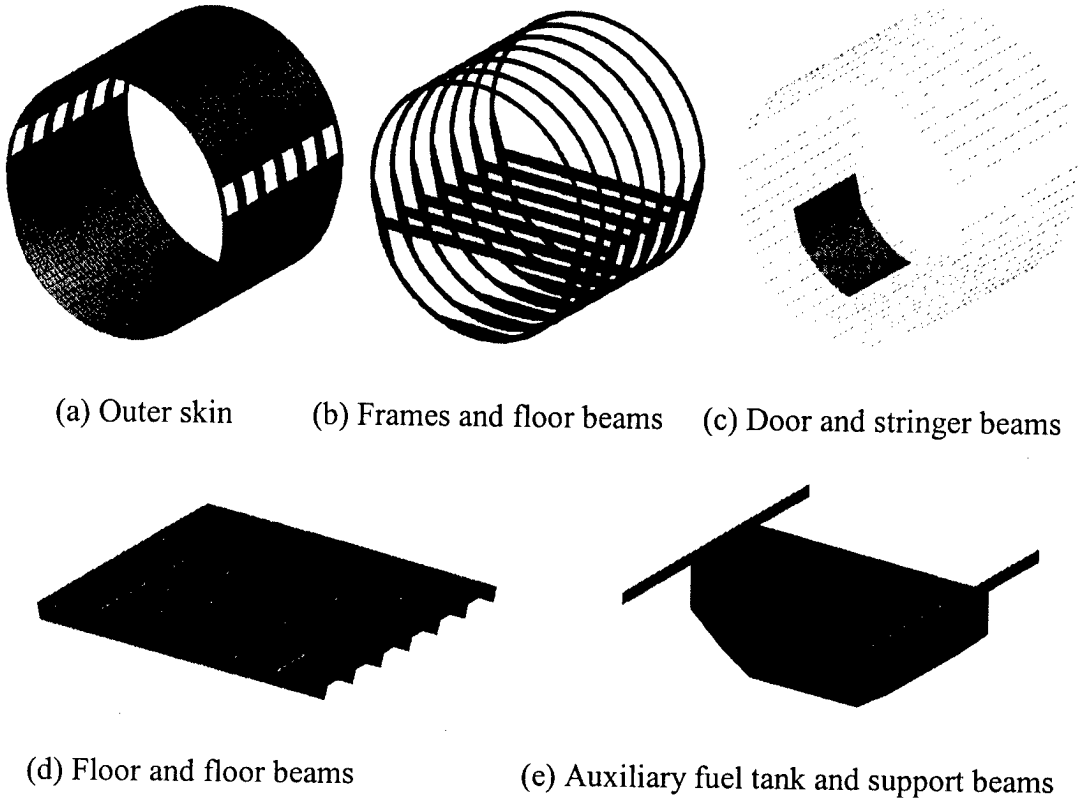


FIGURE 12. COMPONENTS OF THE MSC.DYTRAN MODEL OF THE B737 FUSELAGE SECTION

Most of the primary structure was assumed to be either 2024-T3 or 7075-T6 aluminum. The material formulation chosen for the model, DMATEP, is a general-purpose isotropic bilinear elastic-plastic material property with yielding and ultimate failure strain. The yield stress of 2024-T3 was assumed to be 47,000 psi, while the yield stress of 7075-T6 was assumed to be 60,000 psi. The yield stress of the 7075-T6 aluminum was lowered from handbook values (73,000 psi) to partially account for stress risers, fatigue damage, size effects, and corrosion. A failure strain of 5 percent was assigned to the 7075-T6 aluminum based on experience gained during an earlier project involving simulation of a Boeing 720 fuselage section drop test [12]. A list of material properties used in the model is provided in table 1.

TABLE 1. MATERIAL PROPERTIES USED IN MSC.DYTRAN MODEL OF THE B737 FUSELAGE SECTION WITH AN AUXILIARY FUEL TANK

Material Name	Type of Formulation	Young's Modulus (psi)	Density lb-s <sup>2</sup> /in <sup>4</sup>	Poisson's Ratio	Yield Stress (psi)	Ultimate Failure Strain (in/in)
Aluminum 2024-T3	DMATEP	1.06e07	0.0002525	0.33	47,000	N/A
Aluminum 7075-T6	DMATEP	1.04e07	0.0002525	0.33	60,000	0.05
Fuel Tank Material	DMATEP	1.04e07	0.000449	0.3	99,000	N/A

The entire fuselage model weighed 8,800 lbs, which is close to the total weight of the fully-instrumented test article which was 8,780 lbs. Seats and dummies were not modeled; however, the mass of the seats and dummies was combined and accounted for as 24 concentrated masses that were assigned to nodes located at each seat leg-seat track position on the floor. All nodes in the model, except those forming the impact surface, were assigned an initial vertical velocity of 30 ft/s. The model was executed for 0.1 seconds, which required 21.2 hours on a Sun Ultra 450 workstation computer. The time step for the solution was approximately 2 microseconds. The requested output included the deformed geometry and acceleration, velocity, and displacement time histories for several nodes whose positions correspond to the locations of selected transducers.

ANALYTICAL CORRELATION WITH EXPERIMENTAL DATA FROM THE  
B737 VERTICAL DROP TEST WITH AN AUXILIARY FUEL TANK

COMPARISON OF SIMULATION PREDICTIONS AND EXPERIMENTAL DATA.

An analysis of the test data indicated that the auxiliary fuel tank came loose from the mounting track shortly after impact [6]. Consequently, the model was changed to allow the tank to move freely within the cargo hold with contact surfaces to prevent penetration of the tank through the surrounding structure. A portion of the contact force between the tank and the surrounding fuselage structure is plotted in figure 13.

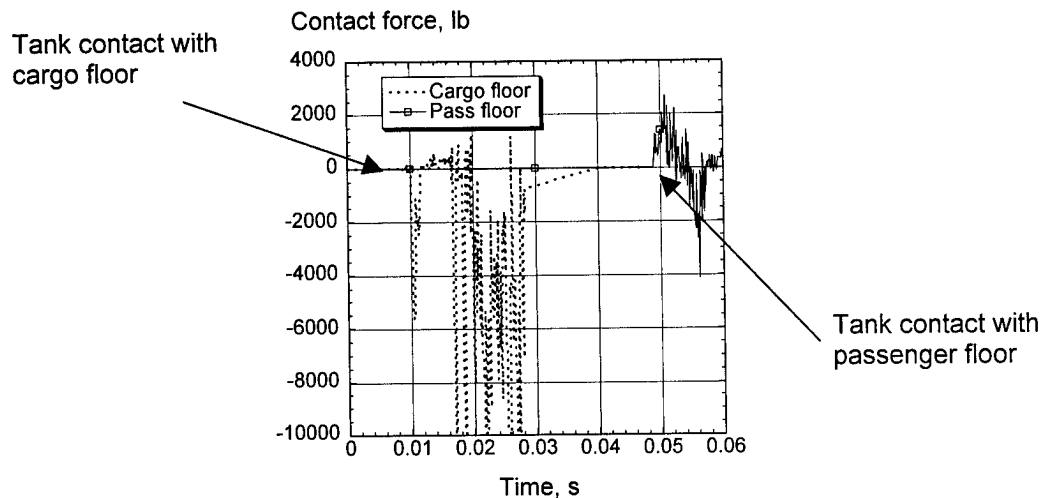


FIGURE 13. CONTACT FORCE OF THE TANK INTO THE CARGO (0.01 s) AND PASSENGER (0.05 s) FLOOR

The plot indicates that the tank initially contacted the lower cargo floor at approximately 0.01 s after impact and contacted the upper floor beams slightly before 0.05 s. These time values correspond closely with the values measured experimentally, as reported in reference 6. The accurate simulation of the tank behavior is critical to achieving good prediction of the fuselage response. The fact that the tank was not constrained by the support beams adds even more complexity to the simulation. Figure 14 shows the tank intruding into the floor beams at FS460 and 480 at time 0.07 s. This intrusion caused failure of the beams and damaged the integrity of

the floor. Front- and rear-view deformed plots of the fuselage section are compared with posttest pictures in figures 15 and 16, respectively. The plots show that the observed deformation pattern of the fuselage is closely captured by the simulation results.

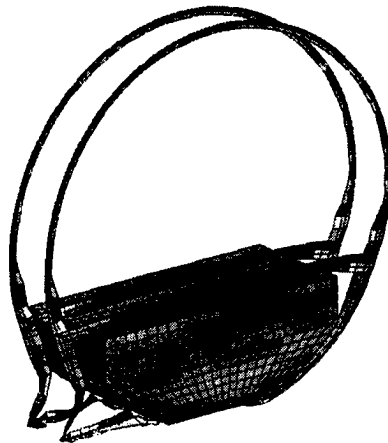
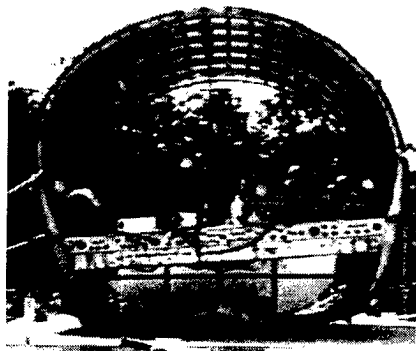
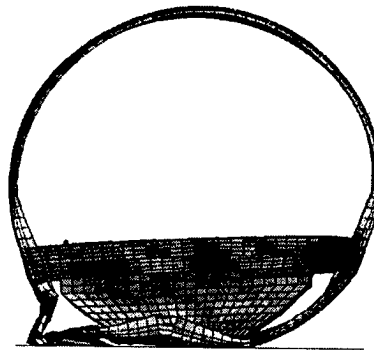


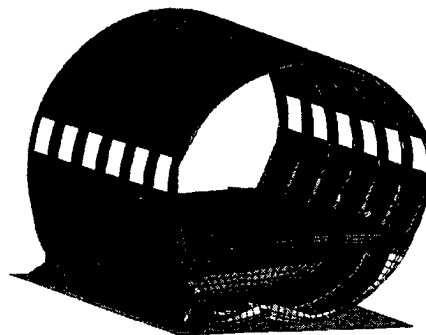
FIGURE 14. TANK INTRUSION INTO THE FLOOR BEAMS AT FS 460 AND 480 AT TIME 0.07 s



(a) Posttest picture rear view

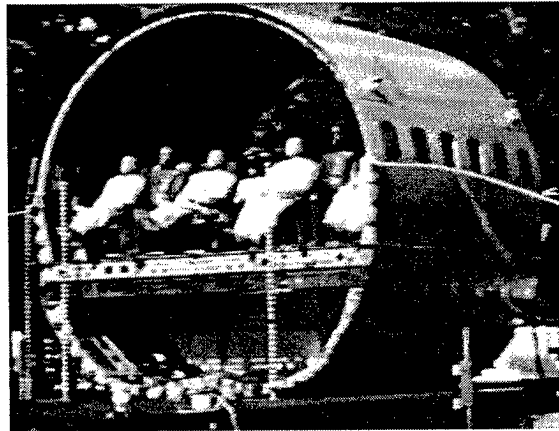
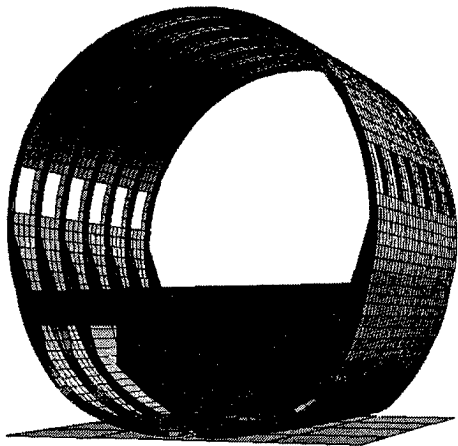


(b) Analysis rear view at time 0.07 second

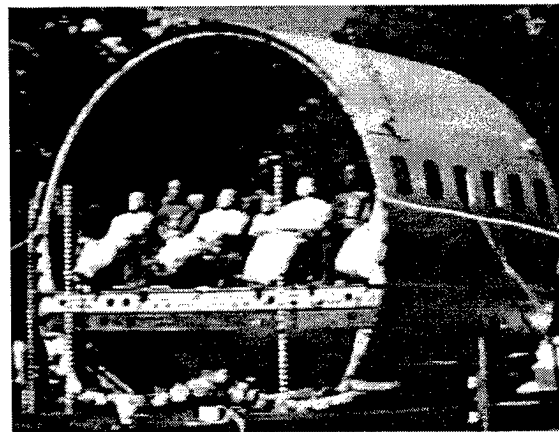


(c) Analysis rear view at time 0.1 second

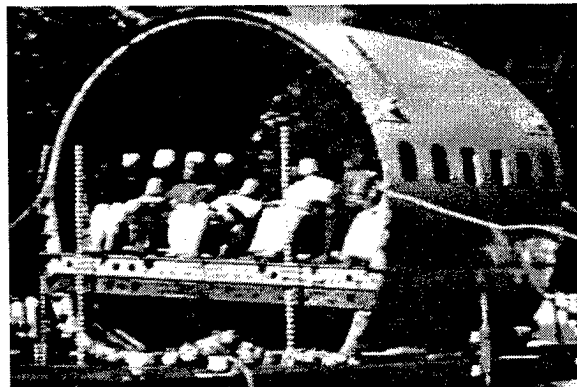
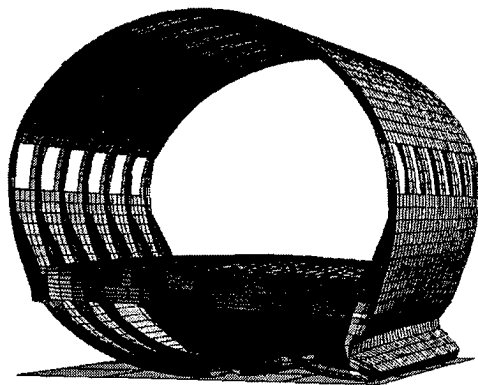
FIGURE 15. POSTTEST REAR VIEW OF TEST ARTICLE COMPARED WITH THE ANALYSIS



(a) Front view at time = 0.02 seconds



(b) Front view at time = 0.06 seconds



(c) Front view at time = 0.10 seconds

FIGURE 16. FRONT VIEWS OF THE DROP TEST COMPARED WITH ANALYSIS

The deformation measured at the floor level is asymmetric from left to right due to the stiff cargo door on the right side and is asymmetric front to rear due to the placement of the tank. The maximum predicted deformation for the left side of the floor was 24 inches near the front edge and 21 inches near the aft edge of the fuselage, compared to 21.7 and 20.7 inches measured experimentally posttest. The maximum deformation on the right side of the fuselage was predicted to be 18 inches on the front edge and 16 inches on the aft edge, compared with the posttest measured values of 10.7 and 10.5 inches, respectively. Note that the posttest measurements were taken at rest, while the predicted values are the maximum dynamic values that occur at approximately 0.1 second. The predicted values should be larger than the equilibrium posttest values since some elastic spring-back is to be expected, especially on the right side.

Comparisons of the predicted velocity response with the experimental velocity response for the left and right edges of the fuselage floor are plotted in figure 17. The experimental velocity responses were obtained from integration of the corresponding acceleration traces, whereas the analytical velocity responses were output directly from the MSC.Dytran simulation. The comparison between data and analysis is good and shows the correct trends. The analytical velocity is quite noisy, however, the velocity was not filtered because filtering would alter the shape of the initial curve. The results shown in figure 17 verify that the right side slows down more quickly due to the stiff cargo door.

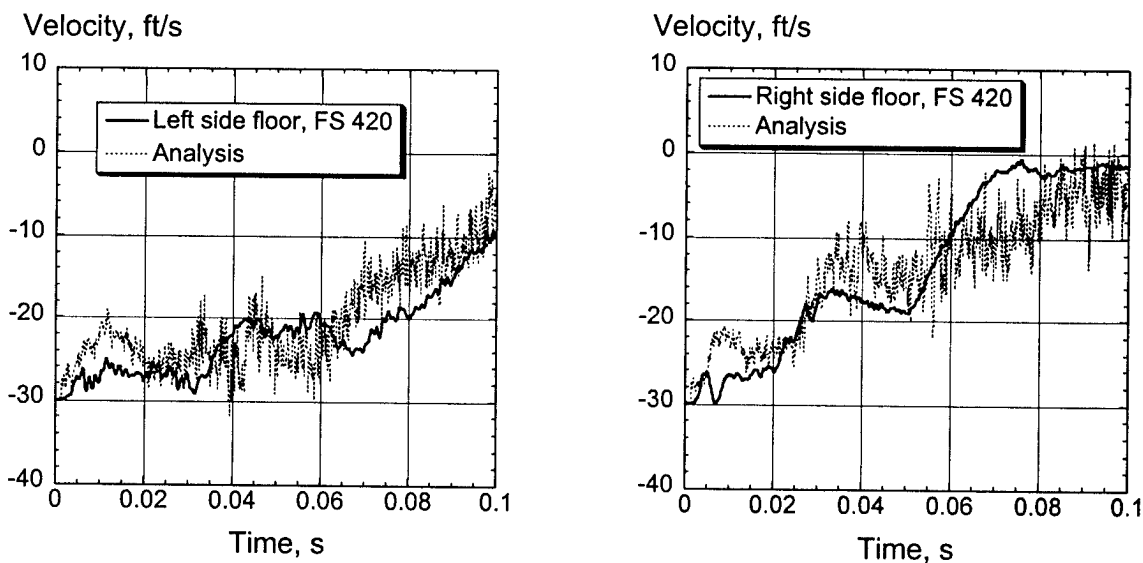


FIGURE 17. LEFT AND RIGHT SIDE MEASURED FLOOR VELOCITY AT FS 420 COMPARED WITH ANALYSIS

The predicted and measured acceleration responses of the left and right sides of the fuselage floor are shown in figure 18. All acceleration data were filtered using a 48-Hz, four-pole Butterworth low-pass digital filter to remove the high frequency ringing from the underlying crash pulse. The filtering was performed forward in time, then backward in time to eliminate the phase shift. The predicted peak acceleration of 33 g's is comparable to the experimental peak value of 36 g's. The predicted right side acceleration response follows the experimental trace

quite well; whereas, the predicted left side acceleration response does not correlate as well due to the complex failure of the frames in that region. The maximum acceleration predicted for the left side floor is 30 g's, which is slightly higher than the measured peak value of 26 g's. Acceleration comparisons for other locations on the floor are shown in figures 19 through 21 for the right rear seat track, the right front seat track, and the left front seat track. In general, the predicted peak values of floor accelerations are typically within 10 to 20 percent of the experimentally measured values; however, some time shift is seen in most of the traces.

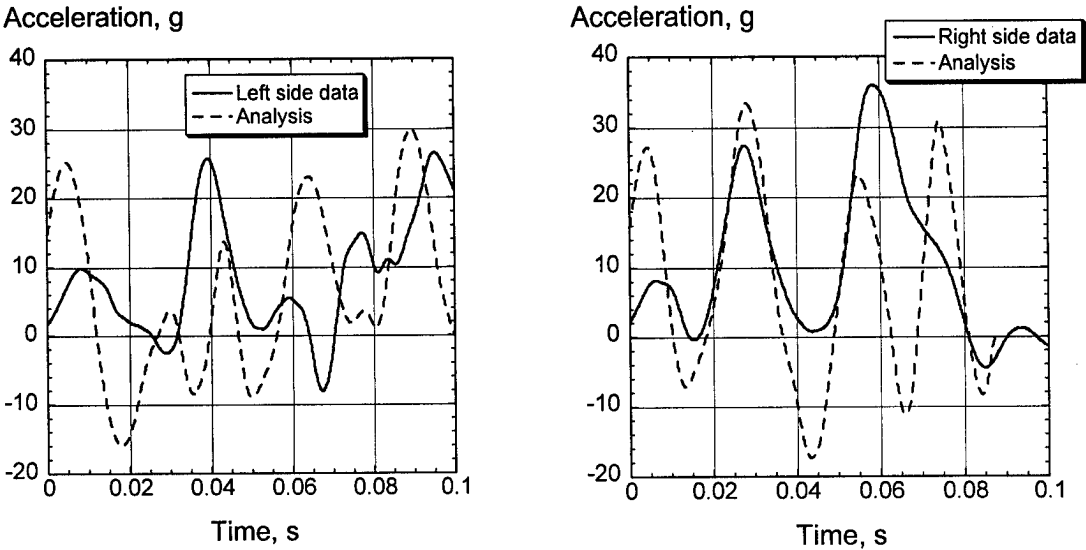


FIGURE 18. LEFT AND RIGHT SIDE MEASURED FLOOR ACCELERATION COMPARED WITH ANALYSIS

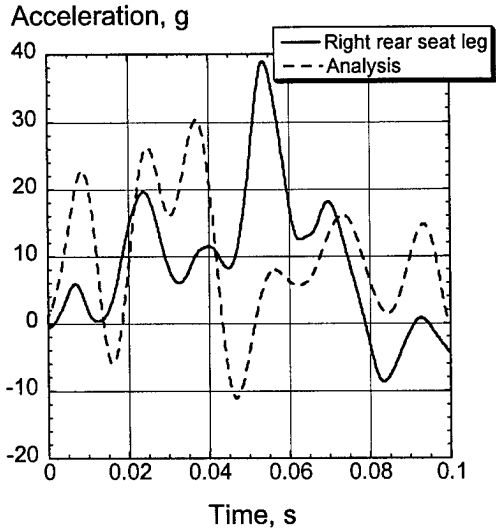


FIGURE 19. COMPARISON OF THE ACCELERATION ON THE FLOOR AT THE RIGHT REAR SEAT (RIGHT REAR LEG) BETWEEN EXPERIMENT AND ANALYSIS

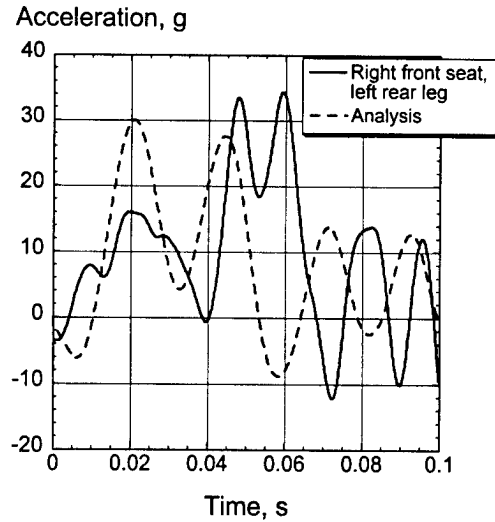


FIGURE 20. COMPARISON OF THE ACCELERATION ON THE FLOOR AT THE RIGHT FRONT SEAT (LEFT REAR LEG) BETWEEN EXPERIMENT AND ANALYSIS

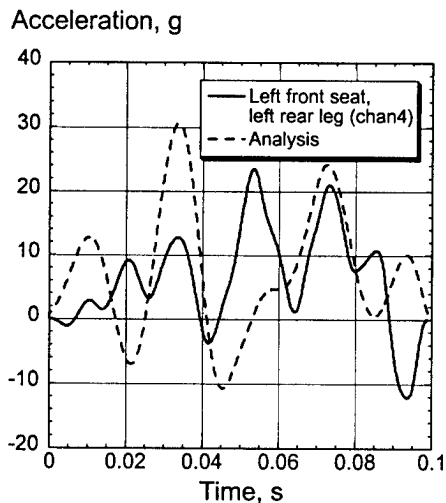


FIGURE 21. COMPARISON OF THE ACCELERATION ON THE FLOOR AT THE LEFT FRONT SEAT (LEFT REAR LEG) BETWEEN EXPERIMENT AND ANALYSIS

ASSESSMENT OF MODEL ACCURACY.

The correlation between the analytical predictions from the MSC.Dytran crash simulation and the experimental results from the vertical drop test of the B737 fuselage section with an auxiliary fuel tank shows that the simulation properly predicted the sequence of events, including the contact times between the fuel tank and the cargo and passenger floors. The predicted velocities for the left and right sides of the floor closely matched the experimental data. The predicted buckling of the left side of the fuselage and the failures of the bulkhead frames in the center and on the right side were nearly identical to the observed deformations and failures. Also, the

predicted peak values of floor accelerations were typically within 10 to 20 percent of the experimentally measured values.

Several factors may have influenced the accuracy of the simulation. As mentioned previously, many approximations were made in defining the geometry of the fuselage section and in estimating the material properties for the fuselage structure and the fuel tank. Because the seats and dummies were represented in the model using concentrated masses applied to nodes on the floor, the failure of the seats on the right-hand side of the fuselage floor could not be simulated. Consequently, the change in floor loading due to the seat failure was not captured in the model. Also, even though MSC.Dytran has the capability to model fluid-structure interaction problems, a simpler approach was taken to represent the water in the fuel tank using concentrated masses. It is likely, however, that the sloshing of the water may have had an effect as well. A more complicated fluid-structure interaction model (coupled Eulerian-Lagrangian approach) would be necessary to accurately predict the failure of the fuel tank. Considering the complexity of this problem due to the presence of the fuel tank and the number of approximations made in the model development, the crash simulation performed well in predicting the outcome of the test.

One purpose of this crash simulation was to validate the structural model of the B737 fuselage section through correlation of the analytical predictions and experimental data obtained during the drop test with the auxiliary fuel tank. Then, the validated fuselage section model was to be used to make pretest predictions of the B737 fuselage section drop test with overhead bins and luggage. This approach was used, however, the presence of the fuel tank in the first drop test dominated the structural response, making validation of the structural model of the fuselage section alone extremely difficult. A better approach would have been to perform a drop test of a similar B737 fuselage section with seats and dummies, but without the auxiliary fuel tank or luggage. Such a test would have permitted fine-tuning of the model to correctly match the observed deformation and structural response. Once validated, the model could then be used to simulate a number of different crash scenarios with good confidence in the simulation accuracy.

#### MODIFICATIONS TO THE B737 MODEL TO REPRESENT THE SECOND DROP TEST CONFIGURATION

Several modifications were made to the MSC.Dytran finite element model of the B737 fuselage section to represent the second test configuration. These changes included removing the fuel tank and adding the two overhead stowage bins. However, the basic structural model, including the outer skin, fuselage frames, stringers, cargo door and its associated stiffened structure, and the floor and floor beams, was nearly identical to the previous model shown in figures 11 and 12. The B737 fuselage section model representing the second test configuration is shown in figure 22. The model contains 9,759 nodes and 13,638 elements, including 9,322 shell and 4,316 beam elements, and 250 concentrated masses. Two new contact surfaces were defined between the fuselage structure and the Heath Tecna and Hitco bins. These contact surfaces were defined to prevent the bins from passing through the fuselage during impact. The contact between the lower half of the fuselage section and the impact surface was unchanged from the previous model. As shown in figure 22, the camera mounts were included in the model and the inertial properties of the cameras were represented using concentrated masses.

As described previously, 3,229 lbs of luggage were placed in the cargo hold beneath the floor of the fuselage section prior to the impact test. The luggage was tightly packed and secured using straps and netting. Several techniques were used to represent the inertial properties of the luggage in the finite element model. The final approach was to use a “percentage area method.” A line was drawn horizontally at the expected height of the luggage, which was approximately 1 ft below the floor. The total area encompassed below the horizontal line and the inner fuselage frames was calculated. Next, lines were drawn vertically from each node in the region to intersect the horizontal line. The percentage area of each “rectangle” formed was determined by dividing the small area in each rectangle by the total area. These ratios were then used to determine the percentage of the 3,229 lbs of luggage to be assigned to the nodes at that location. Using this approach, 60% of the weight of the luggage, or 1,937 lbs, was attached to the nodes forming the cargo floor. The remaining weight of 1,292 lbs was applied in decreasing amounts to the nodes along both sides of the fuselage frames. It was assumed that the fuselage section was loaded uniformly from front to back by the luggage.

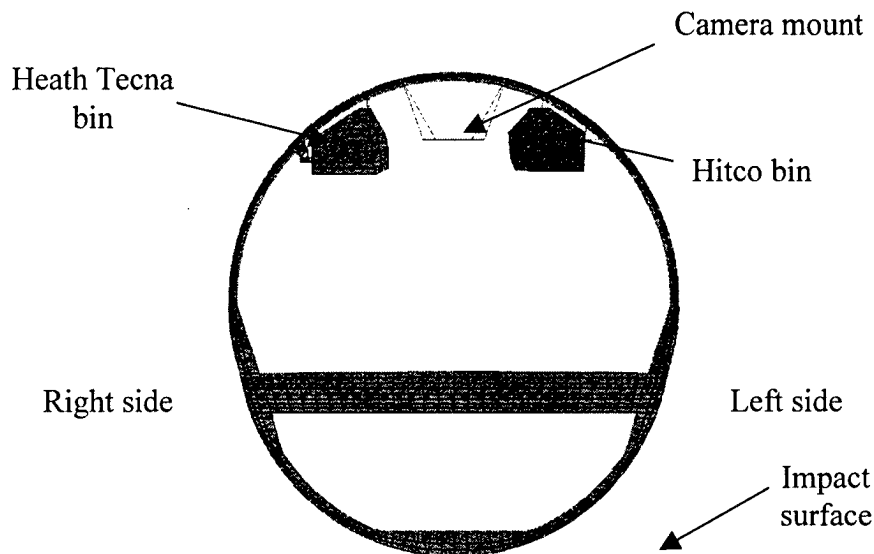


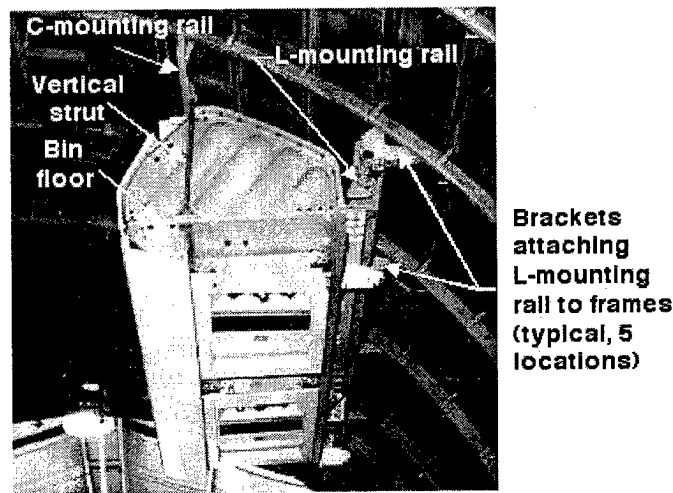
FIGURE 22. FRONT VIEW OF THE MODEL OF THE B737 FUSELAGE SECTION WITH OVERHEAD BINS

This method of modeling the luggage was selected because it is efficient and represents a fairly accurate distribution of the loading provided by the luggage to the fuselage frames at initial impact. However, several important properties of the actual luggage are not modeled using this approach. For example, the inertia of the luggage is approximated and distributed to the nodes on the fuselage frames. During the impact, the weight of the luggage can shift and provide a different loading path to the fuselage structure, which cannot be modeled using the current approach. The frictional contact between the fuselage section and the luggage is not modeled. Since the individual pieces of luggage are not modeled, no material properties are assigned to represent the “compressibility” of the luggage. During the actual impact, the luggage will react the loads applied by the fuselage floor and the lower fuselage frames and skin. However, since the luggage is not physically modeled, there is no mechanism to develop and apply these reactive forces. One obvious way to correct these deficiencies in the model is to represent the luggage

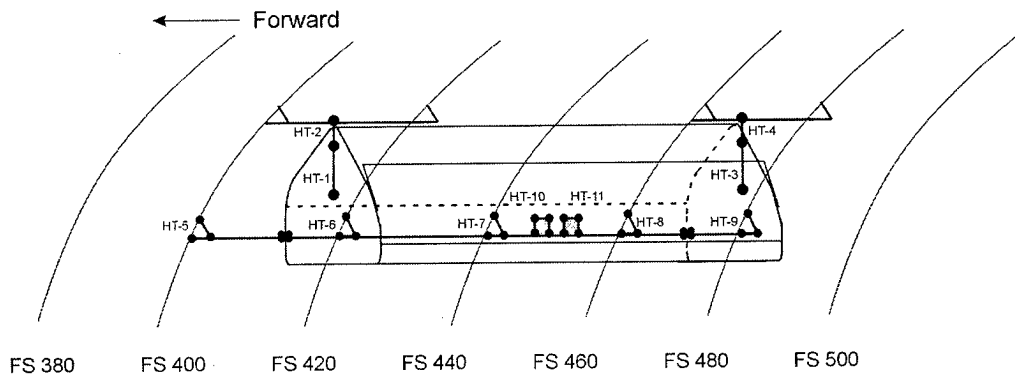
using solid elements and to assign a material property that accurately represents the compressive properties of the luggage. However, this approach was not taken due to the fact that no data on the material properties of luggage were available.

MODEL OF THE HEATH TECNA OVERHEAD BIN.

A photograph of the Heath Tecna bin installed in the fuselage section is shown in figure 23(a). The bin is located on the right, or door side, of the fuselage section. The bin weighs 56 lbs and consists of a fiberglass shell and a composite sandwich floor. The bin is secured to the aircraft by instrumented support brackets and cylindrical struts, including C- and L-cross-section mounting rails attached to the fuselage frames. Two vertically-mounted struts and mating supports, designated HT-1, HT-2, HT-3, and HT-4 in figure 23(b), are used to attach the bin to the ceiling of the test section and to provide support for vertical loading. The vertical struts are 0.5-inch diameter solid cylindrical rods, approximately 14 inches in length. For the drop test, the bin was loaded with 120 lbs of wood.



(a) Photograph of the Heath Tecna bin installed in the B737 fuselage section



(b) Component designations for the Heath Tecna overhead bin

FIGURE 23. HEATH TECNA BIN PHOTOGRAPH AND COMPONENT DESIGNATIONS

The finite element model of the Heath Tecna bin is shown in figure 24. The outer surfaces and floor of the bin are modeled using shell elements. The vertical struts that attach the bin floor to the C-mounting rails are modeled using one-dimensional beam elements. Beam elements can carry axial load, as well as bending, torsional, and shear loads. As shown in figure 23, the struts are inclined at an angle of approximately 5° from true vertical. The elements representing these struts are inclined at the same angle in the model.

The C-mounting rails are modeled using shell elements. In the test article, the C-rails are attached to the fuselage frames using brackets. In the model, the C-rails are attached using beam elements. The bin floor is also secured to the fuselage section through an L-mounting rail that is attached to the fuselage frames at five locations, as shown in figures 23 and 24. The bin is attached to the L-mounting rail at two locations by brackets. In the model, the L-mounting rail and brackets are modeled using shell elements. Individual components of the model of the Heath Tecna bin are shown in figure 25. The wood that was placed in the Heath Tecna bin is modeled as 15 concentrated masses, each weighing 8 lbs. These masses are attached to nodes on the bin floor and are uniformly spaced along the length and width of the platform.

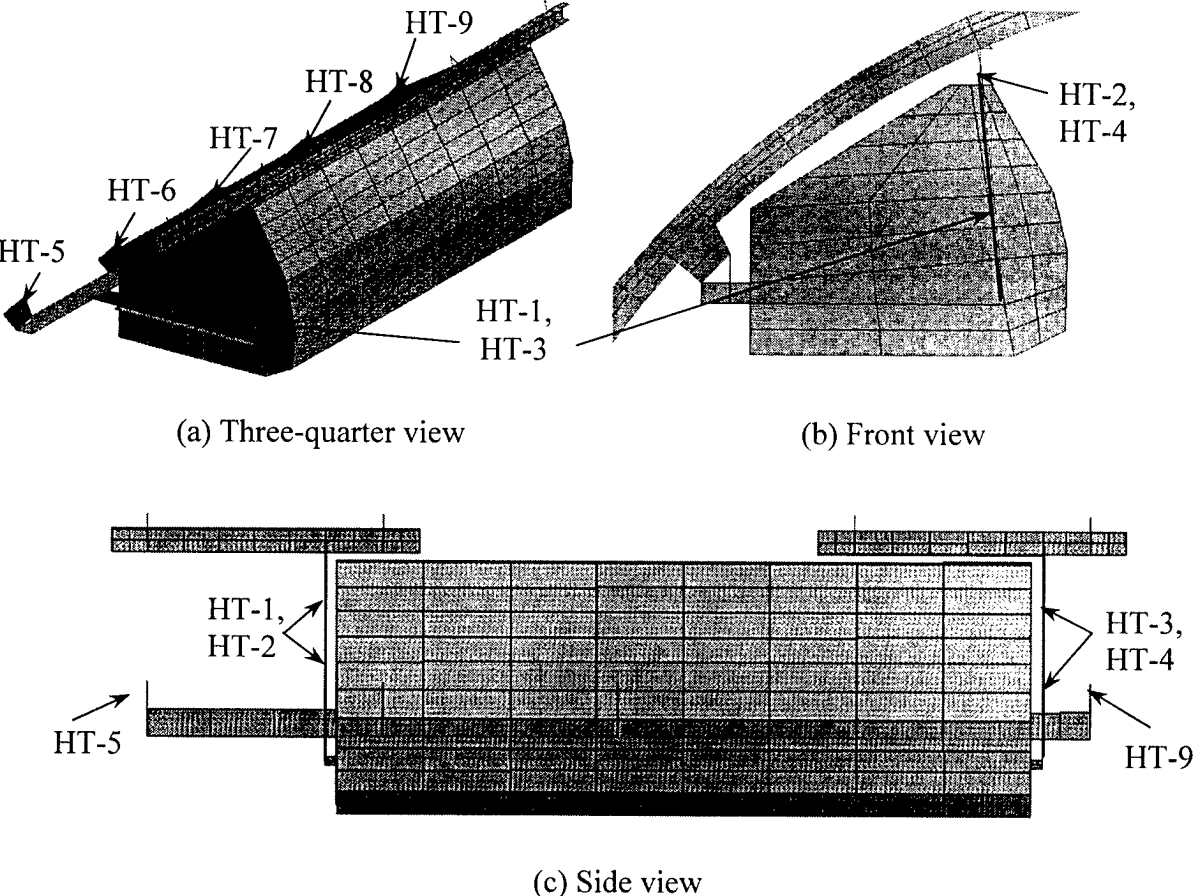


FIGURE 24. FINITE ELEMENT MODEL OF THE HEATH TECNA BIN

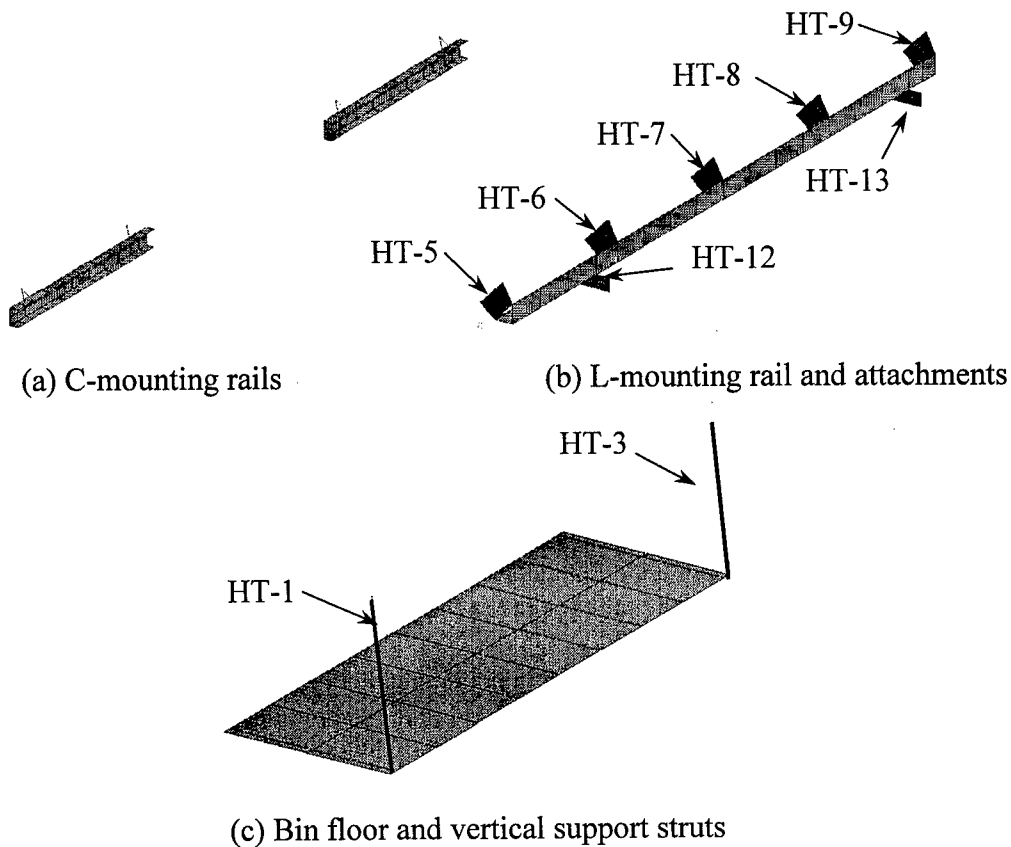


FIGURE 25. COMPONENTS OF THE FINITE ELEMENT MODEL OF THE HEATH TECNA BIN

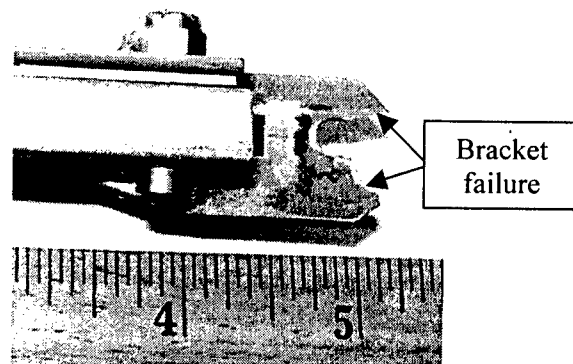
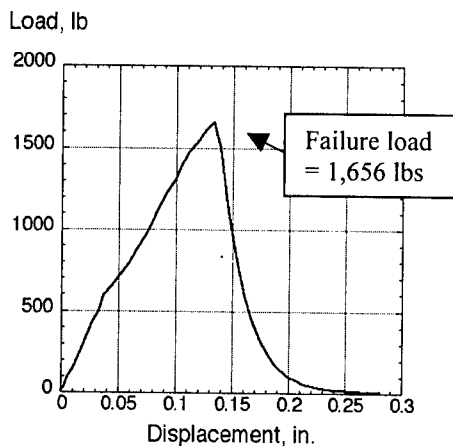
Three unique material properties were assigned to the elements forming the outer surface of the bin, the bin floor, and the vertical struts. The densities of the materials assigned to the outer shell and bin floor were adjusted such that the total empty weight of the Heath Tecna bin was 56 lbs. A third material property was assigned to the elements representing the vertical struts. The specific material properties used in the model are listed in table 2. It should be noted that the material properties of the outer shell and floor of the Heath Tecna bin are unknown and that the values assigned to them are estimates based on engineering judgement. Until these properties are known and input into the model, it is not possible to accurately determine the effective stress or strain in the bin as a function of time. Also, it is important to note that the door latch of the bin is not modeled.

Following inspection of the Heath Tecna bin, it was determined that the components most critical for maintaining structural integrity during impact were the vertical support struts and mating brackets. The FAA supplied one of the 0.5-in.-diameter struts and its mating bracket for testing. The strut is notched on one end and is attached to the bracket by a through bolt, while the other end is threaded. An 0.25-in.-diameter eyebolt is screwed into the strut and is attached to a triangular bracket on the loading platform with a single 0.25-in.-diameter bolt and lock nut.

TABLE 2. MATERIAL PROPERTIES USED IN THE MSC.DYTRAN MODEL OF THE B737 FUSELAGE SECTION WITH OVERHEAD BINS AND LUGGAGE

Material Name	Material Type	Young's Modulus (psi)	Density (lb-s <sup>2</sup> /in <sup>4</sup> )	Poisson's Ratio	Yield Stress (psi)
Aluminum 2024-T3	DMATEP	1.06e07	.0002525	0.33	47,000
Aluminum 7075-T6	DMATEP	1.04e07	.0002525	0.33	60,000
Heath Tecna vertical struts	DMATEP	1.04e07	.0002525	0.33	N/A
Heath Tecna outer shell	DMATEP	2.75e06	.0000638	0.35	N/A
Heath Tecna floor	DMATEP	5.0e06	.0001146	0.35	N/A
Hitco outer shell	DMATEP	2.75e06	.00012	0.33	N/A
Hitco bin floor	DMATEP	2.75e06	.0001137	0.33	N/A
Hitco linkages	DMATEP	1.04e07	.0002525	0.33	N/A
Impact surface	DMATEP	9.0e08	0.00075	0.3	N/A

A tensile test was performed on the Heath Tecna vertical strut and bracket assembly. The notched end of the strut was loaded through the bracket and the threaded end was loaded through the eyebolt. To ensure that only tensile loads were applied, a test fixture was fabricated to align the bracket with the eyebolt. The strut was loaded quasi-statically using a bench-top load test machine. The measured load-deflection curve is shown in figure 26(a). The assembly failed at the hole where the bolt connects the notched end of the strut to the bracket, as shown in figure 26(b). The measured ultimate failure load was 1,656 lbs. This test result provides a single data point that can be used as a guideline for evaluating failure of the strut and mating bracket. However, it must be noted that the actual components may experience a much more complex loading scenario, including shear and bending during the impact test. In the model, the vertical support struts were assigned material properties typical of 7075-T6 aluminum with no yielding or failure. The axial force responses of the beam elements representing the struts were output for correlation with the calibrated load data obtained from the strain gages.



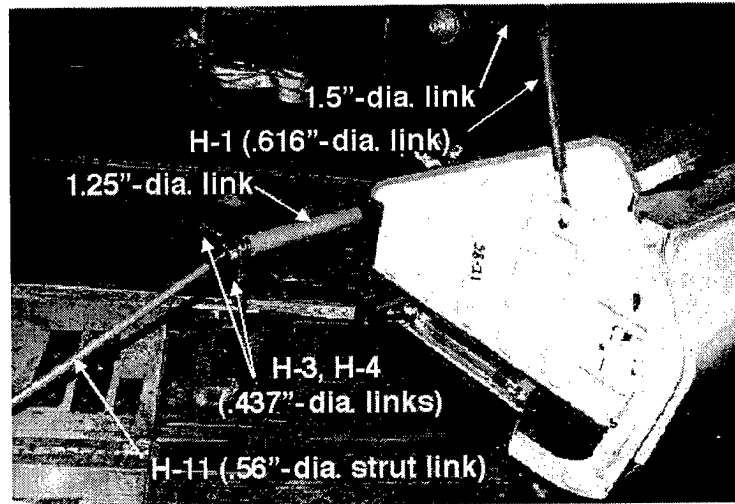
(a) Load versus displacement response

(b) Photograph showing failed bracket

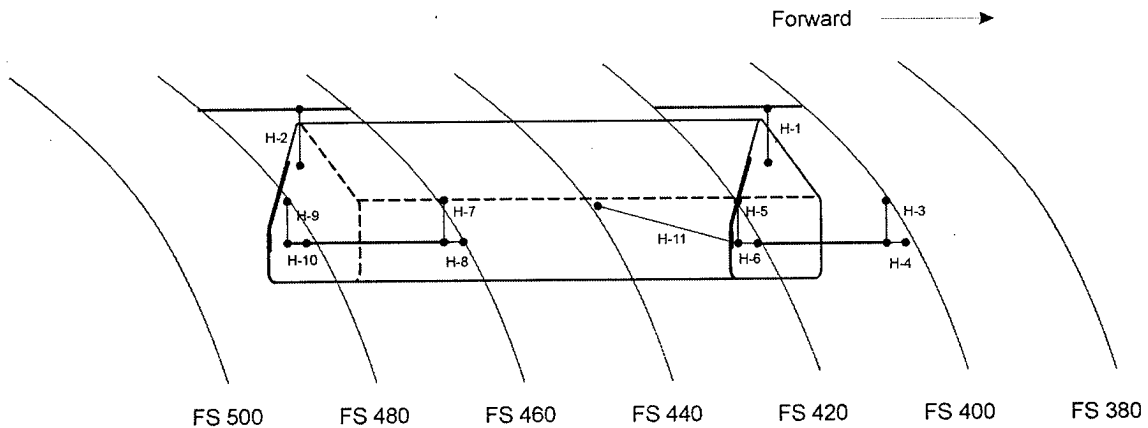
FIGURE 26. LOAD VERSUS DISPLACEMENT RESPONSE OF A HEATH TECNA VERTICAL SUPPORT STRUT ASSEMBLY

MODEL OF THE HITCO OVERHEAD BIN.

A photograph of the Hitco overhead bin is shown in figure 27(a) prior to installation on the fuselage section. This bin is located on the left side of the fuselage section and consists of an outer shell, floor, and several support linkages. The empty bin weighs 57 lbs. For the test, the bin was loaded with 200 lbs of wood and instrumented with five accelerometers. The bin is secured to the airframe by 11 support linkages, as shown in figure 27(b), which were instrumented with strain gages for the test. Vertical support is provided by two 1.5-in.-diameter links that are attached to the fuselage frames at FS 400 and FS 420 and at FS 460 and FS 480. These links are attached to the overhead bin through two 0.616-in.-diameter tie-rod links that are approximately 10 inches in length and are threaded on one end to receive an 0.25-in.-diameter eye-screw. The eye-screws are attached to brackets located on both ends of the bin with a bolt and lock nut. When the bin is mounted to the fuselage section, the 0.616-in.-diameter tie-rod links are oriented vertically.



(a) Photograph of the Hitco overhead stowage bin and support linkages



(b) Component designations for the Hitco bin

FIGURE 27. PHOTOGRAPH AND COMPONENT DESIGNATIONS FOR THE HITCO BIN

In addition, the bin is supported by two 1.25-in.-diameter links that are attached at FS 400 and FS 420 and at FS 460 and FS 480 using two 0.437-in.-diameter support links at each frame. The 1.25-in.-diameter links are attached to the rear of the bin through brackets. Finally, a 0.56-in.-diameter strut link was attached from the end of the 1.25-in.-diameter link to the fuselage frame located at FS 440 to provide longitudinal support for the bin. The FAA performed tensile tests on the 0.437- and 0.616-in.-diameter links in which ultimate failure loads of approximately 4,000 and 5,000 lbs were obtained, respectively. These loads can be used as guidelines for evaluating failure of the linkages.

The finite element model of the Hitco bin is shown in figure 28. The outer surfaces and floor of the bin are modeled using shell elements, and the support linkages are modeled using beam elements. A wall thickness of 0.125 inch was specified for each of the tubular support links. The individual components of the finite element model of the Hitco bin are shown in figure 29.

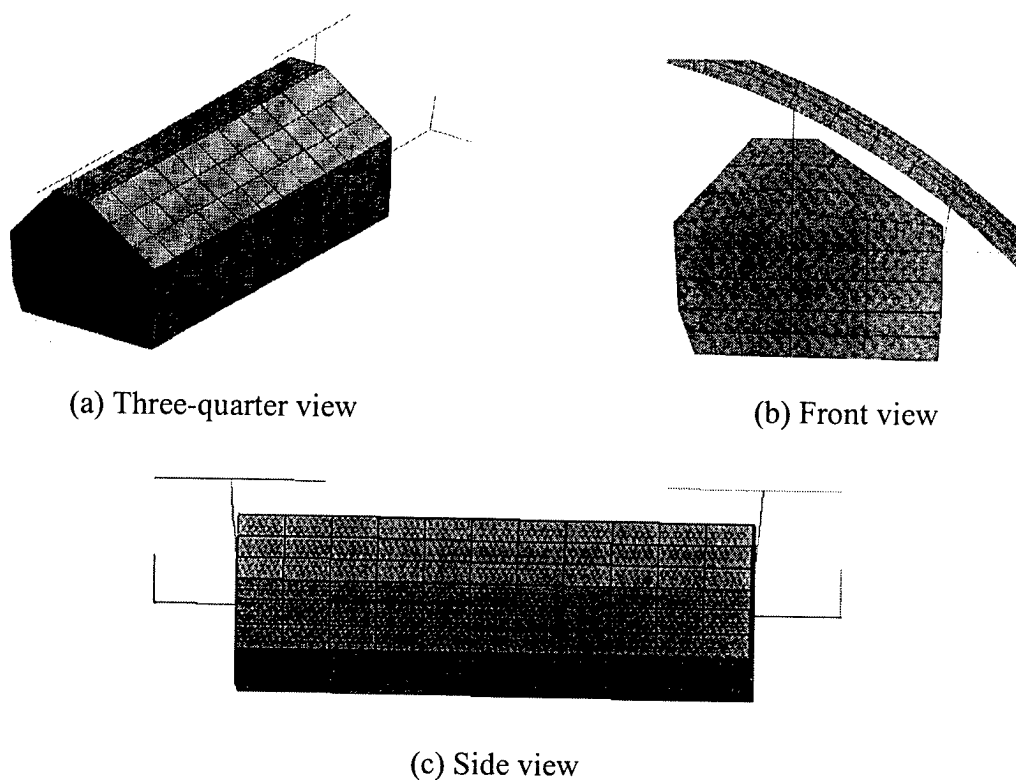
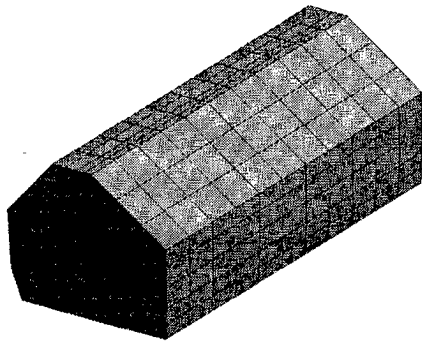


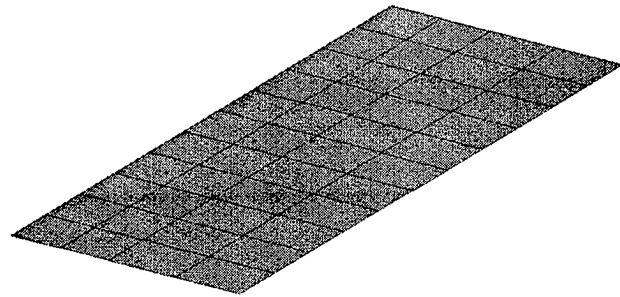
FIGURE 28. FINITE ELEMENT MODEL OF THE HITCO BIN

The mass and inertial properties of the 200 lbs of wood added to the Hitco bin are represented as 24 concentrated masses, each weighing 8.33 lbs. These masses are attached to nodes on the bin floor and are uniformly spaced along the length and width of the platform. Three different material properties were defined for the elements forming the Hitco bin (see figure 29). The densities of the materials assigned to the outer shell and floor were adjusted such that the total weight of the empty bin is 57 lbs. The support linkages were assigned material properties typical of 7075-T6 aluminum with no yielding or failure, and the axial force response was requested as output. The specific material properties are listed in table 2. As with the Heath Tecna bin, the

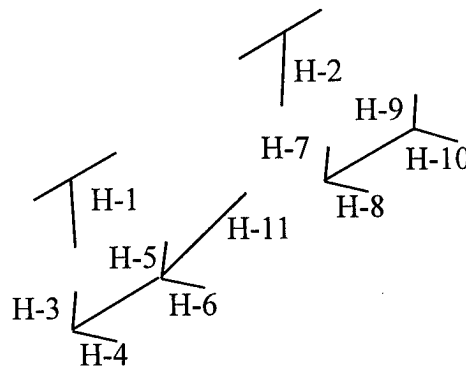
material properties of the outer shell and floor of the Hitco bin are unknown and the values assigned to them are estimates based on engineering judgement. Until these properties are known and input into the model, it is not possible to accurately determine the effective stress or strain in the bin as a function of time. Also, it is important to note that the door latch of the bin is not modeled. It is assumed that the door of the bin cannot open during the impact test.



(a) Shell elements forming the Hitco bin



(b) Hitco bin floor



(c) Model of the Hitco bin support linkages

FIGURE 29. COMPONENTS OF THE FINITE ELEMENT MODEL OF THE HITCO BIN

B737 FUSELAGE SECTION MODEL EXECUTION.

One check of the integrity of the finite element model is to compare the mass of the individual components with the corresponding weights of the test article. A weight comparison of the test article and model is shown in table 3. The total weight of the model is 4.5% heavier than the actual B737 fuselage section. The differences in mass appear in the empty weight of the fuselage section and in the combined seat, occupant, and other weights that are accounted for in the model using concentrated masses. The empty weight of the model is expected to be somewhat heavier than the actual fuselage due to the fact that most of the cutouts were not included. Also, average thicknesses were used in the model, whereas the geometry of the actual fuselage section varied greatly from location to location. The total weight of all concentrated masses is somewhat higher than the experimental value due to the fact that many small masses

(2-3 lbs each) were assigned to nodes where output was requested as a means of lowering the high-frequency response.

Another check of the model is to compare the locations of the center of gravity for the test article and the model. The center of gravity of the finite element model is located at  $x = 60.88$ ,  $y = -4.2083$ , and  $z = 62.426$  inches, where  $x$  is the longitudinal direction,  $y$  is the lateral direction, and  $z$  is the vertical direction. This location is slightly forward of the mid-plane, slightly left of the centerline, and approximately 1 inch above the floor. Thus, the center of gravity location of the model reflects the asymmetry caused by the door. The center of gravity location of the test article was not determined experimentally.

TABLE 3. WEIGHT COMPARISON OF THE MODEL AND TEST ARTICLE

Component	Test Weight (lbs)	Model Weight (lbs)
Fuselage section, empty	1,360	1,526
Combined seats, occupants, and misc.	3,620	3,845
Hitco bin and wood mass	257	257
Heath Tecna bin and mass	176	176
Cameras and mount	228	240
Luggage	3,229	3,230
Total	8,870	9,274

Prior to discussion of the correlation between the pretest predictions and the experimental data, it is important to fully understand the assumptions and approximations made in developing and executing the model. For example, since engineering drawings were not available, the gross geometry of the section was determined through measurements made by hand using tape measures and digital calipers. The level of accuracy of the analytical and experimental correlation will determine, in some respects, whether the approximations used were valid. The assumptions and approximations made in development of the model are listed as follows:

- It is assumed that the impact occurs with no roll, pitch, or yaw.
- The impact condition is assumed to be 30-ft/s vertical velocity, with no lateral, longitudinal, or rotational velocity components.
- The wooden impact platform at the Dynamic Drop Test Facility at the FAA is assumed to behave as a rigid surface.
- The geometry of the outer fuselage skin, frames, stringers, floor, and other features is approximated as uniform along the length of the fuselage section. Inconsistencies in the geometry were averaged. For example, a large variation in the skin thickness was measured around the circumference of the fuselage. Instead of incorporating these variations in the model, an average value was determined and used.

- The material properties assigned to the elements representing the fuselage section are estimated. Based on corrosion, stress concentrations, fatigue damage, and a multitude of other factors, the numbers used for Young's modulus, yield stress, and ultimate failure strain may be reduced by an order of magnitude from the original material properties, or values obtained in engineering handbooks. No tests were performed on components from the fuselage to determine the actual material properties. Thus, the values used in the model are based on engineering judgement, past experience, and material handbook data.
- Many of the cutouts, fittings, attachments, doublers, and joints are not included in the model. For example, none of the rivets were included. The cutouts were accounted for by decreasing the average thickness of the specific component. Some large cutouts, e.g., the windows, were included in the model.
- The seats, occupants, and other weights on the floor are assumed to behave as concentrated masses attached to nodes at their approximate location in the model. The inertial properties of the components are approximated.
- Where possible, the components of the fuselage section are modeled using shell elements since these elements are extremely efficient in MSC.Dytran. However, beam elements were used to represent the stringers, door and window frames, and other reinforcing structure.
- The luggage is modeled using concentrated masses located on nodes forming the lower fuselage frames. This approximation of the luggage was made for efficiency of the simulation and because material property data for luggage were not available. However, as discussed previously, this nongeometric, nonphysical representation cannot accurately simulate the behavior of the luggage during the test.
- The Heath Tecna and Hitco support linkages are modeled using one-dimensional beam elements, instead of rod elements. Beam elements can support axial, bending, and shear loads, whereas rod elements can only react axial loads. The decision to use beam versus rod elements was made to reflect the fact that the support linkages are constrained such that they are primarily loaded in the axial direction. However, it is possible that the support links may experience a more complex loading scenario.
- It is assumed that the door latches on the Heath Tecna and Hitco bins cannot be opened. Consequently, they were not included in the models of the bins.

The model was executed in MSC.Dytran, Version 2000, for 0.2 second of simulation time on a Sun Ultra Enterprise 450 workstation computer. The simulation required 36 hours of CPU with a final time step of 2.67 microseconds. Requested output included the deformed geometry and acceleration, velocity, and displacement time histories for several nodes whose positions correspond to the locations of selected transducers. Postprocessing of the model was performed using MSC.Patran [11].

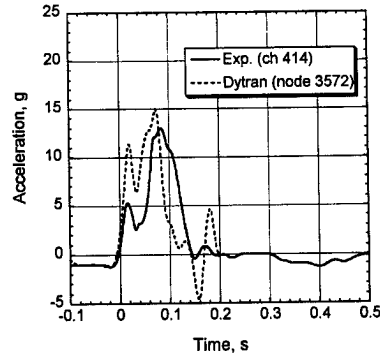
## ANALYTICAL CORRELATION WITH EXPERIMENTAL DATA FROM THE B737 VERTICAL DROP TEST WITH OVERHEAD BINS AND LUGGAGE

### COMPARISON OF PRETEST PREDICTIONS AND EXPERIMENTAL DATA.

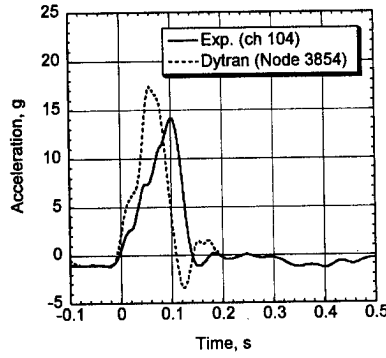
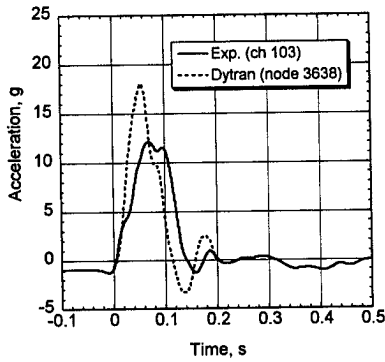
In this section, the pretest predictions are correlated with data from the November 2000 vertical drop test of the B737 fuselage section with overhead bins and luggage. The correlation results are presented in several categories including (1) seat track acceleration and velocity time histories, (2) fuselage upper and lower sidewall acceleration time histories, (3) Heath Tecna bin acceleration and load time histories, and (4) Hitco bin acceleration and load time histories. In addition, the report includes the predicted displacement time histories of the four corners of the floor. Maximum deflections of the four corners of the floor were determined by the FAA, using motion analysis of the high-speed films, and these values are provided for correlation with the predicted displacement responses. Finally, an assessment of model accuracy is provided with suggestions for improvements to achieve better agreement.

For the acceleration time histories, both the analytical and experimental data are filtered using a 16-Hz, four-pole Butterworth low-pass digital filter to remove the high-frequency ringing from the underlying crash pulse. The filtering was performed forward in time, then backward in time to eliminate any phase shift. A lower cutoff frequency was used for this test to more adequately capture the underlying crash pulse. For the force time histories, the analytical predictions contained high-frequency oscillations. As a result, a smoothed curve fit of the analytical data is plotted versus the raw experimental data. A discussion of the importance of the choice of filter frequency, as well as other important aspects of filtering, are provided in appendix A.

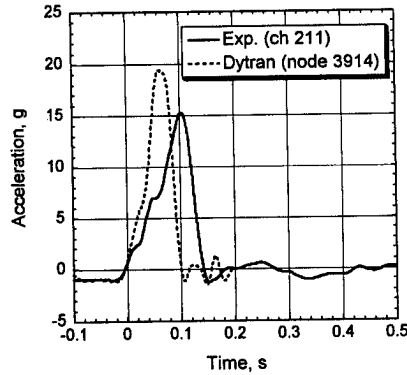
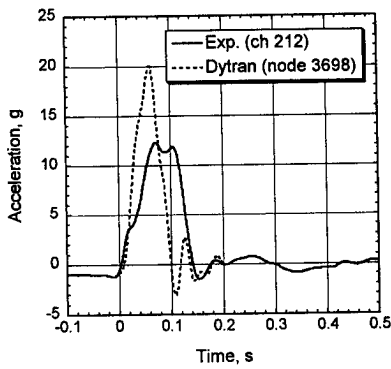
SEAT TRACK LOCATIONS. The predicted acceleration time histories are correlated with the experimental data obtained from accelerometers located on the left and right seat tracks at FS 380, 418, 452, and 484 are shown in figures 30 and 31, respectively.



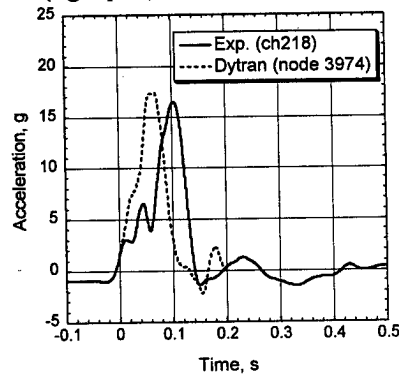
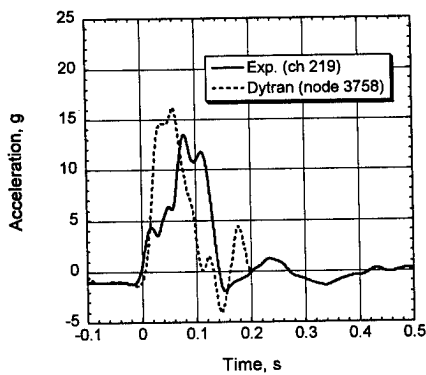
(a) Left side inner seat track at FS 380



(b) Left side inner (left plot) and outer (right plot) at FS 418

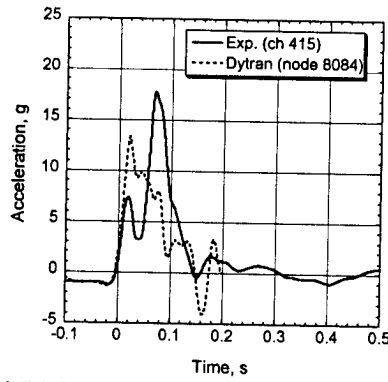


(c) Left side inner (left plot) and outer (right plot) at FS 452

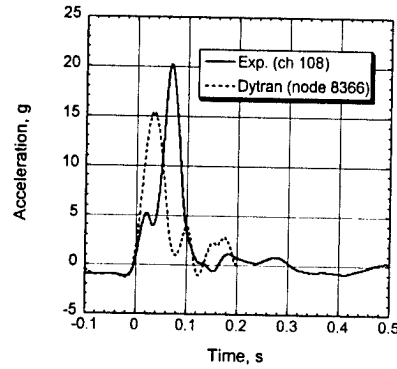
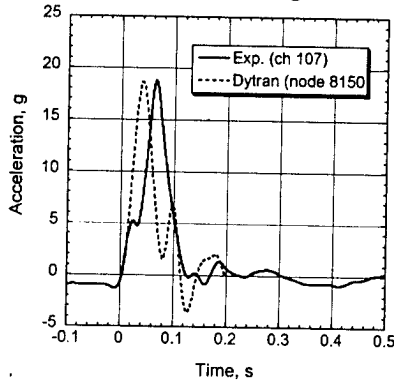


(d) Left side inner (left plot) and outer (right plot) at FS 484

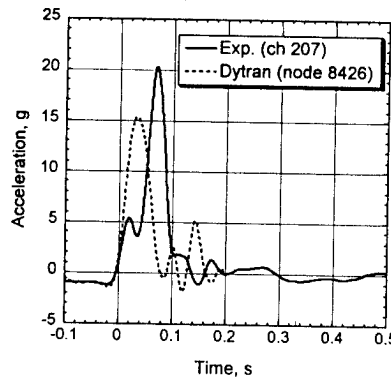
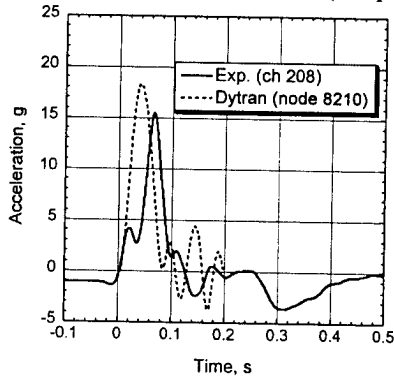
FIGURE 30. PREDICTED AND EXPERIMENTAL LEFT SEAT TRACK ACCELERATION RESPONSES



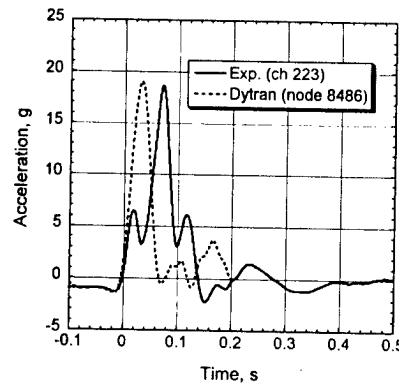
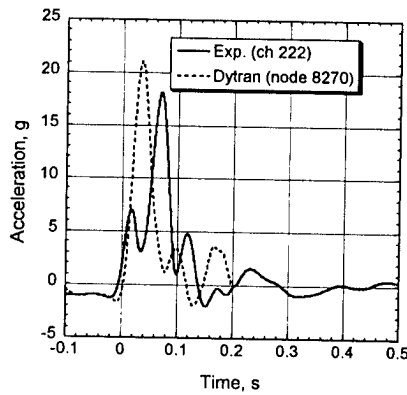
(a) Right side inner seat track at FS 380



(b) Right side inner (left plot) and outer (right plot) at FS 418



(c) Right side inner (left plot) and outer (right plot) at FS 452



(d) Right side inner (left plot) and outer (right plot) at FS 484

FIGURE 31. PREDICTED AND EXPERIMENTAL RIGHT SEAT TRACK ACCELERATION RESPONSES

Comparisons of the predicted and experimental velocity responses of the left and right outer seat track locations at FS 418 are plotted in figure 32. The experimental velocity responses were obtained by integrating the corresponding acceleration traces. The analytical velocity responses were obtained directly from output of the simulation, i.e., they were not obtained by integration of the analytical acceleration traces. It should be noted that the accelerometer located on the right outer seat track at FS 418 is directly above the rear edge of the door. These plots indicate that the model is removing velocity more quickly than the test article. For the left outer seat track, the predicted response has reached zero velocity at 0.085 second, while the experimental response reaches zero velocity at 0.115 second. For the right outer seat track, the experimental velocity response reaches zero velocity at 0.11 seconds with no rebound velocity shown. However, the predicted response levels at a velocity of -5 ft/s at 0.11 second never crosses zero velocity. One explanation for this behavior is that, in the model, the floor is rotating, as well translating. The left-to-right, or clockwise, rotational velocity subtracts from the translational velocity on the left side causing it to be removed more quickly, and adds to the velocity on the right side keeping it from crossing zero velocity.

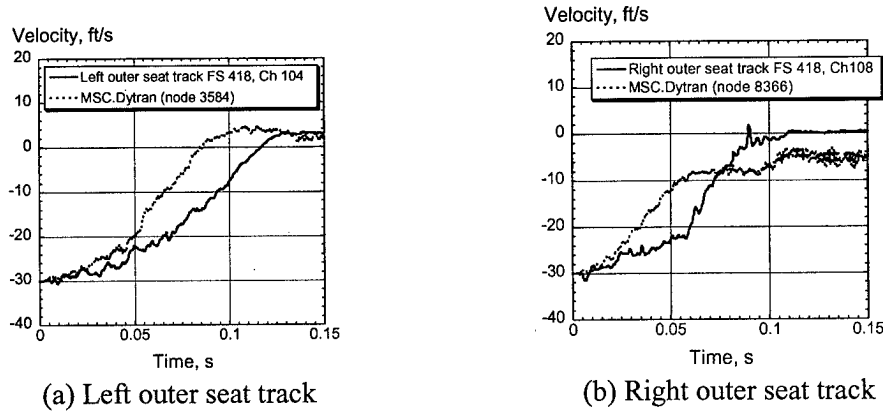


FIGURE 32. PREDICTED AND EXPERIMENTAL VELOCITY TIME HISTORIES OF THE OUTER SEAT TRACKS AT FS 418

FUSELAGE SIDEWALL LOCATIONS. The predicted and experimental acceleration responses for locations on the upper and lower fuselage sidewalls at FS 400, 440, 480, and 500 are presented. The location of the nodes used for correlation with the lower sidewall accelerometers is shown in figure 33. Left and right sidewall acceleration time histories are shown in figures 34 and 35, respectively. Note that plots for some locations are missing due to anomalies in the test data.

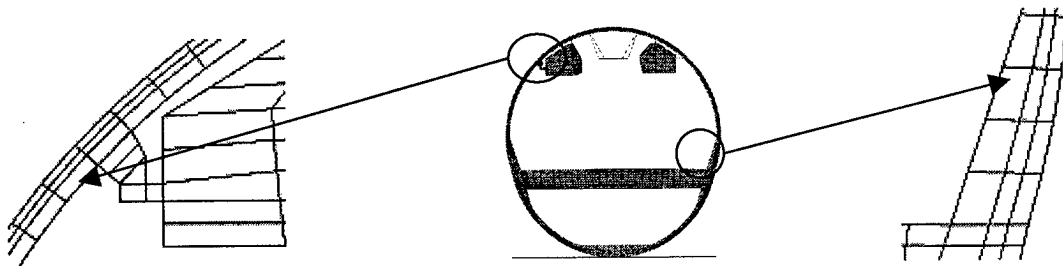
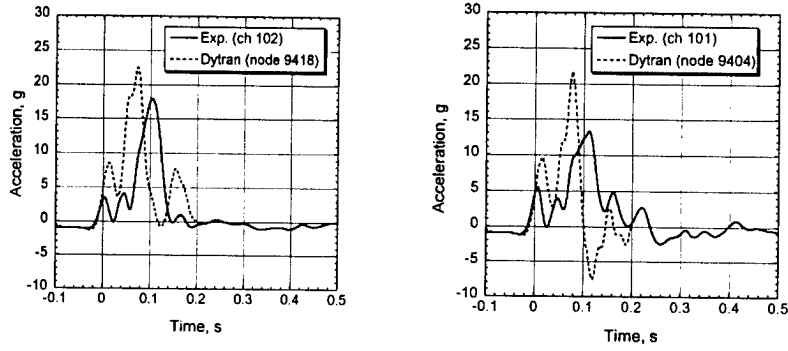
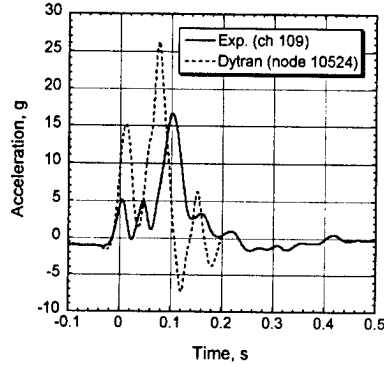


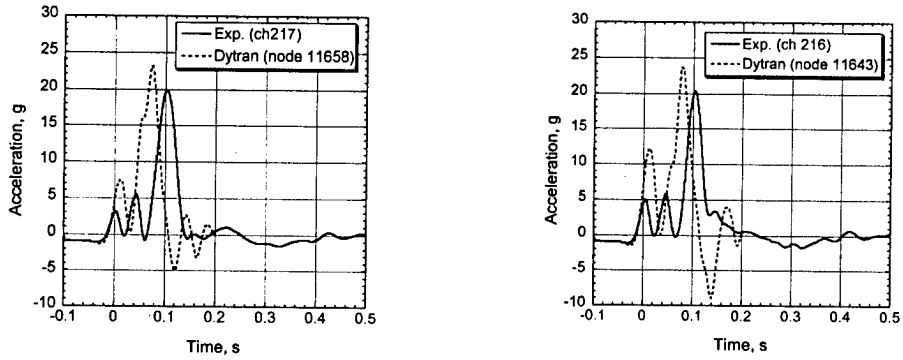
FIGURE 33. TYPICAL LOCATIONS OF THE NODES USED TO PREDICT THE UPPER AND LOWER SIDEWALL RESPONSES



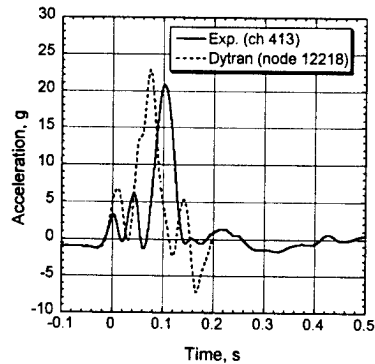
(a) Left side lower (left plot) and upper (right plot) sidewall at FS 400



(b) Left side upper sidewall at FS440

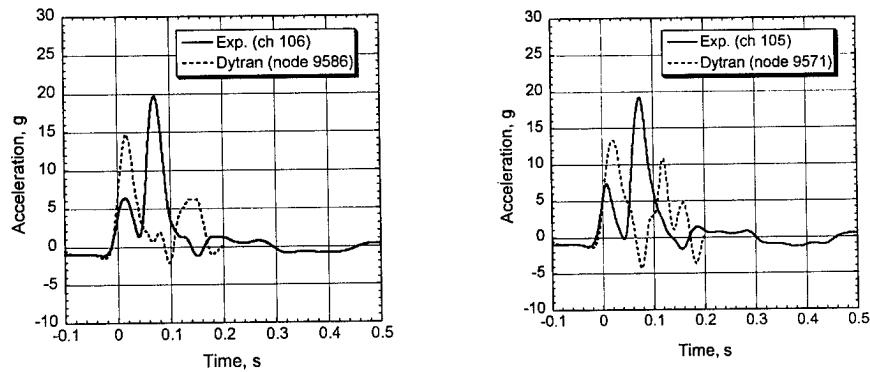


(c) Left side lower (left plot) and upper (right plot) sidewall at FS 480

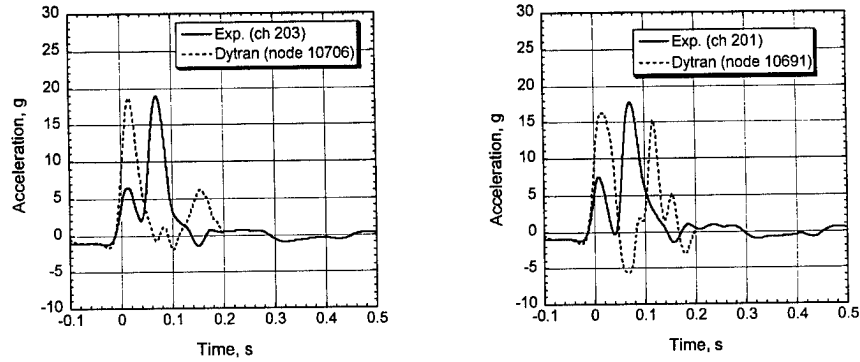


(d) Left side lower sidewall at FS 500

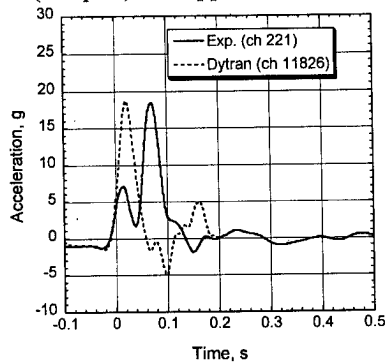
FIGURE 34. PREDICTED AND EXPERIMENTAL LEFT SIDEWALL ACCELERATION RESPONSES



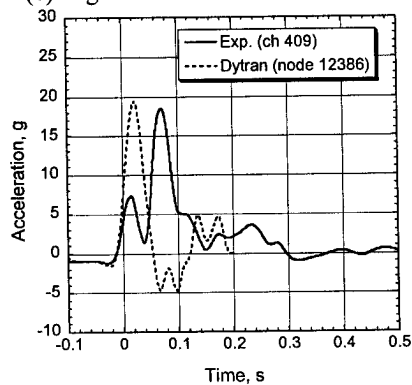
(a) Right side lower (left plot) and upper (right plot) sidewall at FS 400



(b) Right side lower (left plot) and upper (right plot) sidewall at FS 440



(c) Right lower sidewall at FS 480



(d) Right lower sidewall at FS 500

FIGURE 35. PREDICTED AND EXPERIMENTAL RIGHT SIDEWALL ACCELERATION RESPONSES

HEATH TECNA BIN. The predicted and experimental vertical acceleration responses for locations on the center of the front and rear ends of the Heath Tecna bin and at the bottom center of the bin are shown in figure 36. The predicted and experimental axial force time histories of the vertical support struts HT-1 and HT-3 are shown in figure 37. Since the pulse durations of the experimental force time histories of the bin linkages were generally found to be between 0.2 and 0.3 second, the simulation was rerun to provide analytical data for up to 0.3 second.

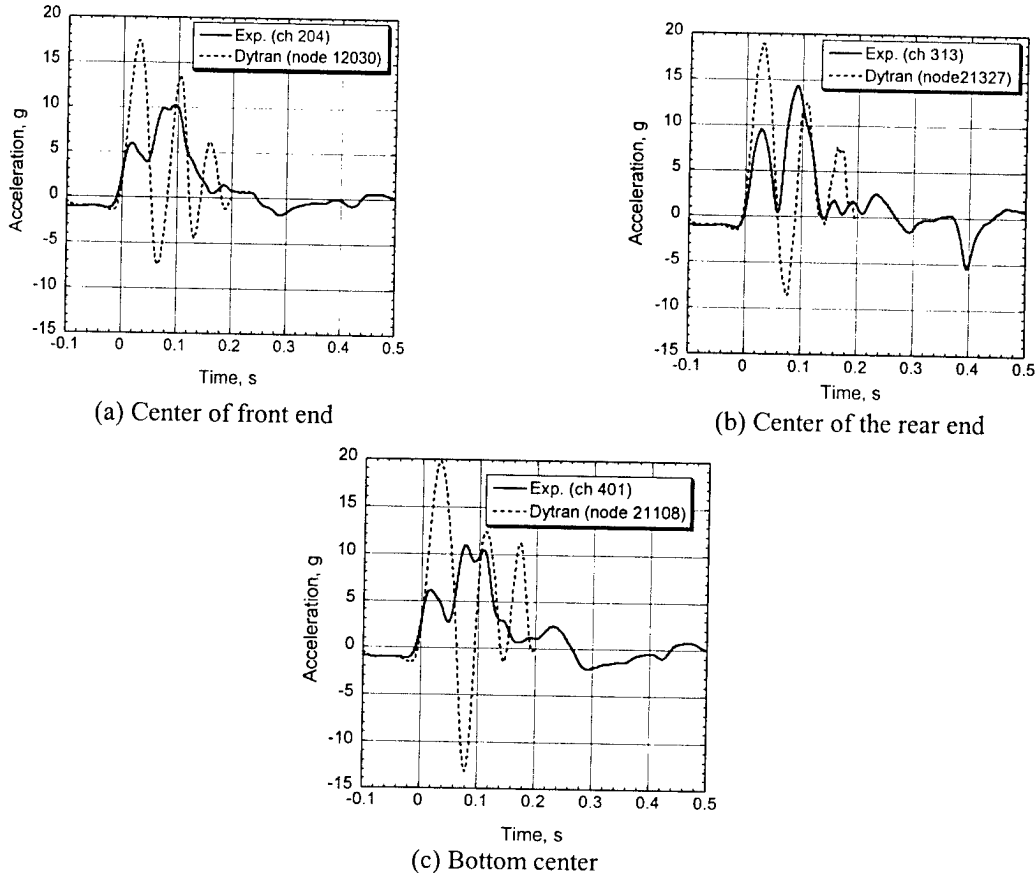


FIGURE 36. PREDICTED AND EXPERIMENTAL VERTICAL ACCELERATION RESPONSES OF THE HEATH TECNA BIN

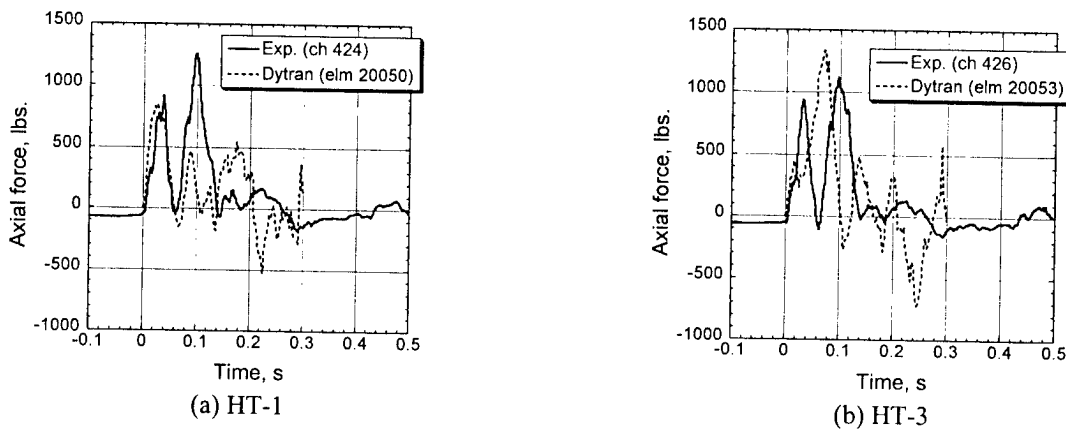
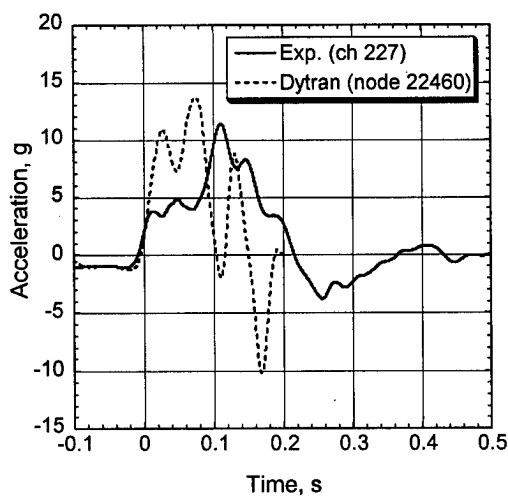
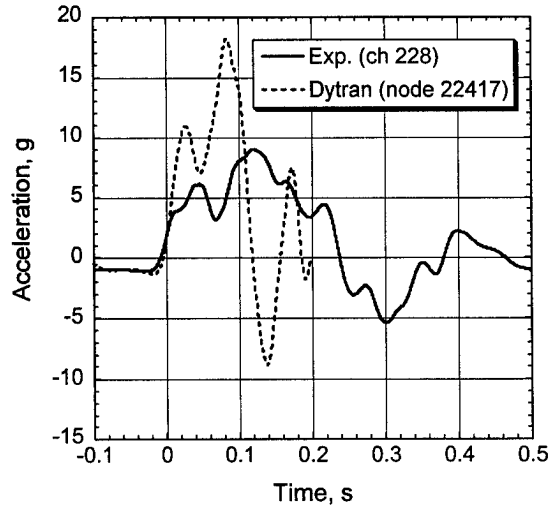


FIGURE 37. PREDICTED AND EXPERIMENTAL AXIAL FORCE RESPONSES OF THE VERTICAL SUPPORT STRUTS HT-1 AND HT-3 OF THE HEATH TECNA BIN

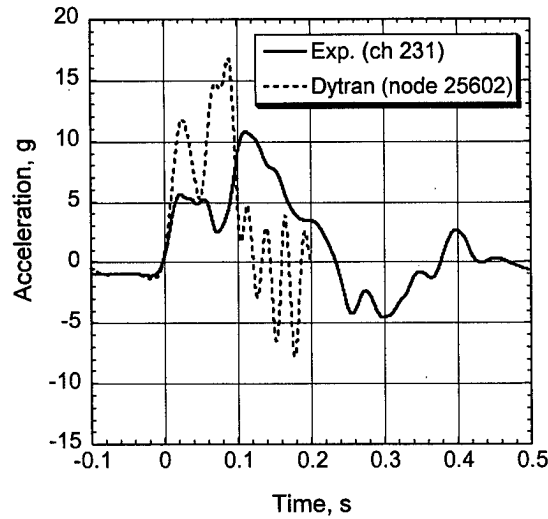
HITCO BIN. The predicted and experimental vertical acceleration responses for the center of the front and rear ends of the Hitco bin and at the bottom center of the bin are shown in figure 38. The predicted and experimental axial force time histories of the Hitco bin support linkages H-1 through H-11 are shown in figures 39 through 49.



(a) Center of the front end



(b) Center of the rear end



(c) Center of the bottom of the bin

FIGURE 38. PREDICTED AND EXPERIMENTAL VERTICAL ACCELERATION RESPONSES OF THE HITCO BIN

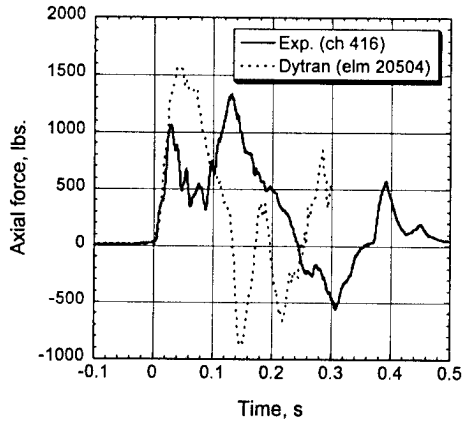


FIGURE 39. PREDICTED AND EXPERIMENTAL AXIAL FORCE TIME HISTORIES OF HITCO BIN LINK H-1

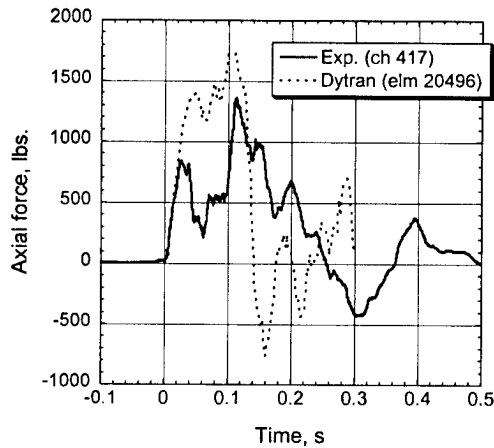


FIGURE 40. PREDICTED AND EXPERIMENTAL AXIAL FORCE TIME HISTORIES OF HITCO BIN LINK H-2

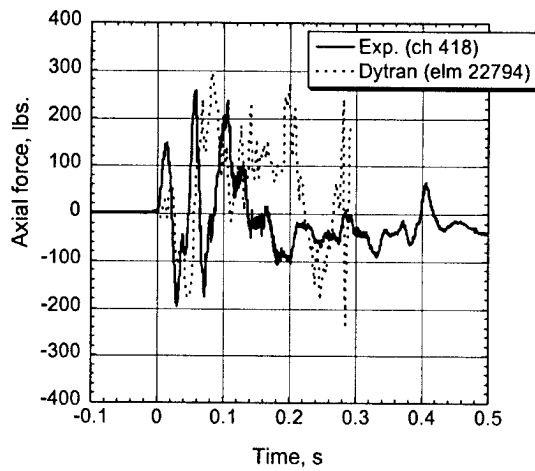


FIGURE 41. PREDICTED AND EXPERIMENTAL AXIAL FORCE TIME HISTORIES OF HITCO BIN LINK H-3

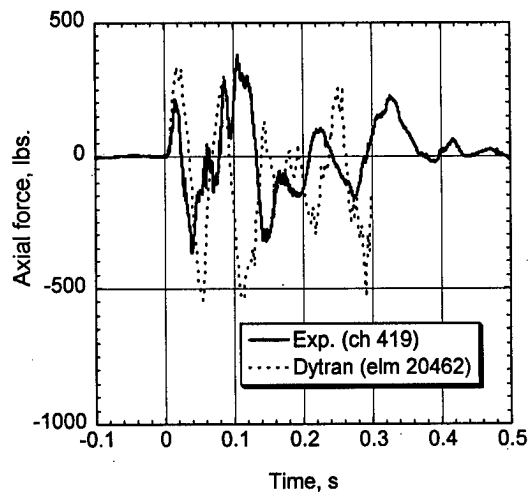


FIGURE 42. PREDICTED AND EXPERIMENTAL AXIAL FORCE TIME HISTORIES OF HITCO BIN LINK H-4

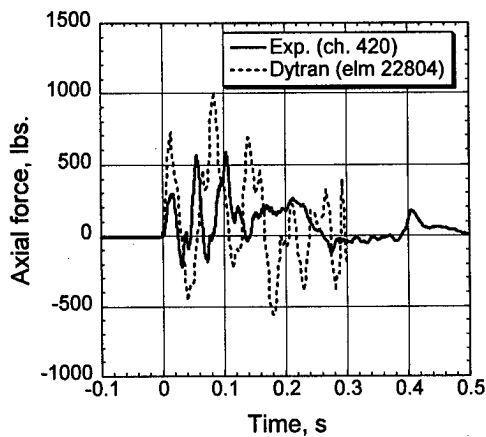


FIGURE 43. PREDICTED AND EXPERIMENTAL AXIAL FORCE TIME HISTORIES OF HITCO BIN LINK H-5

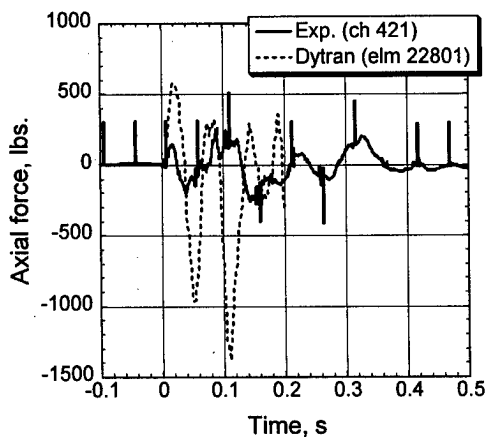


FIGURE 44. PREDICTED AND EXPERIMENTAL AXIAL FORCE TIME HISTORIES OF HITCO BIN LINK H-6

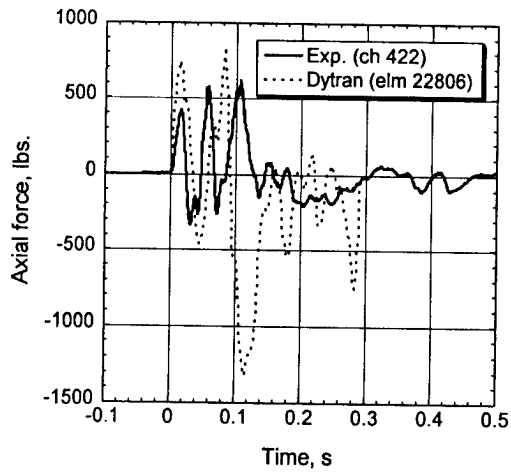


FIGURE 45. PREDICTED AND EXPERIMENTAL AXIAL FORCE TIME HISTORIES OF HITCO BIN LINK H-7

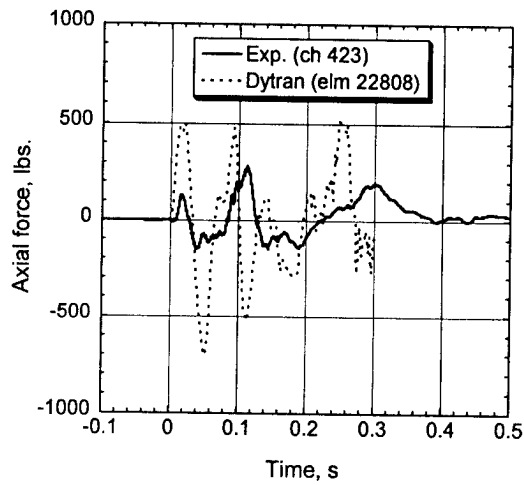


FIGURE 46. PREDICTED AND EXPERIMENTAL AXIAL FORCE TIME HISTORIES OF HITCO BIN LINK H-8

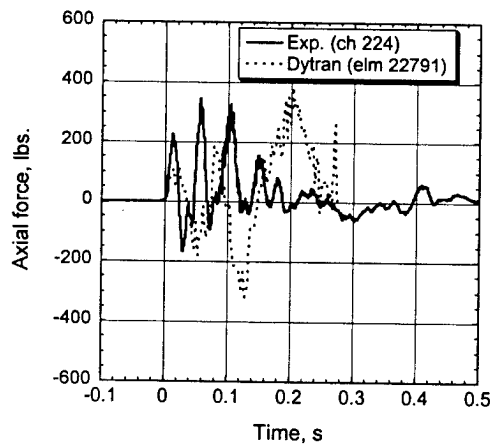


FIGURE 47. PREDICTED AND EXPERIMENTAL AXIAL FORCE TIME HISTORIES OF HITCO BIN LINK H-9

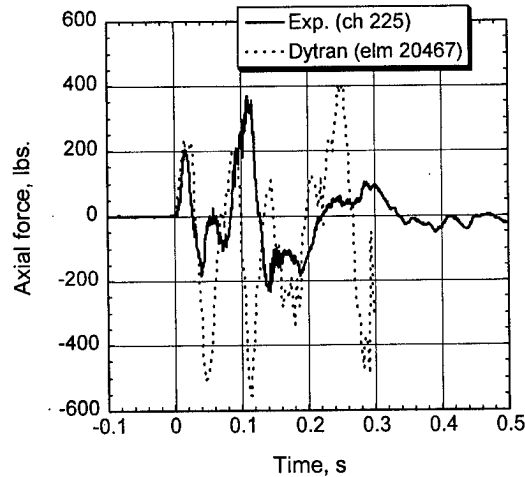


FIGURE 48. PREDICTED AND EXPERIMENTAL AXIAL FORCE TIME HISTORIES OF HITCO BIN LINK H-10

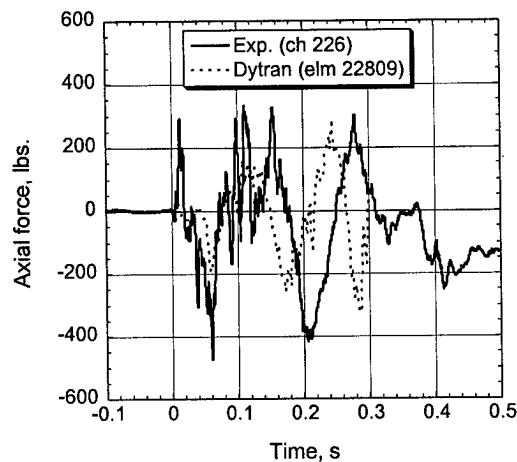
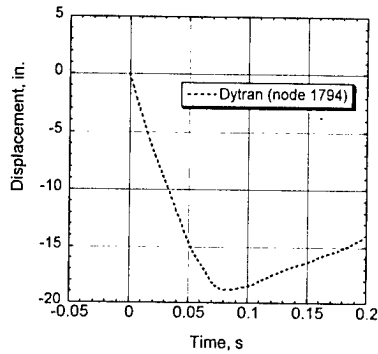
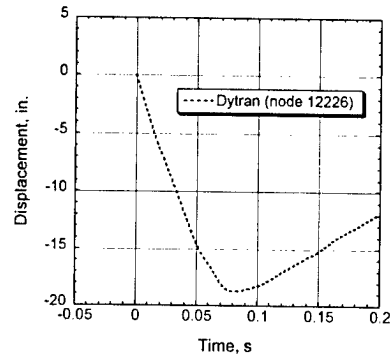


FIGURE 49. PREDICTED AND EXPERIMENTAL AXIAL FORCE TIME HISTORIES OF HITCO BIN LINK H-11

FLOOR CORNERS. The predicted vertical displacement time histories of the corners of the fuselage floor are shown in figures 50 and 51 for the left and right sides of the fuselage, respectively. These responses were output directly from the MSC.Dytran simulation and were not obtained by double integration of the acceleration time histories. Maximum dynamic deflection values of the four corners of the floor were determined from detailed analyses of the high-speed film and video of the test. These values are shown in parentheses in the caption of each plot in figures 50 and 51.

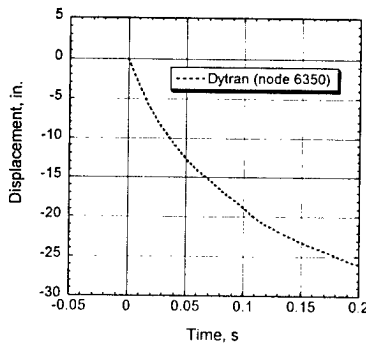


(a) Left front corner (28 in. maximum)

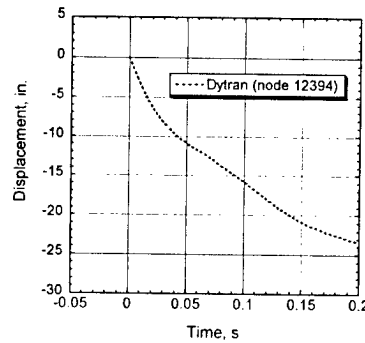


(b) Left rear corner (30 in. maximum)

FIGURE 50. PREDICTED VERTICAL DISPLACEMENT RESPONSES OF THE LEFT FRONT AND REAR CORNERS OF THE FLOOR



(a) Right front corner (21 in. maximum)



(b) Right rear corner (24 in. maximum)

FIGURE 51. PREDICTED VERTICAL DISPLACEMENT RESPONSES OF THE RIGHT FRONT AND REAR CORNERS OF THE FLOOR

### ASSESSMENT OF MODEL ACCURACY.

Based on the test and analysis correlation presented in the previous section of this report, several general statements can be made regarding model accuracy. The predicted seat rail acceleration responses, shown in figure 30 and 31, matched the overall shape and duration of the experimental acceleration pulses fairly well. Also, the peak acceleration values were well predicted, i.e., within 25%, except for the left inner seat rail at FS 418. However, a phase shift in the time of occurrence of the peak acceleration was typically seen. In general, the degree of correlation was surprising given the large number of approximations used in the model development. One suggestion that would result in a more accurate representation of the test article is to model the luggage using solid elements. These elements would be assigned material properties typical of the compressive response of luggage.

Another issue that might affect the floor-level acceleration response is the fact that all of the triple-occupant aircraft seats located on the right side of the fuselage failed during the test, as shown in figure 52. This factor is important since a large portion of the occupant weight is transmitted to the fuselage structure through the seats. In the model, the weight and inertial

properties of the seats and occupants are represented using concentrated masses attached to nodes on the floor. The use of concentrated masses is a good approach as long as the load transfer path remains constant. In this case, the load transfer path was altered by the failure of the seats. For a more accurate simulation, the seats and dummies would have to be added to the model. However, this approach is not feasible at this time. A possible alternative would be to incorporate the seats into the fuselage model, and then represent the mass and inertial properties of the dummies by attaching concentrated masses to the seat nodes.

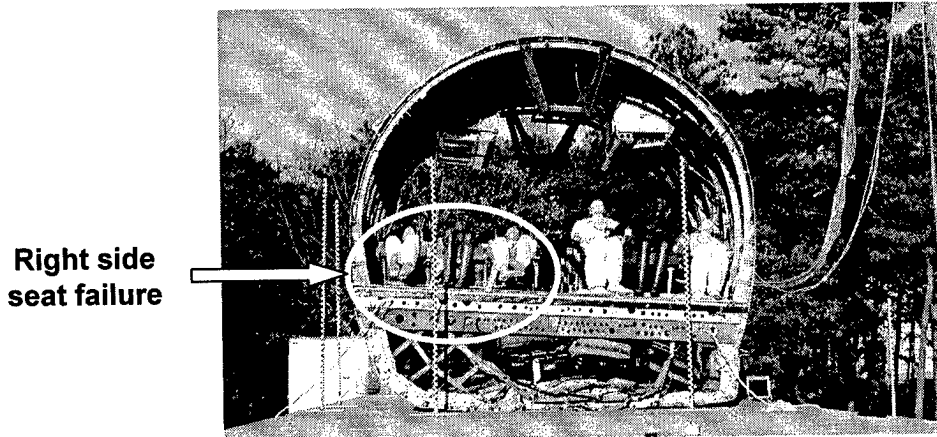


FIGURE 52. POSTTEST PHOTOGRAPH OF THE B737 FUSELAGE SECTION WITH OVERHEAD BINS

For the fuselage sidewall locations, the correlation with test data varied according to position. For the accelerometers located on the left side of the fuselage, the simulation predicted the overall shape, duration, and peak g's of the acceleration pulses quite well, as shown in figure 34. However, the correlation for channels located on the right side of the fuselage section was not as good. The experimental acceleration responses on the right side of the fuselage section, shown in figure 35, typically exhibit a 2-peak pulse with a 7-g peak occurring first and a 17- to 20-g peak occurring next. In general, the predicted acceleration responses exhibited the opposite shape, a large initial peak with a smaller second peak. It is anticipated that the addition of a physical model of the luggage and a more accurate model of the cargo door and its associated stiffened structure will help to eliminate this problem. In addition, it is possible that the seat failures on the right side of the fuselage floor influenced the fuselage sidewall acceleration responses, as well.

The predicted axial force responses of the Heath Tecna vertical support struts, shown in figure 37, compare favorably with the experimental data. These linkages were represented using beam elements, and the axial force was correlated with the calibrated load response measured during the test. It is useful to note that the predicted and experimental axial force responses of both struts did not exceed the 1,656-lb failure load determined previously from the tensile test. The predicted axial force responses of the Hitco bin support linkages correlated fairly well with the measured force responses (see figures 39 through 49). As with the Heath Tecna bin, it is useful to note that the predicted and experimental axial force responses for the 0.437-in.-diameter links (H-3 through H-10), shown in figures 41 through 48, did not exceed their ultimate failure load of 4,000 lbs. Likewise, the predicted and experimental axial force responses for the 0.616-in.-

diameter links (H-1 and H-2), shown in figures 39 and 40, did not exceed their ultimate failure load of 5,000 lbs. Neither the Heath Tecna struts nor the Hitco bin linkages failed during the test.

The predicted force responses are given in the local coordinate system in which the x axis is defined as the axial direction of the individual beam element. The beam elements shared common nodes with the bin on one end and the fuselage frame on the other end. This modeling approach did not allow the beam elements to rotate in response to bending loads. Another suggested improvement would be to add rotational springs to represent the various joints or connections between the individual linkages and between the linkages and the bin and fuselage structure, as shown in figure 53. One difficulty in implementing this approach will be determining the appropriate stiffness to input for the joints.

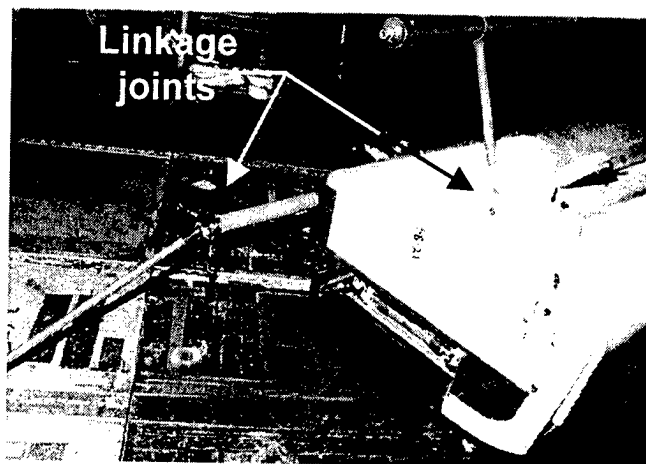


FIGURE 53. PHOTOGRAPH SHOWING THE VARIOUS LINKAGES AND CONNECTIONS OF THE HITCO BIN

The predicted displacement time history responses of the four corners of the fuselage floor are shown in figures 50 and 51. The results show that the displacement responses of the front and rear locations on each side of the fuselage floor exhibit the same overall shape and magnitude. However, there is a large difference between the left and right side responses. The front and rear displacement responses on the left side exhibit a maximum displacement of approximately 19 inches at 0.08 second. Following the maximum value, the displacement decreases monotonically with time. However, the front and rear displacement responses on the right side do not exhibit a maximum value and continue to increase with time, reaching 23 to 25 inches at 0.2 second. The displacement time histories shown in figures 50 and 51 suggest counter-intuitive results. For example, it would be expected that the displacement on the right side of the fuselage section would be less than that of the left side due to the presence of the door and its associated stiffened structure, located on the right side of the cargo hold. Actually, up to about 0.08 second, this behavior is found. For example, at 0.05 second, the displacement of the right side of the floor is 13 inches, while the displacement of the left side of the floor is 15 inches. However, this trend reverses after approximately 0.10 second. The explanation for these results can be found by examining the structural deformation patterns of the model and the film-capture photographs from the test shown in figure 54.

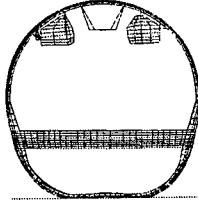
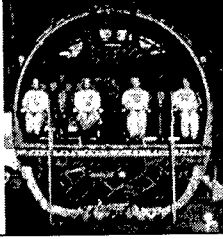
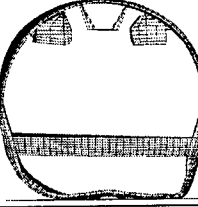
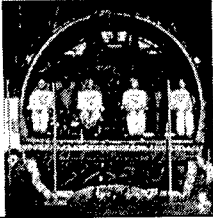
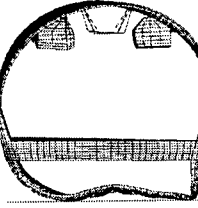
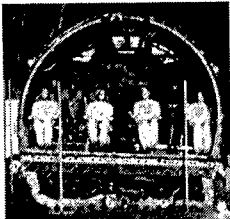
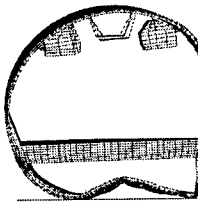
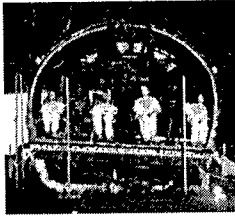
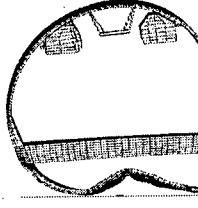

Pretest Model	Experiment
 <p data-bbox="509 474 672 499">t = 0.03 second</p>	 <p data-bbox="922 474 1084 499">t = 0.03 second</p>
 <p data-bbox="509 737 672 762">t = 0.06 second</p>	 <p data-bbox="922 737 1084 762">t = 0.06 second</p>
 <p data-bbox="509 991 672 1016">t = 0.09 second</p>	 <p data-bbox="922 991 1084 1016">t = 0.09 second</p>
 <p data-bbox="509 1262 672 1287">t = 0.12 second</p>	 <p data-bbox="922 1262 1084 1287">t = 0.12 second</p>
 <p data-bbox="509 1524 672 1549">t = 0.15 second</p>	 <p data-bbox="922 1524 1084 1549">t = 0.15 second</p>

FIGURE 54. FRONT VIEWS OF THE DEFORMED MODEL AND FILM-CAPTURE PHOTOGRAPHS

The model deformation closely matches the experiment up to 0.09 second. However, by 0.12 second, the model shows excessive deformation of the lower fuselage structure. The large plastic hinge formed at the bottom of the fuselage has significantly invaded the space that is occupied by the luggage in the test. Also, a pronounced second hinge forms on the lower left side of the fuselage. As time progresses, the fuselage section begins to rotate in a clockwise

direction, left to right. Note that by 0.15 second the lower left side of the fuselage has lost contact with the impact surface. Obviously, after about 0.1 second, the model deformation does not match the experiment. It is suggested that the excessive deformation of the lower fuselage frames and skin that occurs after 0.1 second can be corrected by representing the luggage physically using solid elements in the model. It is expected that once the luggage is modeled properly, it will limit the amount of deformation seen in the lower fuselage structure. It is also possible that the material properties assigned to the elements forming the lower fuselage structure are not correct. Since no materials testing was performed, the properties used were estimated based on engineering judgement. Consequently, variations in Young's modulus, yield stress, strain-hardening modulus, and ultimate failure strain should be investigated as well.

It is also important to note that by 0.06 second, a second damage site on the lower right side of the fuselage section has developed. This secondary damage site is not predicted by the model. Instead, the cargo door area on the lower right side of the fuselage model remains intact with no sign of buckling or failure. These results indicate that the model of the cargo door does not have sufficient fidelity to capture the observed failure. A suggested model improvement is to re-examine the cargo door model and to make adjustments as necessary to obtain a better representation of the actual structure.

## EVALUATION OF POSTTEST MODEL IMPROVEMENTS

Several of the modifications discussed in the previous section have been implemented and the effects of the changes on model accuracy have been evaluated. These modifications can be categorized into three groups: (1) changes in the contact definition between the lower fuselage structure and the wooden platform, (2) changes in model features including material and inertial properties, and (3) changes in the model to achieve a more accurate physical representation of the problem. The contact modifications include adjustments in the contact force penalty factor (FACT) and the addition of friction. The changes in model features include a 25 percent reduction in yield stress for the 2024-T3 and 7075-T6 aluminum and a correction in the inertial properties of the model. Finally, the modifications to gain a better physical representation of the impact problem involve development of a more accurate representation of the lower cargo door and surrounding structure and the addition of a physical model of the luggage, as well as the development of a platform model.

It is important to note that each of the modifications to the model have been performed independently of one another, thus, allowing an understanding of the influence of the change on the results. For each modification, the same initial model was used which was the one used to generate the pretest predictions, as described in the previous section of the paper. In most cases, comparisons are made between the test data, the pretest model, and the modified posttest model as a means of evaluating the improvement in model accuracy.

### CONTACT SURFACE MODIFICATIONS.

ADJUSTMENTS TO THE CONTACT FORCE PENALTY FACTOR. The FACT is used in the contact definition to adjust the stiffness of the contact. For example, once the code has detected that a slave node has passed through a master surface, it applies a restoring force to move the node to the original side of the surface. The magnitude of the force can be adjusted using FACT.

In MSC.Dytran, the default value of FACT is 0.1. To increase or decrease the stiffness of the contact force, FACT can be set greater or less than 0.1. The default value of FACT is generally acceptable for most simulations.

The default value of FACT was used in the pretest simulation. To determine if changes in the value of FACT affect the accuracy of the analytical predictions for this problem, the simulation was executed with a FACT of 0.01, which is an order of magnitude decrease in the default value. The posttest simulation results are plotted with the experimental data and the pretest predictions in figures 55 and 56 for the left and right seat tracks at FS 452, respectively. The comparisons shown in figures 55 and 56 indicate that only minor changes in the predicted acceleration responses were obtained due to the order of magnitude decrease in FACT.

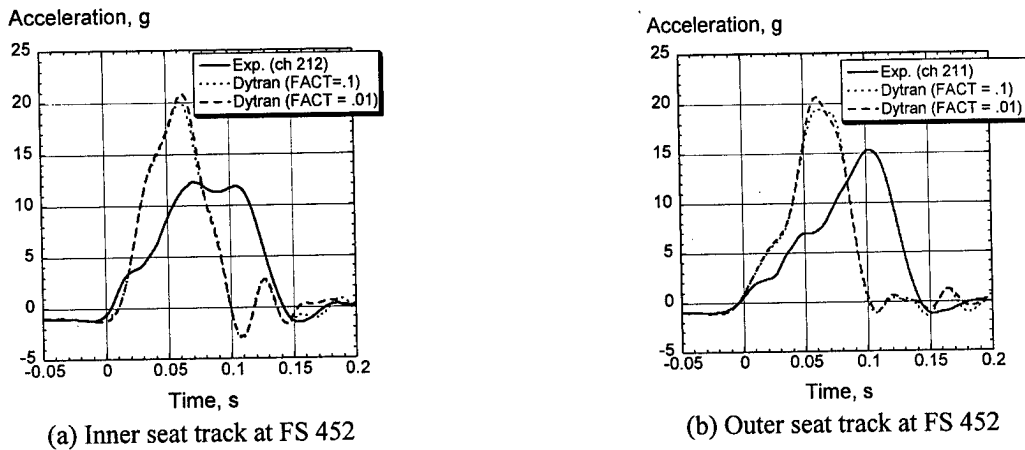


FIGURE 55. EFFECT OF CONTACT FORCE PENALTY FACTOR (FACT) ON LEFT SEAT TRACK ACCELERATION RESPONSES

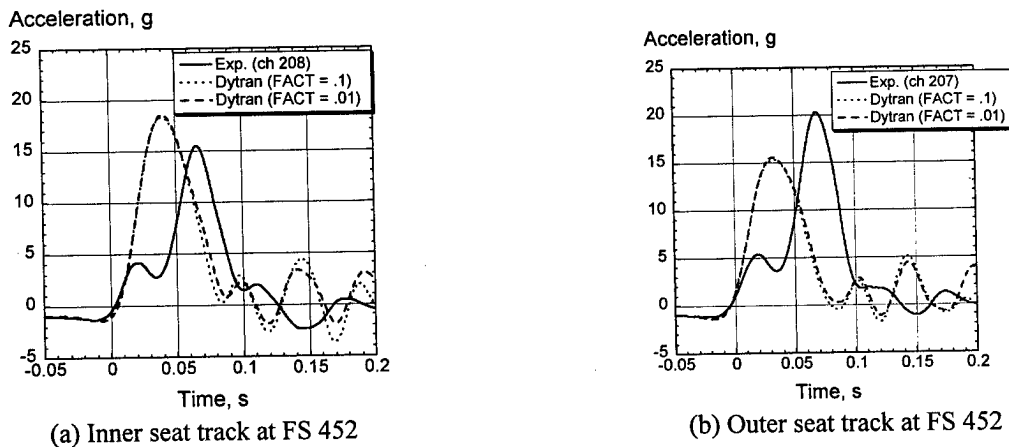


FIGURE 56. EFFECT OF CONTACT FORCE PENALTY FACTOR (FACT) ON RIGHT SEAT TRACK ACCELERATION RESPONSES

FRICITIONAL CONTACT. The pretest simulation was performed assuming frictionless contact. This assumption is appropriate for a vertical impact onto a flat surface, even though some sliding contact of the fuselage against the wooden platform probably occurs during crushing and

deformation of the lower structure. To better account for friction, the contact definition was modified to add both static and dynamic coefficients of friction. Since no direct experimental measurements of these coefficients were possible, the coefficients of friction were estimated based on engineering handbook values to be 0.54 for the static coefficient and 0.32 for the dynamic coefficient. The results of this modification are shown in figures 57 and 58 in which the left and right seat track acceleration responses at FS 452 are plotted, respectively, with the pretest simulation predictions (no friction) and the posttest predictions with friction. The results indicate that the addition of friction had minimal effect on the floor-level acceleration responses on the left side of the fuselage. For the right side, the peak acceleration responses increased by 10% and 15% over the pretest predictions for the inner and outer seat tracks, respectively. For the right inner seat track at FS 452, this increase caused the correlation with test data to be worse, whereas the correlation for the right outer seat track improved.

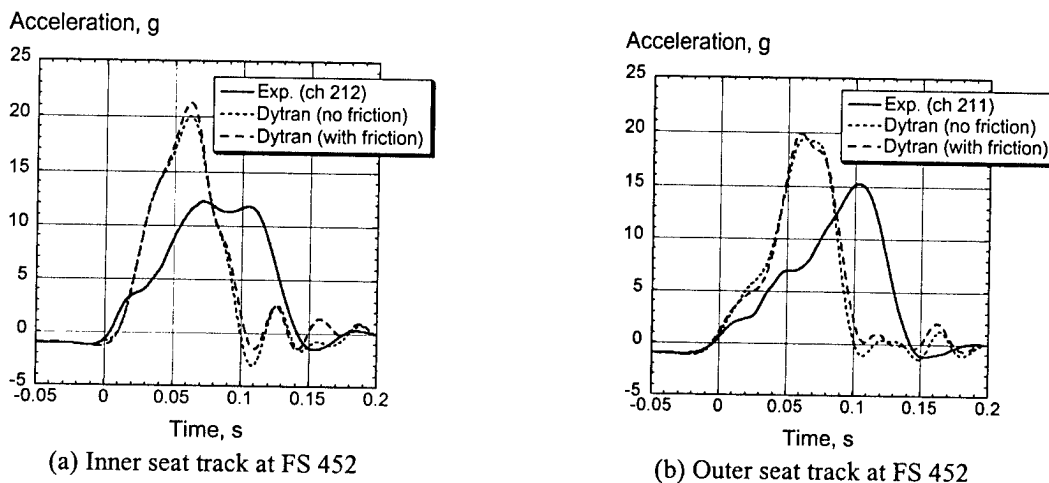


FIGURE 57. EFFECT OF FRICTION ON LEFT SEAT TRACK ACCELERATION RESPONSES

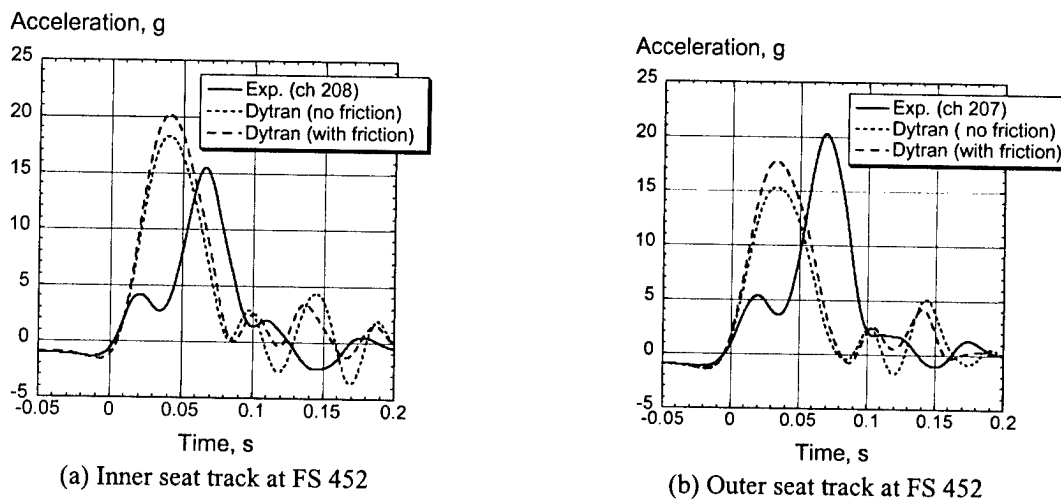


FIGURE 58. EFFECT OF FRICTION ON RIGHT SEAT TRACK ACCELERATION RESPONSES

MODIFICATIONS TO MODEL FEATURES.

REDUCTION IN YIELD STRESS. The material properties that were assigned to the elements forming the fuselage model were estimates based on engineering handbook values for 2024-T3 and 7075-T6 aluminum, see tables 1 and 2. As mentioned previously, the handbook values of yield stress were reduced to partially account for stress risers, fatigue damage, and stress corrosion. This approach was necessary since no materials testing was performed to determine the actual properties. A modification was implemented in which the yield stresses assigned to the 2024-T3 and 7075-T6 aluminum were reduced by 25% over the values used in the pretest simulation. No other changes were made, and the simulation was executed for 0.2 second of simulation time. The deformation pattern of the reduced yield model is compared with the pretest model and test results are shown in figure 59. The crushing of the cargo floor and lower fuselage structure is more uniform than that of the pretest model, and the formation of the center plastic hinge is much less pronounced. Comparisons of the measured vertical acceleration responses with the predictions from the pretest model and the reduced yield stress model are shown in figures 60 and 61 for the left and right side seat track locations, respectively.

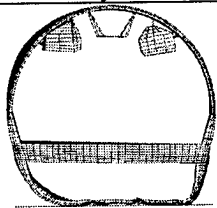
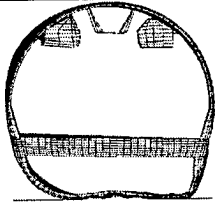
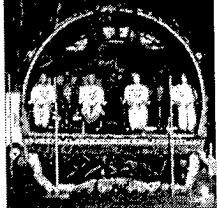
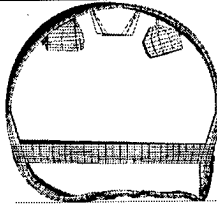
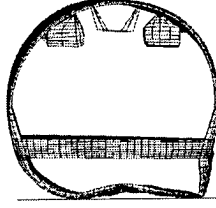
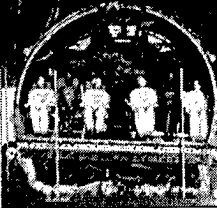
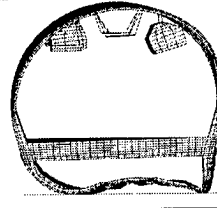
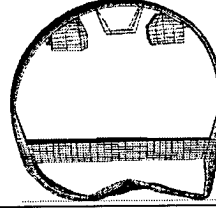
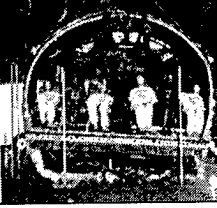
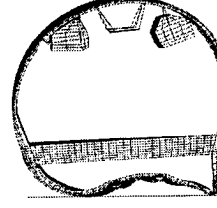
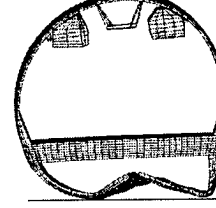
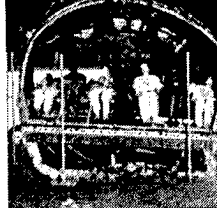
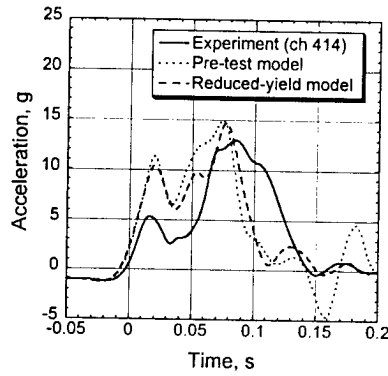
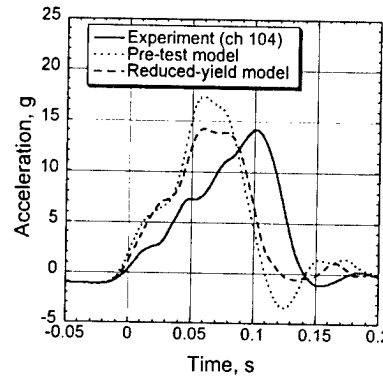
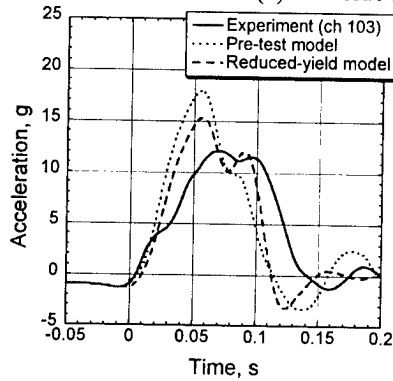
Reduced-yield model	Pretest model	Experiment
		
t = 0.06 second	t = 0.06 second	t = 0.06 second
		
t = 0.09 second	t = 0.09 second	t = 0.09 second
		
t = 0.12 second	t = 0.12 second	t = 0.12 second
		
t = 0.15 second	t = 0.15 second	t = 0.15 second

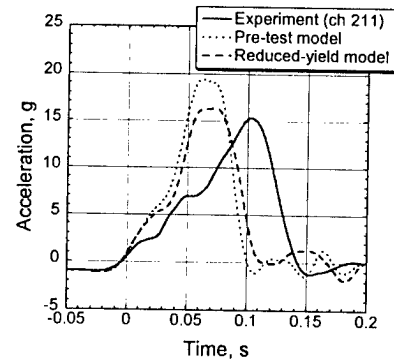
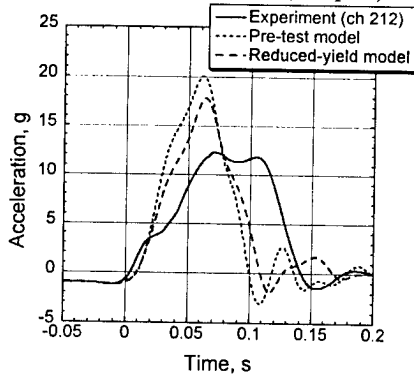
FIGURE 59. DEFORMATION PATTERNS OF THE REDUCED YIELD AND PRETEST MODELS AND TEST RESULTS



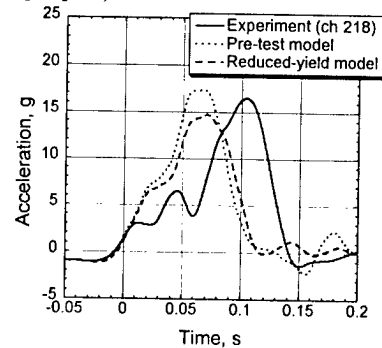
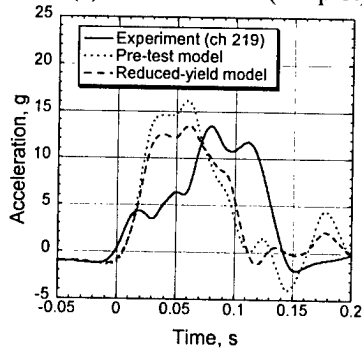
(a) Left side inner seat track at FS 380



(b) Left side inner (left plot) and outer (right plot) seat track at FS 418

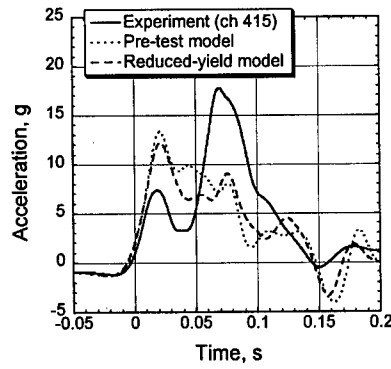


(c) Left side inner (left plot) and outer (right plot) seat track at FS 452

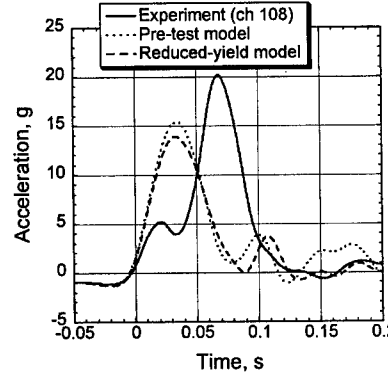
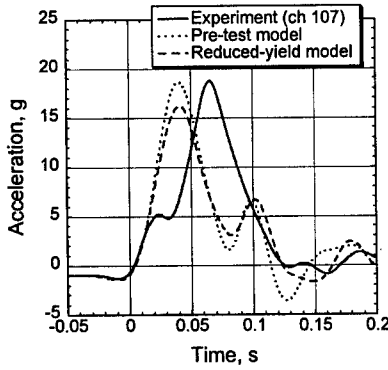


(d) Left side inner (left plot) and outer (right plot) seat track at FS 484

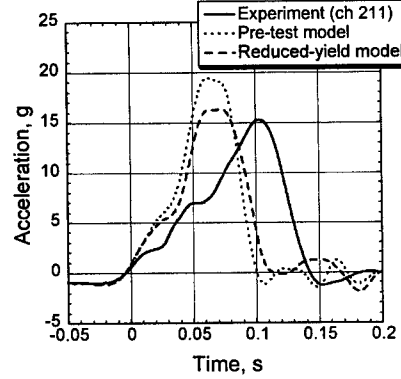
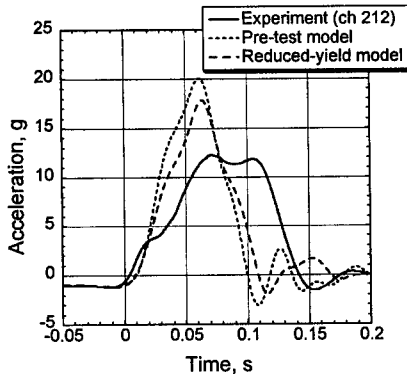
FIGURE 60. MEASURED VERTICAL ACCELERATION RESPONSES PLOTTED WITH THE PRETEST AND REDUCED YIELD MODEL PREDICTIONS FOR THE LEFT SIDE SEAT TRACK AT FOUR LOCATIONS



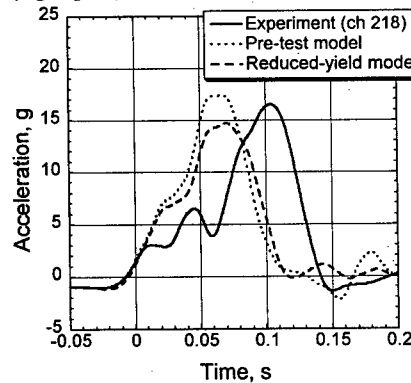
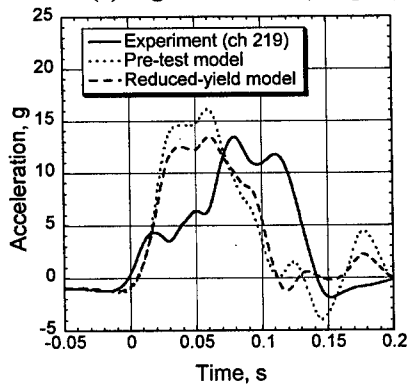
(a) Right side inner seat track at FS 380



(b) Right side inner (left plot) and outer (right plot) seat track at FS 418



(c) Right side inner (left plot) and outer (right plot) seat track at FS 452



(d) Right side inner (left plot) and outer (right plot) seat track at FS 484

FIGURE 61. MEASURED VERTICAL ACCELERATION RESPONSES PLOTTED WITH THE PRETEST AND REDUCED YIELD MODEL PREDICTIONS FOR THE RIGHT SIDE SEAT TRACK AT FOUR LOCATIONS

In general, the reduction in yield stress lowered the predicted peak acceleration values from 4% to 18%, resulting in improved correlation with the experimental data for most of the seat track locations. The overall shape of the predicted acceleration curves from the reduced-yield model closely matched those of the pretest simulation, except that they were slightly lower in magnitude and there was a slight increase in pulse duration.

**CORRECTED MASS PROPERTIES.** An additional change was made to adjust the inertial properties of the model to better match the total weight of the test article. As noted in table 3, the weight of the pretest model was 404 lbs heavier than the actual fuselage section. Most of this 4.5% increase was in the empty weight of the fuselage section and in the concentrated masses used to represent the combined seats, occupants, and miscellaneous floor masses. The excess weight was attributed to the fact that average thickness values were used in the model and few of the cut-outs were included. Also, extra concentrated masses were added at nodal locations where output was requested to reduce the amount of high-frequency noise in the analytical responses. To determine if the weight overage in the pretest model had a significant influence on the accuracy of the analytical predictions, the model was adjusted such that the total weight more closely matched that of the test article. This change was implemented by adjusting the densities of the 2024-T3 and 7075-T6 aluminum materials such that the total empty weight of the fuselage section was 1,360 lbs. Also, the material density of the camera mount was adjusted. Finally, most of the extra concentrated masses were removed. The total weight of the revised model was 8,900 lbs, which was only 30 lbs heavier than the test article.

The simulation was executed to determine if changes in the mass of the model affect the accuracy of the analytical predictions for this problem. The posttest simulation results are plotted with the experimental data and the pretest predictions in figures 62 and 63 for the left and right seat tracks at FS 452, respectively. The comparisons shown in figures 62 and 63 indicate that only minor changes in the predicted acceleration responses were obtained due to the 4.5 % decrease in overall mass.

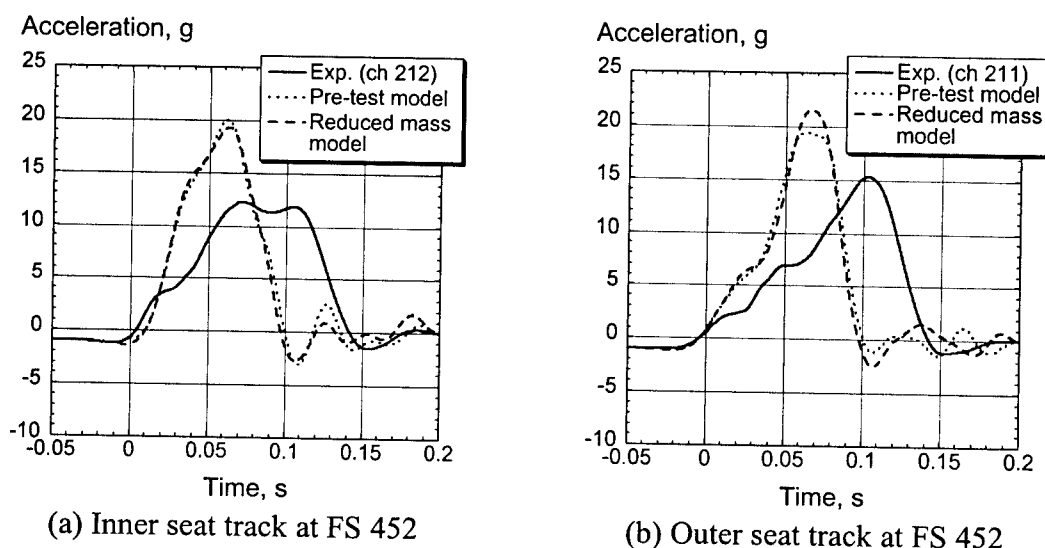
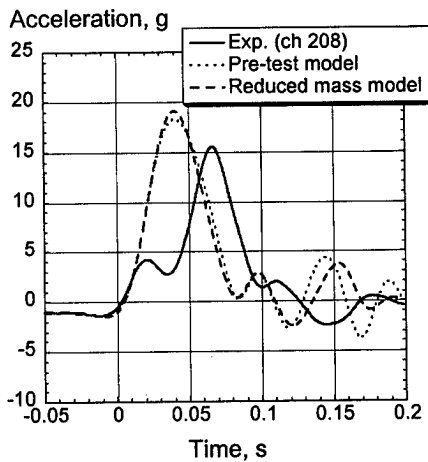
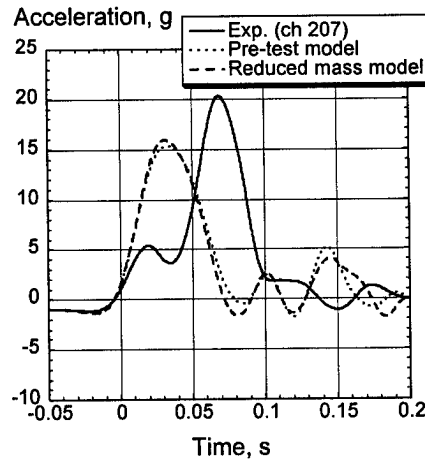


FIGURE 62. LEFT SEAT TRACK ACCELERATION RESPONSES COMPARED WITH PRETEST AND REDUCED MASS MODEL PREDICTIONS



(a) Inner seat track at FS 452



(b) Outer seat track at FS 452

FIGURE 63. RIGHT SEAT TRACK ACCELERATION RESPONSES COMPARED WITH PRETEST AND REDUCED MASS MODEL PREDICTIONS

MODIFICATIONS TO GAIN A MORE ACCURATE PHYSICAL REPRESENTATION OF THE PROBLEM.

INCORPORATION OF A PLATFORM MODEL. A modification to achieve a more accurate physical representation of this impact experiment was to include the drop test platform in the B737 fuselage section model. In the pretest simulation, the platform was represented as a rigid surface, as shown in figure 22. A master-surface to slave-node contact was defined between the rigid surface and the nodes forming the lower fuselage mesh. The motivation for adding a physical representation of the platform to the model is to correlate analytical predictions with test data obtained from the platform as a further means of validating the model. Also, it may be possible to determine what influence, if any, the platform has on the simulation results.

The 15-ft by 36.5-ft wooden platform, shown schematically in figure 64, rests on steel I-beams and is supported by 12 load cells. A photograph of the platform is shown in figure 65. For the test, the platform was instrumented with 12 load cells, 12 string potentiometers, and 12 accelerometers. The 12 load cells have capacities of 50,000, 100,000, and 200,000 pounds. All platform load cells are dual output and their locations are shown in figure 64. Prior to the drop test, the platform was leveled and the tare weight electronically zero balanced. The platform load cells are used to measure the impact loads and to determine their distribution. The reaction forces generated during the impact of the fuselage section may then be determined. In addition, 12 accelerometers were mounted to the bottom of the platform to characterize the platform response to the impact (see figure 64). Platform response is measured because of the potential influence it may have on fuselage accelerometer readings. Finally, 12 string potentiometers were attached to the platform to measure platform displacement (see figure 64).

The MSC.Dytran model of the B737 fuselage section was modified to incorporate a physical representation of the drop test platform. The integrated B737 fuselage section and platform model is shown in figure 66. The wooden platform was represented using 774 shell elements and the I-beam supports were modeled using 177 beam elements. The platform shell elements

were assigned a thickness of 10 inches, and a material density that is typical of dense, hard wood. The I-beams were assigned material properties typical of steel with a Young's modulus of 30e06-psi. The 12 load cells were modeled as tubular beam elements. In addition, a rigid surface was added below the beam elements to represent the concrete surface beneath the platform. A master-surface to slave-node contact was defined between the load cell nodes and the rigid surface. A new master-surface to slave-node contact was defined between the nodes forming the lower fuselage structure and the shell elements forming the wooden impact surface. The default value of FACT was assigned to both contact surfaces.

The integrated B737 fuselage section and drop test platform model was executed for 0.2 second of simulation time, which required 28.7 hours of CPU time on a Sun Ultra Enterprise 450 workstation computer. Requested output included vertical acceleration responses at nodal locations corresponding with the placement of accelerometers on the platform, axial force responses of the beam elements representing the loads cells, and nodal displacement responses corresponding to the string potentiometer locations. The acceleration traces recorded from the accelerometers on the platform were oscillatory in shape and had a magnitude of less than 1-g. Likewise, the displacement time histories recorded by the string potentiometers were generally parabolic in shape with magnitudes of less than 0.2 inch. Given these extremely low levels of test data, it was felt that correlation with the accelerometer and string pot data was not useful. Consequently, the analytical correlation was focused on the load cell data.

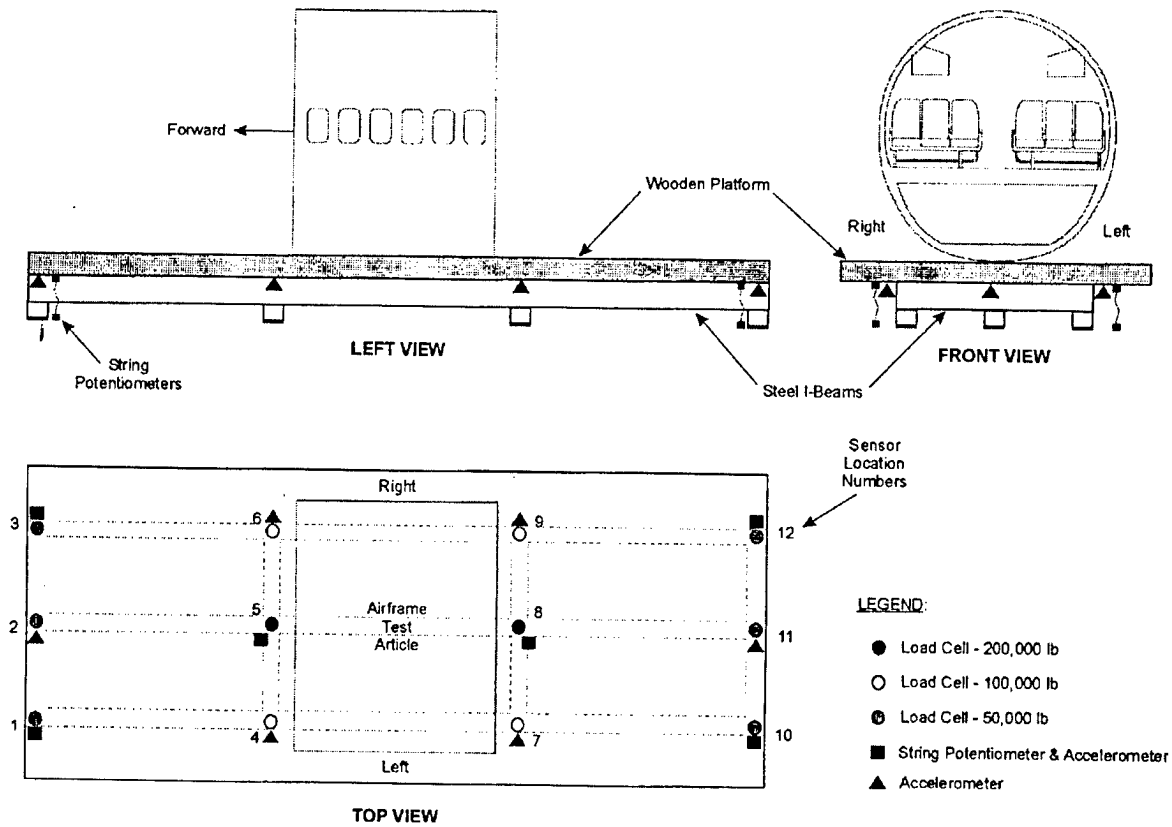


FIGURE 64. SCHEMATIC DRAWING OF THE DROP TEST PLATFORM AND INSTRUMENTATION LAYOUT

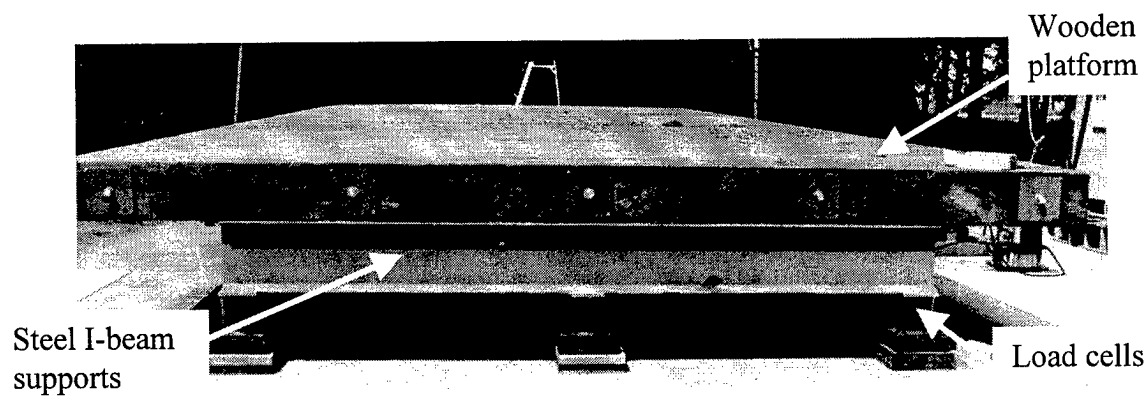


FIGURE 65. PHOTOGRAPH OF THE DROP TEST PLATFORM

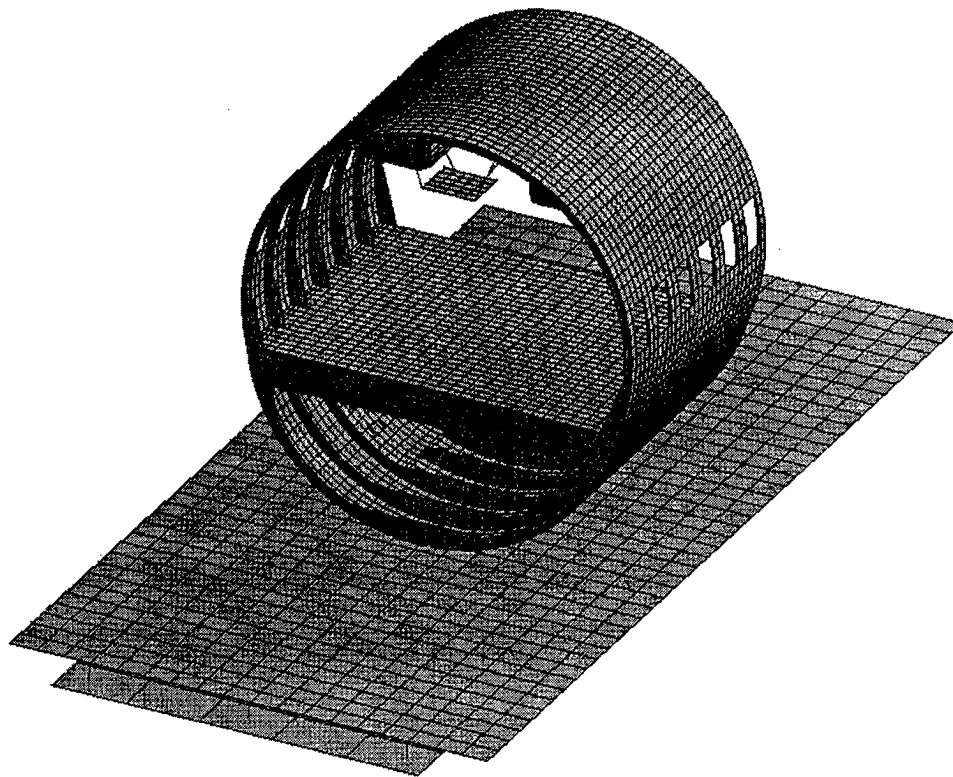
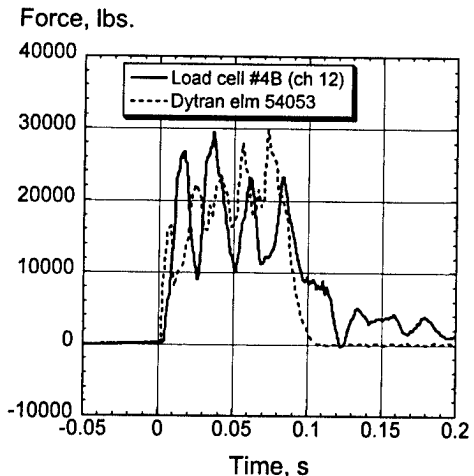
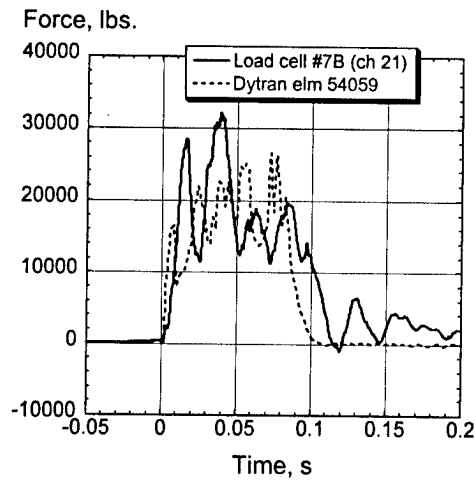


FIGURE 66. THREE-QUARTER VIEW OF THE INTEGRATED B737 FUSELAGE SECTION AND PLATFORM MODEL

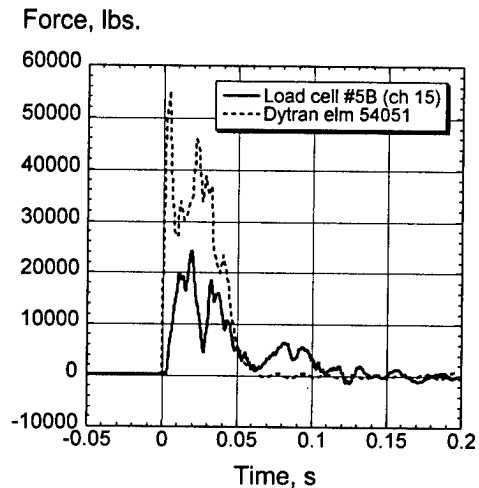
The experimental force time histories recorded by the six central load cells (load cells 4-9 in figure 64) are plotted with the analytical predictions in figure 67. The analytical predictions are the axial force responses of the lower beam elements representing each load cell. The experimental data is the raw unfiltered data, whereas the analytical force responses have been smoothed using a data reduction software program to remove some of the high-frequency oscillations. The correlation in the overall shape and duration of the force responses for the four "corner" load cells (4, 6, 7, and 9) is excellent; however, it is apparent that the predicted responses for load cells 5 and 8 are much higher in magnitude than the experimental data.



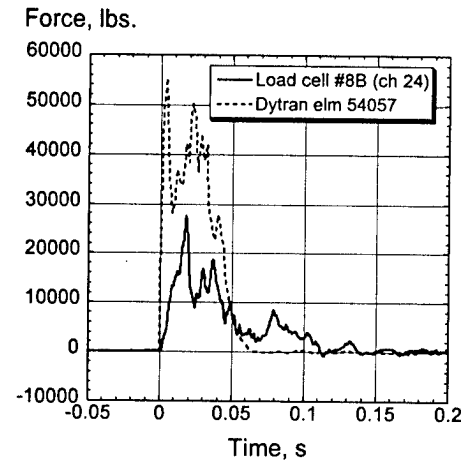
(a) Load cell #4



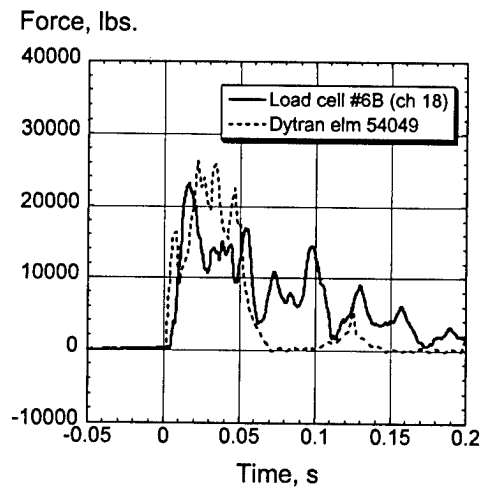
(b) Load cell #7



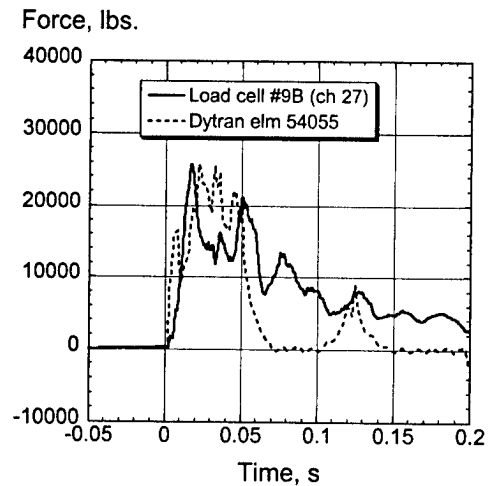
(c) Load cell #5



(d) Load cell #8



(e) Load cell #6



(f) Load cell #9

FIGURE 67. COMPARISON OF EXPERIMENTAL AND ANALYTICAL FORCE RESPONSES FOR SIX PLATFORM LOAD CELLS

Different boundary conditions were tried in the simulation in an attempt to understand the over-predicted force responses for these two load cells. In every case, the same results were obtained. It is interesting to note that the impulse (average force multiplied by the pulse duration) is approximately the same for each of the six predicted force time histories shown in figure 67. For example, the predicted average force for load cell 5 is about 34,000 lbs, whereas the predicted average force for load cell number 4 is approximately 17,000 lbs. For the impulse of these two load responses to be equal, the pulse duration for load cell 5 should be about half that of load cell 4. In fact, that is exactly the case.

Several assumptions made in the platform model development could influence the correlation between model and test. For example, the exact material properties of the wood were unknown and estimates were obtained from an engineering handbook. A linear elastic material property was assigned to the wood, yet it is well known that wood is a highly orthotropic material. As such, wood tends to exhibit different types of coupling including extension-flexure and bend-twist coupling. These types of material responses are not simulated using the linear elastic material property card that was specified for the wood. It is also possible that the various connections and constraints between the platform components were not represented accurately. For example, in the model it was assumed that the wooden platform is rigidly connected to the upper flanges of the I-beam supports. If this assumption is not accurate, it could influence the results. For example, if the wood is merely placed on top of the I-beam flanges without any constraints, there can be relative motion between the wood and the I-beams that is not captured by the present model.

The experimental left and right inner and outer seat track acceleration responses at FS 452 are plotted in figures 68 and 69, respectively, with the pretest predicted responses and the responses obtained from the integrated platform and B737 fuselage section model. It is apparent from the results shown in figures 68 and 69 that the incorporation of the platform model had minimal effect on the simulation predictions.

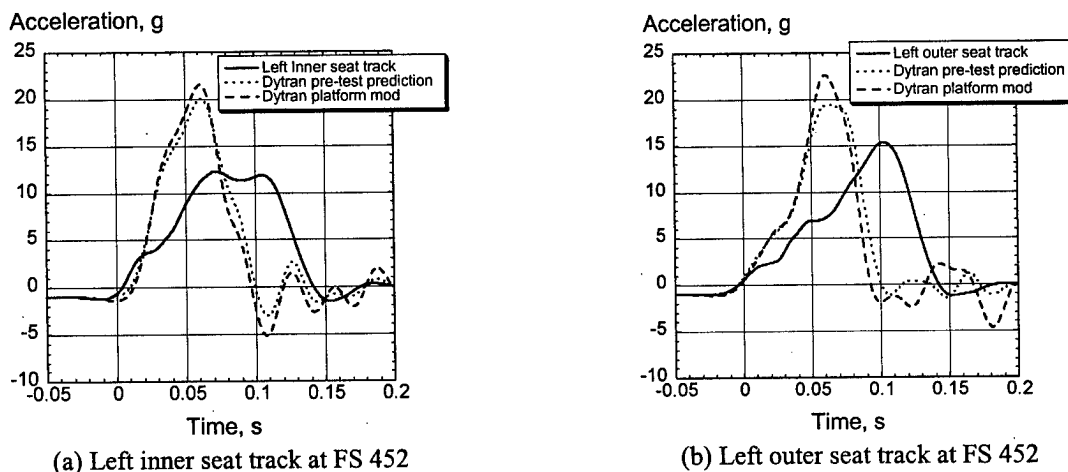
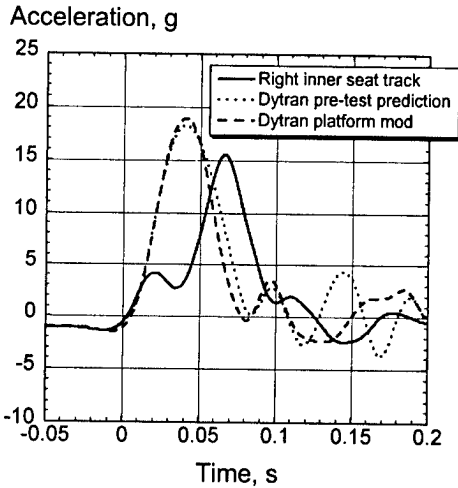
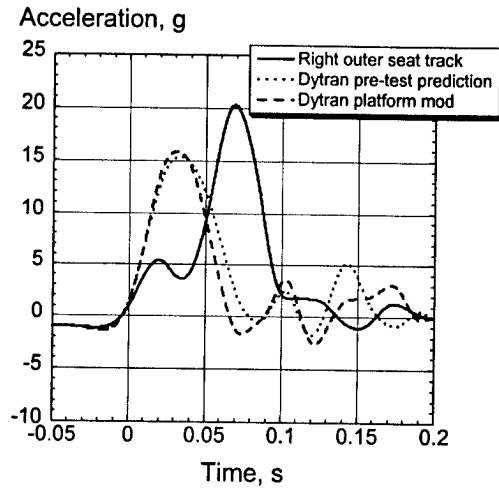


FIGURE 68. ACCELERATION RESPONSES OF THE LEFT INNER AND OUTER SEAT TRACKS AT FS 452 PLOTTED WITH THE PRETEST PREDICTIONS AND THE RESPONSES OBTAINED FROM THE INTEGRATED PLATFORM AND B737 FUSELAGE SECTION MODEL



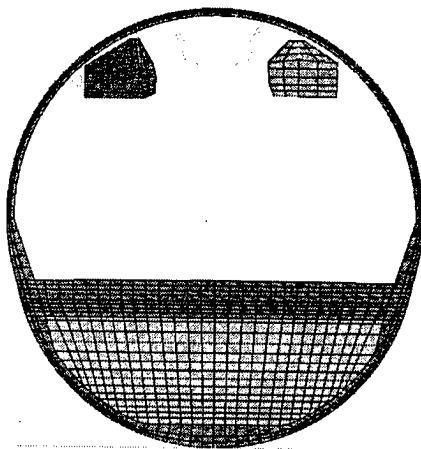
(a) Right inner seat track at FS 452



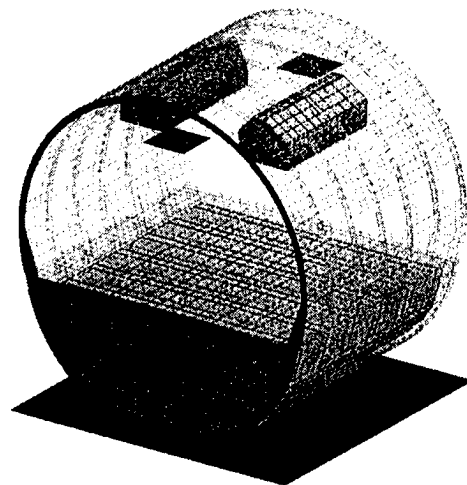
(b) Right outer seat track at FS 452

FIGURE 69. ACCELERATION RESPONSES OF THE RIGHT INNER AND OUTER SEAT TRACKS AT FS 452 PLOTTED WITH THE PRETEST PREDICTIONS AND THE RESPONSES OBTAINED FROM THE INTEGRATED PLATFORM AND B737 FUSELAGE SECTION MODEL

INCORPORATION OF A LUGGAGE MODEL. One obvious deficiency in the pretest model of the B737 fuselage section was that the luggage was represented simply as concentrated masses that were attached to the nodes forming the inner surface of the lower bulkhead webs. To correct this deficiency, the pretest model was modified to incorporate the luggage, as shown in figure 70. The luggage was modeled as 9,072 solid elements including 8,736 hexagonal and 336 pentagonal solid elements. The hexagonal elements are eight-noded solid elements with six faces or sides. The six-noded pentagonal elements are wedge shaped and have five sides. These solid elements fill the lower fuselage volume, as indicated in figure 70, from the bottom of the floor beams to the top of the cargo floor.



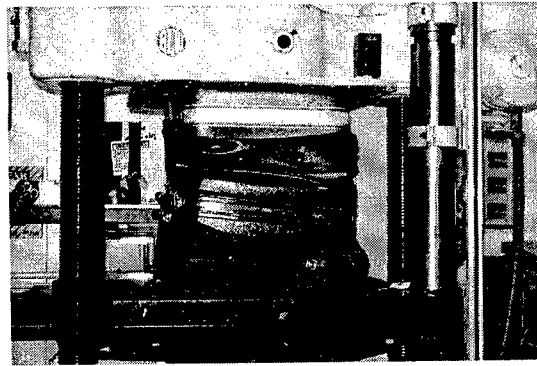
(a) Front view



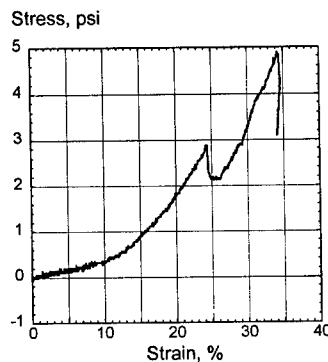
(b) Three-quarter view

FIGURE 70. B737 FUSELAGE MODEL WITH LUGGAGE

The main reason for not including a physical representation of the luggage in the pretest model was that no material property data were available. To overcome this deficiency, a simple crush test of four pieces of stacked luggage was performed. The empty pieces of luggage were obtained from a thrift shop and packed with cloth rags, shoes, and various toiletry items. The four pieces of luggage included two hard-sided and two soft-sided pieces of approximately the same overall size. As shown in figure 71(a), the luggage was stacked vertically and placed on the lower platen of a standard load test machine. An upper platen was fabricated from a 1.0-in. thick aluminum plate that had a cross-sectional area large enough to completely cover the luggage. The luggage was loaded in compression between the platens of the load test machine. The resulting stress versus strain plot is shown in figure 71(b). This test data was used to generate a table of stress and strain values that were assigned to a FOAM2 material property card to define the material response of the solid elements representing the luggage. The FOAM2 material property card in MSC.Dytran was implemented in the code specifically for representing the compressive stress/strain behavior of isotropic, crushable foam materials having a Poisson's ratio that is effectively zero. In addition, the FOAM2 card allows the user to specify the type of unloading curve, a tensile cut-off stress, as well as an energy dissipation factor. The density specified on the FOAM2 card was adjusted such that the total weight of the luggage was exactly 3,229 lbs, matching the experimental weight. Also, the concentrated masses were removed that had been used to represent the luggage in the pretest model.



(a) Photograph of the luggage crush test



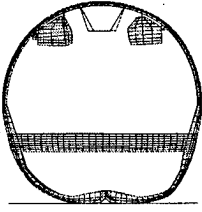
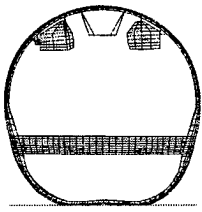

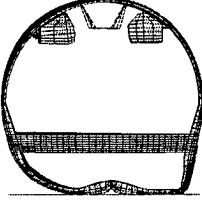
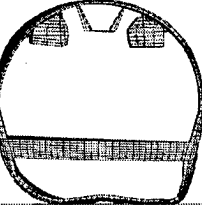
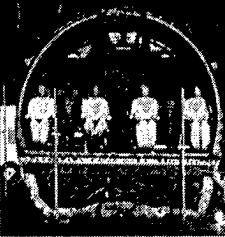
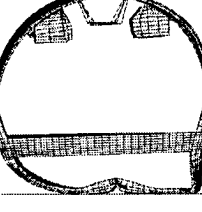
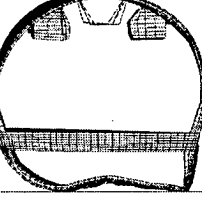
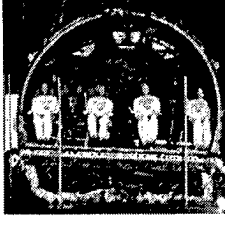
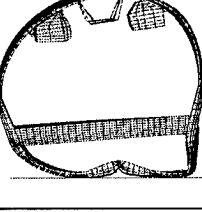
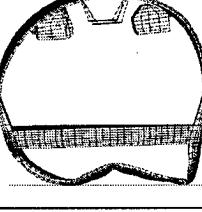
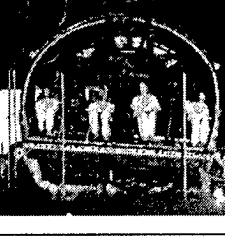
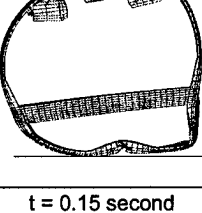
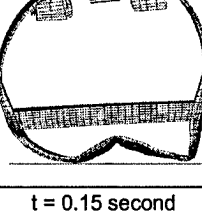
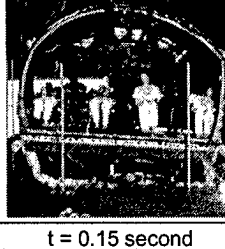
(b) Stress versus strain response

FIGURE 71. LUGGAGE CRUSH TEST RESULTS

In addition to 9,072 new elements, a total of 10,206 nodes were added to the model due to the addition of the luggage. Also, new contact surfaces were created. A master-surface to slave-node contact was defined between the floor and floor beams and the top surface of the luggage. A similar contact surface was defined between the fuselage skin and bulkhead webs and the luggage. The fuselage model with luggage was executed in MSC.Dytran, Version 2000, for 0.2 second of simulation time on a Sun Ultra Enterprise 450 workstation computer. The simulation required 44 hours of CPU with a final time step of 2.54 microsecond. Thus, the luggage modification added considerable complexity to the model and increased the total run time by 8 hours.

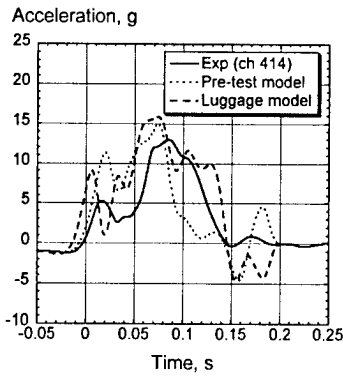
The results of the luggage modification are shown in figure 72, which shows the deformed shape of the pretest and luggage models at five time increments with photographs obtained from the high-speed motion picture coverage. The presence of the luggage has limited the formation and growth of the large plastic hinge at the base of the model. In the pretest model, the lower fuselage frames displace upward toward the floor and intrude into the area occupied by the luggage. In the luggage model, this large displacement is prevented by the luggage. The two deformation patterns are similar in that the formation of a damage site on the lower left side of the fuselage occurs at the same location and at roughly the same time. However, a similar damage site on the lower right side of the fuselage section is not predicted by the luggage model. Comparisons of the measured vertical acceleration responses with the predictions from the pretest and luggage models are shown in figures 73 and 74 for the left and right side seat track locations, respectively.

The results shown in figures 73 and 74 indicate that the addition of the luggage had a pronounced effect on the predicted floor-level acceleration responses on the right side of the fuselage, but minimal effect on the left side. For the left inner and outer seat track locations, the predicted floor-level responses that were output from the luggage model had roughly the same or slightly higher peak acceleration values and longer pulse durations when compared with the pretest model results. However, a much greater difference was observed for the right inner and outer seat track locations. For these locations, the peak acceleration values were substantially less than those predicted by the pretest model, and the time of occurrence of the peak acceleration was delayed. In general, the right side floor-level acceleration responses had a longer pulse duration than did the pretest predictions or the test results.

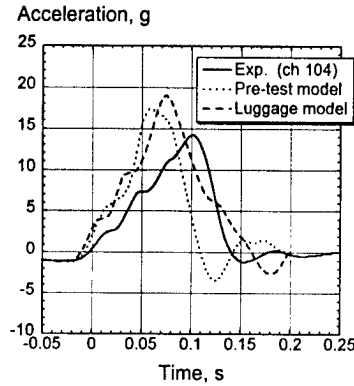
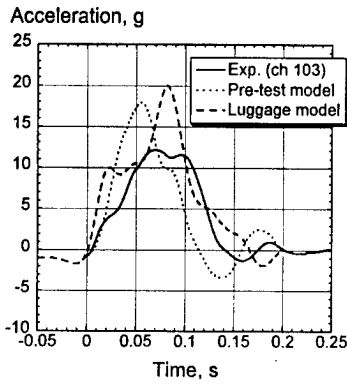
Luggage model*	Pretest model	Experiment
		
t = 0.03 second	t = 0.03 second	t = 0.03 second
		
t = 0.06 second	t = 0.06 second	t = 0.06 second
		
t = 0.09 second	t = 0.09 second	t = 0.09 second
		
t = 0.12 second	t = 0.12 second	t = 0.12 second
		
t = 0.15 second	t = 0.15 second	t = 0.15 second

\* Note the solid elements representing the luggage have been removed for better visualization of the structural deformation.

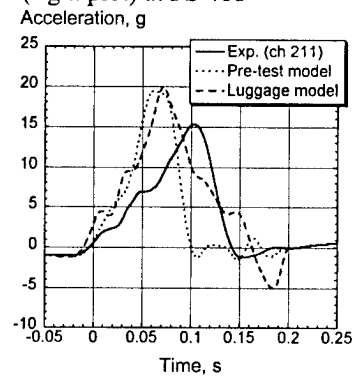
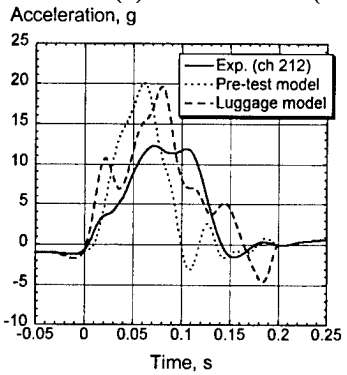
FIGURE 72. COMPARISONS OF THE DEFORMATION PATTERNS OF THE LUGGAGE AND PRETEST MODELS WITH EXPERIMENT



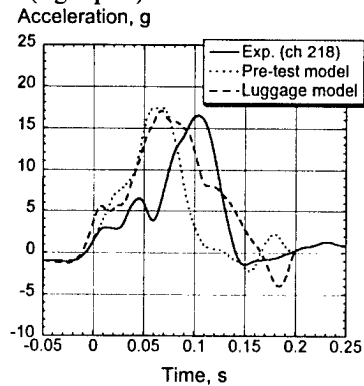
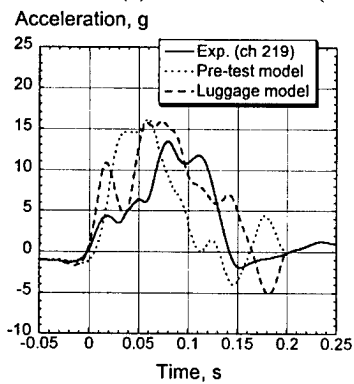
(a) Left side inner seat track at FS 380



(b) Left side inner (left plot) and outer (right plot) at FS 418

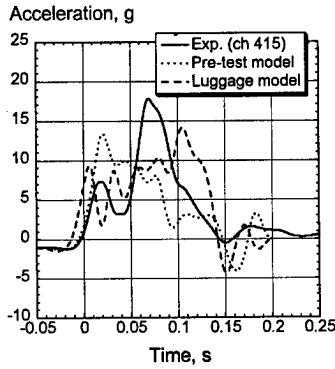


(c) Left side inner (left plot) and outer (right plot) at FS 452

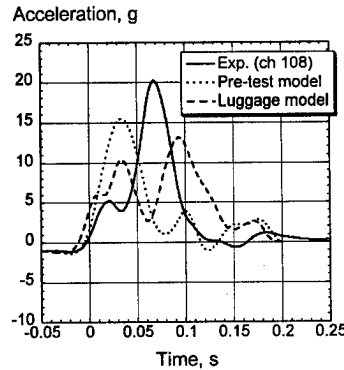
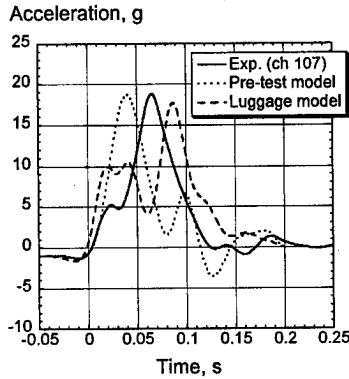


(d) Left side inner (left plot) and outer (right plot) at FS 484

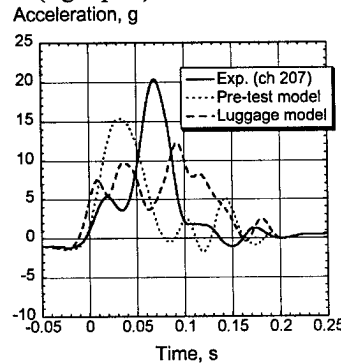
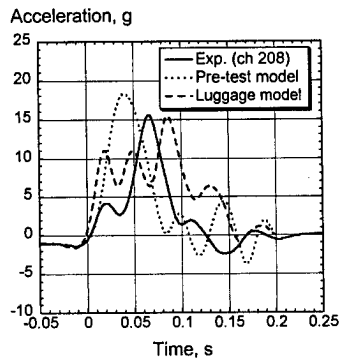
FIGURE 73. MEASURED VERTICAL ACCELERATION RESPONSES PLOTTED WITH THE PRETEST AND LUGGAGE MODEL PREDICTIONS FOR THE LEFT SIDE SEAT TRACK AT FOUR LOCATIONS



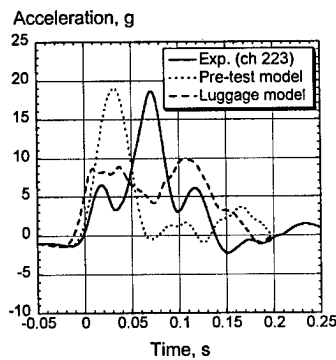
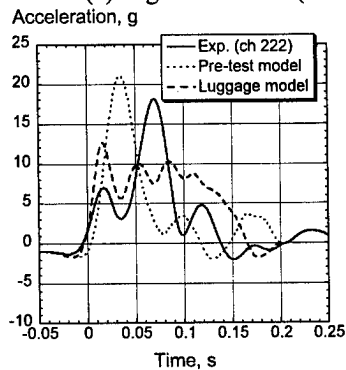
(a) Right side inner seat track at FS 380



(b) Right side inner (left plot) and outer (right plot) at FS 418



(c) Right side inner (left plot) and outer (right plot) at FS 452



(d) Right side inner (left plot) and outer (right plot) at FS 484

FIGURE 74. MEASURED VERTICAL ACCELERATION RESPONSES PLOTTED WITH THE PRETEST AND LUGGAGE MODEL PREDICTIONS FOR THE RIGHT SIDE SEAT TRACK AT FOUR LOCATIONS

The experimental velocity responses of the left and right outer seat tracks at FS 418 are plotted with the simulation results from the pretest and luggage models, as shown in figure 75. For the left outer seat track location, the predicted responses are nearly identical, except that the luggage response has a higher rebound velocity than does the pretest model response. Both predicted curves cross zero velocity at 0.08 second, whereas the experimental curve crosses zero velocity at 0.115 second. For the right outer seat track location, the vertical velocity response predicted by the luggage model is close to the pretest response until 0.05 second. At that time, the two curves deviate from one another. However, by 0.1 second they are close again. Neither curve crosses zero velocity, whereas the experimental velocity curve crosses zero velocity at 0.11 second. Thus, even though the luggage model produced a more uniform deformation pattern in the cargo floor region, the results shown in figure 72 indicate that the damage sites on the lower left and right sides of the fuselage are not well predicted by the simulation. On the left side, the simulation predicted too little crush, causing the floor-level velocity response to come to rest too quickly. On the right side, the simulation predicted too much crush, causing the floor-level velocity to not come to rest during the 0.2 second simulation time.

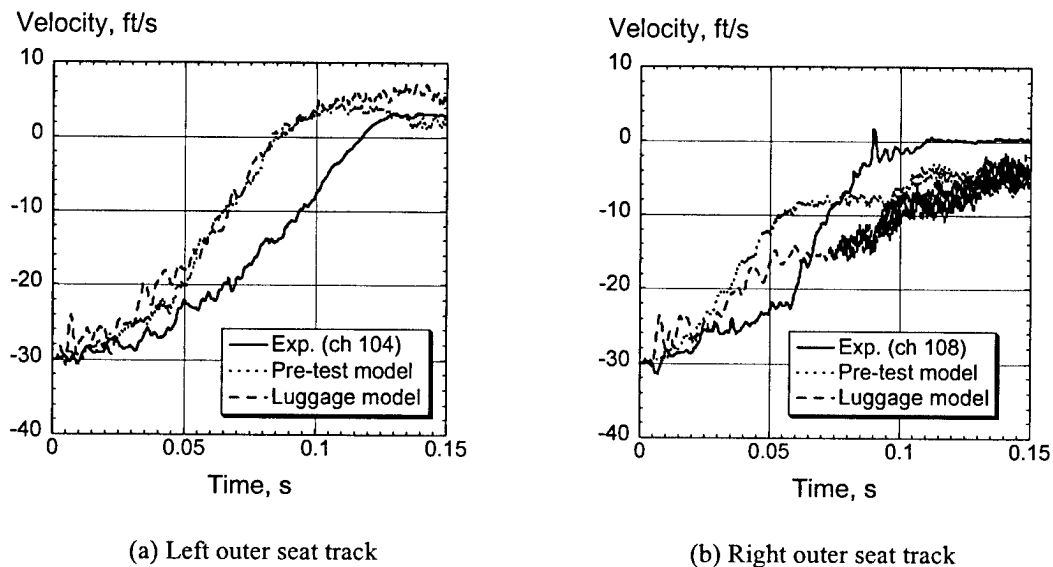


FIGURE 75. COMPARISON OF EXPERIMENTAL VELOCITY RESPONSES OF THE LEFT AND RIGHT OUTER SEAT TRACKS AT FS 418 WITH PRETEST AND LUGGAGE MODEL PREDICTIONS

#### CORRECTIONS TO THE CARGO DOOR AND ASSOCIATED STIFFENED STRUCTURE.

One deficiency of the pretest model was the fact that the deformation and failure of the lower fuselage structure were not well predicted. While the addition of a physical representation of the luggage provided a more uniform crushing of the cargo floor area, the simulation still did not properly predict the location of secondary damage sites on the lower left and right sides of the fuselage structure. One explanation for this deficiency was that the cargo door and its associated stiffened structure were not modeled accurately. The original model of the cargo door is shown in figure 12(c) and a photograph of the actual cargo door is shown in figure 4. In the pretest simulation, the cargo door was represented as a plate attached to the inner flanges of the lower fuselage frames using 252 shell elements with a thickness of 0.125 in. In addition, 66 beam elements were used to represent the surrounding stiffened structure. These beam elements were

modeled as I-beams which were 3.0 in. in height with a web and flange thickness of 0.125 inch. The thickness of the fuselage skin opposite the door was increased from 0.05 to 0.125 in., and the thickness of the bulkhead webs in the door area were increased in the same manner. It is obvious from the deformation pattern of the fuselage section model, shown in figure 54, that the cargo door area is too stiff.

To more accurately represent the complex cargo door, the existing model was modified, as shown in figure 76. These modifications included changing the geometry of the I-beam elements to a rectangular cross-section; reducing the thickness of the door, the skin opposite the door, and the bulkhead webs to 0.05 inch; and adding new beam elements across the width of the door to represent the support structure between the fuselage skin and the door. In addition, beam elements were added to represent the door hinges.

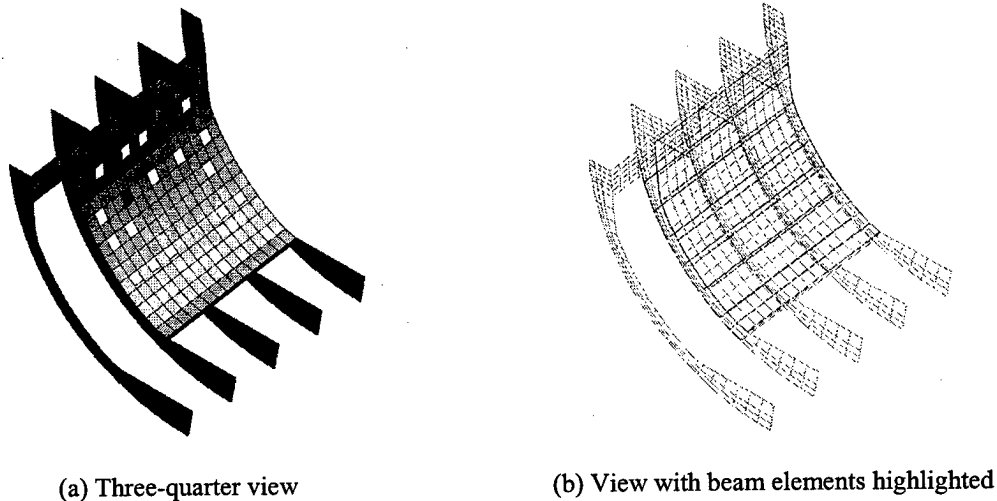
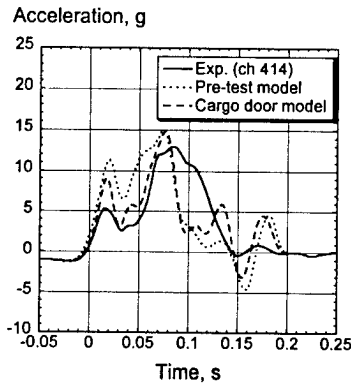


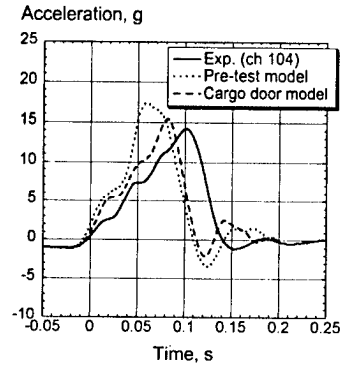
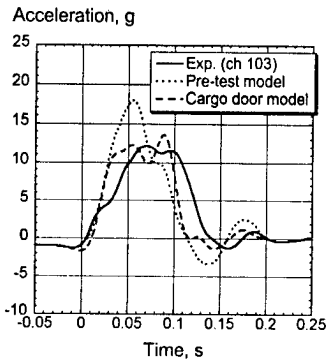
FIGURE 76. REVISED MODEL OF THE CARGO DOOR AND SURROUNDING STRUCTURE

The revised cargo door model was executed for 0.2 second of simulation time and the comparisons between the pretest and cargo door models and the test data for the left and right seat track vertical acceleration responses are shown in figures 77 and 78, respectively. In general, the cargo door model predictions show improved correlation with the test data for the left seat track responses. The peak acceleration values and the time of occurrence of the peak agree well with the test data. However, the correlation for the right seat track locations is not as good as for the pretest simulation.

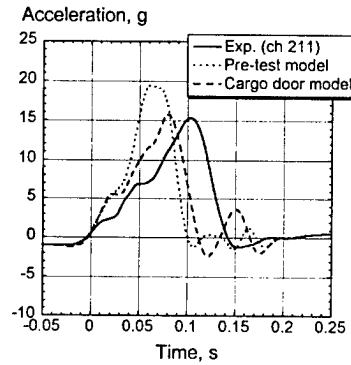
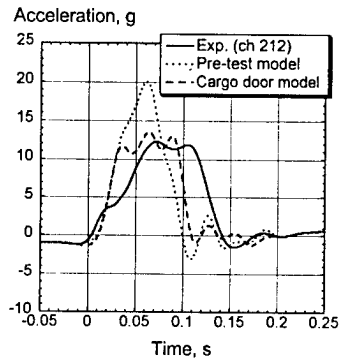
Comparisons of the deformation pattern of the cargo door and pretest models with photographs of the actual fuselage deformation are shown in figure 79. The results indicate that the left-to-right, or clockwise, rotation of the floor is reduced for the cargo door model. Also, there is evidence of a secondary damage site developing on the lower right side of the fuselage model. However, the amount of intrusion of the damaged lower structure into the region occupied by the luggage is greater in the cargo door model than in the pretest simulation.



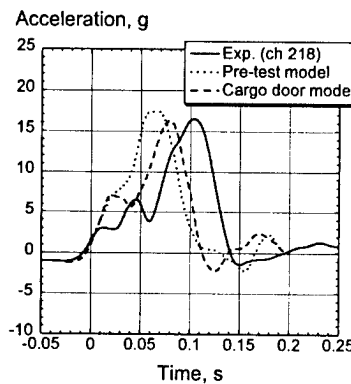
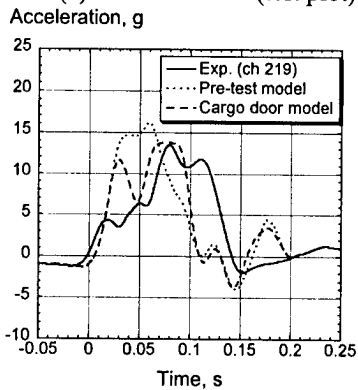
(a) Left side inner seat track at FS 380



(b) Left side inner (left plot) and outer (right plot) seat track at FS 418

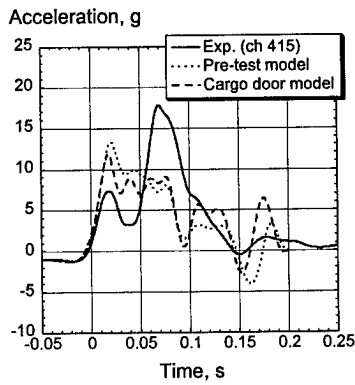


(c) Left side inner (left plot) and outer (right plot) seat track at FS 452

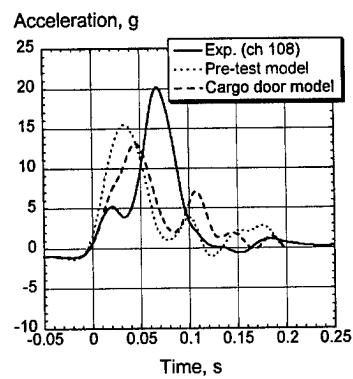
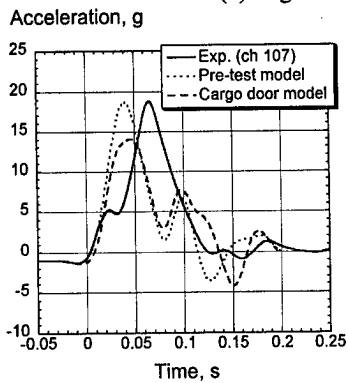


(d) Left side inner (left plot) and outer (right plot) seat track at FS 484

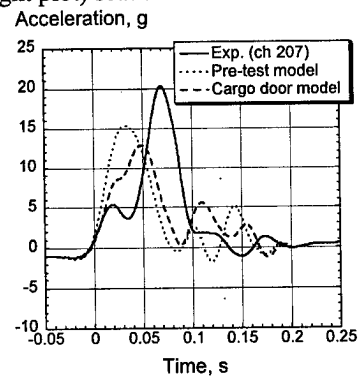
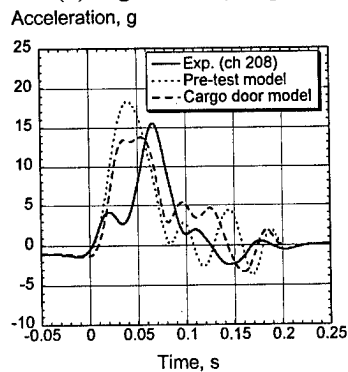
FIGURE 77. MEASURED VERTICAL ACCELERATION RESPONSES PLOTTED WITH THE PRETEST AND CARGO DOOR MODEL PREDICTIONS FOR THE LEFT SIDE SEAT TRACK AT FOUR LOCATIONS



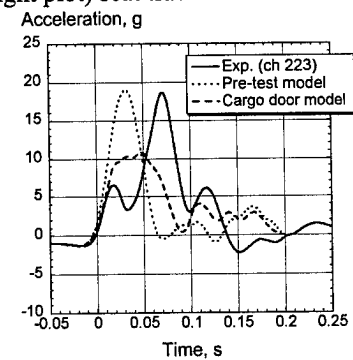
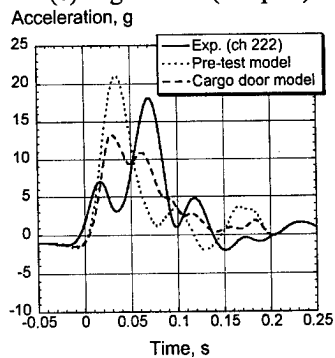
(a) Right inner seat track at FS 380



(b) Right inner (left plot) and outer (right plot) seat track at FS 418



(c) Right inner (left plot) and outer (right plot) seat track at FS 452



(d) Right inner (left plot) and outer (right plot) seat track at FS 484

FIGURE 78. MEASURED VERTICAL ACCELERATION RESPONSES PLOTTED WITH THE PRETEST AND CARGO DOOR MODEL PREDICTIONS FOR THE RIGHT SIDE SEAT TRACK AT FOUR LOCATIONS

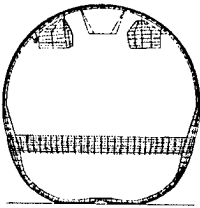
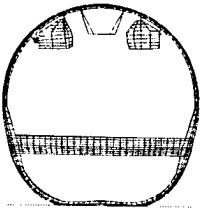
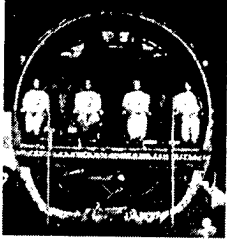
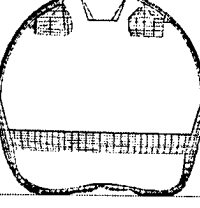
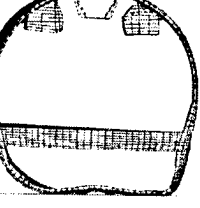
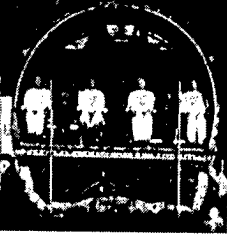
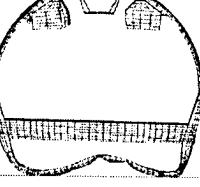
Cargo door model	Pretest model	Experiment
		
t = 0.03 second	t = 0.03 second	t = 0.03 second
		
t = 0.06 second	t = 0.06 second	t = 0.06 second
		
t = 0.09 second	t = 0.09 second	t = 0.09 second
t = 0.12 second	t = 0.12 second	t = 0.12 second
t = 0.15 second	t = 0.15 second	t = 0.15 second

FIGURE 79. COMPARISONS OF THE DEFORMATION PATTERNS OF THE CARGO DOOR AND PRETEST MODELS WITH EXPERIMENT

Finally, it is useful to examine the influence of the model revisions on the floor-level velocity responses. Comparisons of the vertical velocity responses of the pretest and cargo door models with the experimental data are shown in figure 80(a) and (b) for the left and right outer seat track locations at FS 418, respectively. The predicted velocity response of the cargo door model

shows much better agreement with the test data than does the pretest model response for the left outer seat track location. However, the results for the right seat track location are only marginally improved.

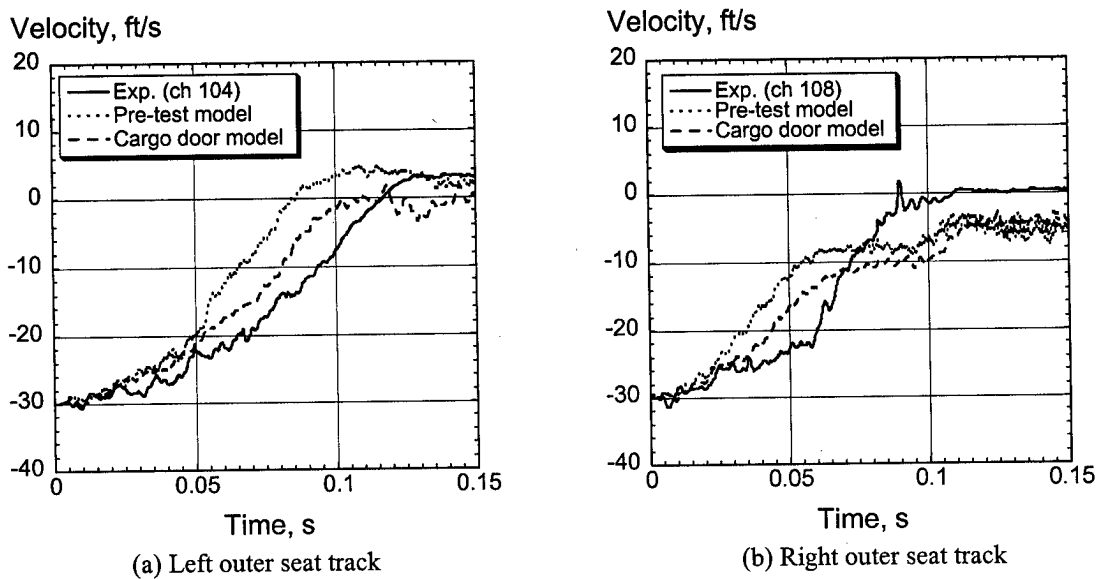


FIGURE 80. COMPARISON OF EXPERIMENTAL VELOCITY RESPONSES OF THE LEFT AND RIGHT OUTER SEAT TRACKS AT FS 418 WITH PRETEST AND CARGO DOOR MODEL PREDICTIONS

#### COMBINED LUGGAGE AND CARGO DOOR MODIFICATIONS.

It is apparent from the previous study of model revisions that the luggage and cargo door modifications had the most influence on model accuracy. It is also true that no one modification was able to correct all of the model inaccuracies. Consequently, a final model was executed that incorporated both the luggage and cargo door modifications. The deformation patterns of the combined luggage and cargo door model, pretest model, and test data are shown in figure 81. The results shown in figure 81 indicate that the combined luggage and cargo door model does not develop the left-to-right, or clockwise, rotation of the floor that is evident in the pretest model deformation. Also, the secondary damage sites on the left and right sides of the lower fuselage are well predicted.

As further indication of the improved correlation of the combined model, the predicted vertical velocity responses of the left and right seat tracks at FS 418 are correlated with the pretest simulation and the test data, as shown in figure 82. For the left seat track location, shown in figure 82(a), the predicted velocity response of the combined model shows much better agreement with the test data than does the pretest model response. However, the response of the combined model has a much greater rebound velocity than either the pretest model or experimental responses. This result is not surprising because the solid elements representing the luggage are capable of storing elastic energy that is returned to the system as kinetic energy in rebound. The improvement in correlation with the velocity response of the right seat track location is not as pronounced as for the left seat track location, as shown in figure 82(b).

However, both the combined model and experimental velocity responses cross zero velocity at approximately the same time. Again, a much larger rebound velocity is noted for the combined luggage and cargo door model than is observed in the experimental response. The pretest velocity response does not cross zero velocity due to the left to right rotation of the floor.

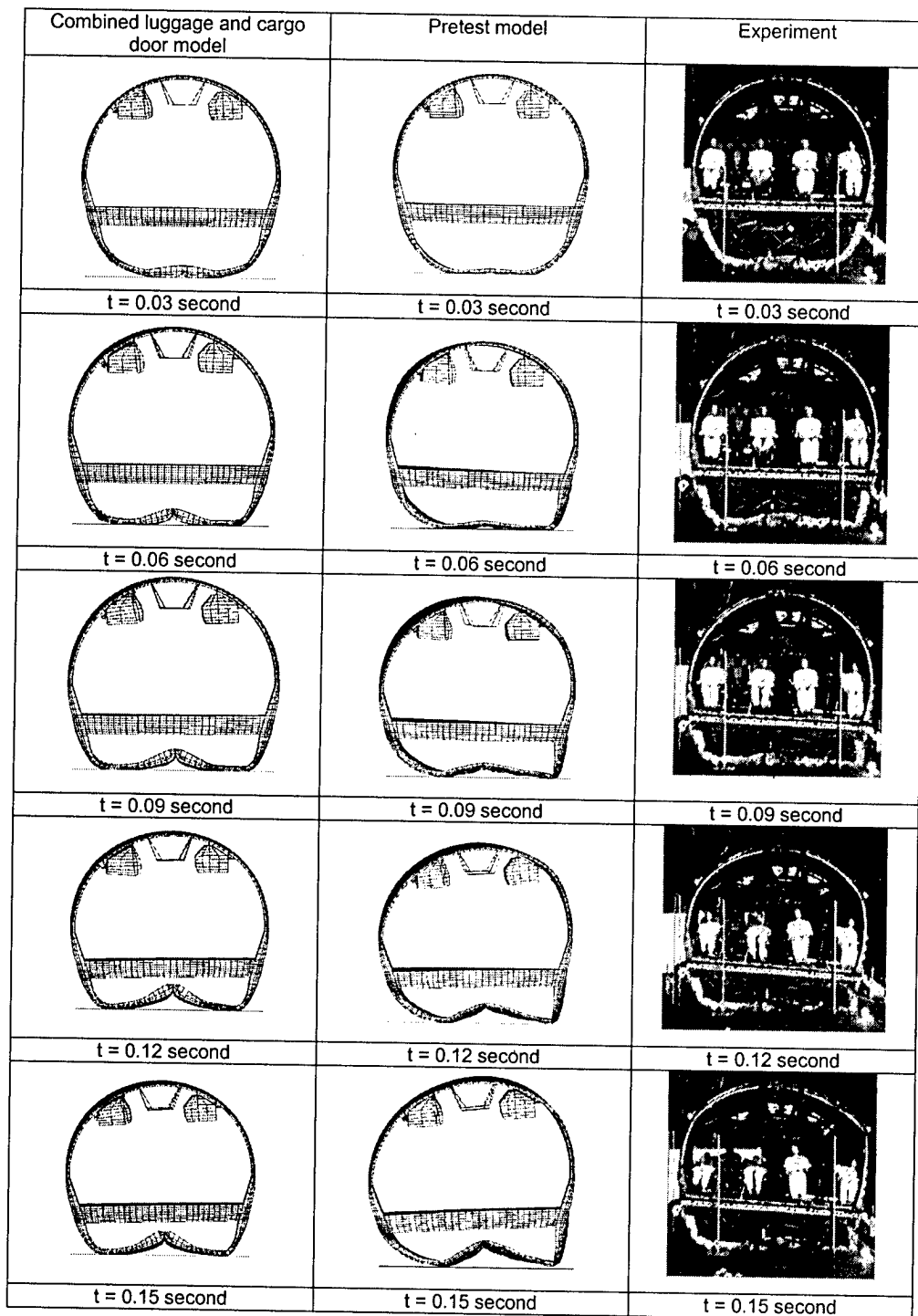
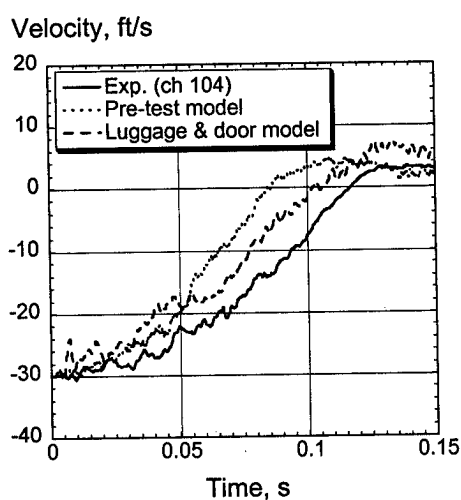
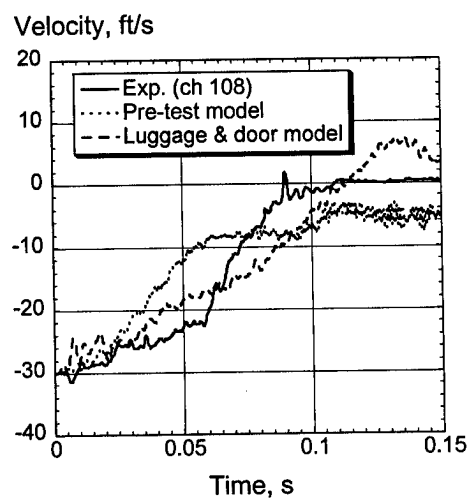


FIGURE 81. COMPARISONS OF THE DEFORMATION PATTERNS OF THE COMBINED LUGGAGE AND CARGO DOOR AND PRETEST MODELS WITH EXPERIMENT



(a) Left outer seat track



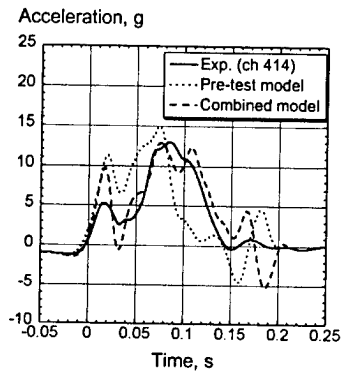
(b) Right outer seat track

FIGURE 82. COMPARISON OF EXPERIMENTAL VELOCITY RESPONSES OF THE LEFT AND RIGHT OUTER SEAT TRACKS AT FS 418 WITH PRETEST AND COMBINED LUGGAGE AND CARGO DOOR MODEL PREDICTIONS

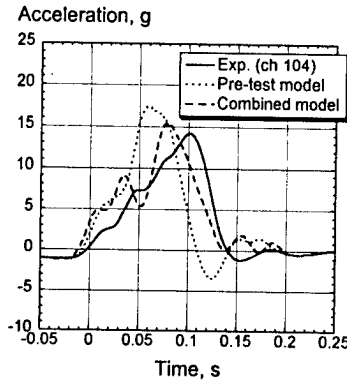
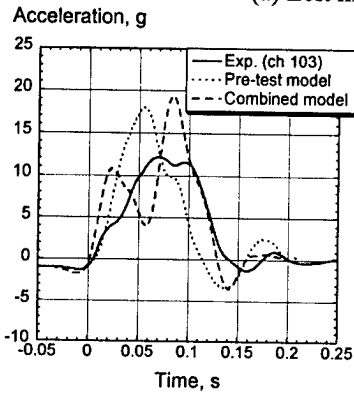
Comparisons of the measured vertical acceleration responses with the predictions from the pretest model and the combined luggage and cargo door model are shown in figures 83 and 84 for the left and right seat track locations, respectively. For the left seat track locations, shown in figure 83, the combined model predictions show improved correlation with the overall shape and duration of the experimental accelerations pulses. In particular, the predicted peak acceleration values are markedly closer to the experimental data for the left outer seat track locations. Also, the time of occurrence of the peak value is much better predicted by the combined model, as compared with the pretest model.

For the right seat track locations, shown in figure 84, the predicted peak acceleration values obtained from the combined model are, in general, similar to the pretest model or lower in magnitude. The greatest change, however, is seen in the time of occurrence of the peak. For the pretest model, the peak acceleration generally occurred much sooner than the experimental peak, whereas the peak acceleration values of the combined model occur somewhat later in time than the experimental peak. Overall, the pulse durations of the combined model are longer than the pretest predictions and show excellent agreement with the experimental data.

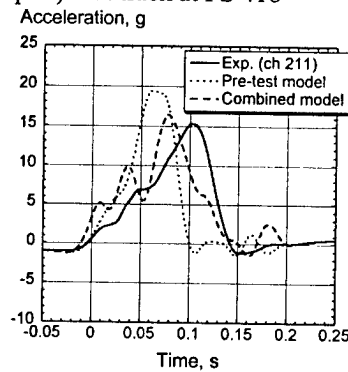
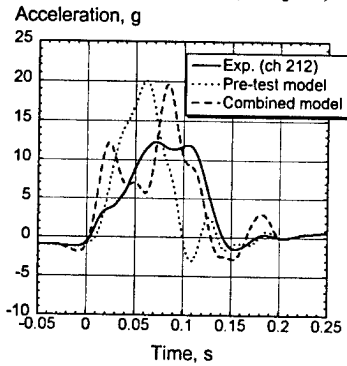
These findings confirm that the cargo door and its associated stiffened structure were modeled with too much structural rigidity in the pretest simulation. This inaccuracy in the pretest model was carried over from the initial fuselage section model with the auxiliary fuel tank. For the initial simulation, the inaccuracies in the cargo door model were overshadowed by the presence of the stiff, heavy fuel tank. A better approach for this crash modeling and simulation exercise would have been to perform the initial simulation on a vertical drop test of a B737 fuselage section without an auxiliary fuel tank or luggage beneath the floor. Such a simulation would have enabled the development and validation of a structural model of the B737 fuselage section, including a robust and accurate model of the cargo door area. Then, this validated model could have been modified to match both test configurations with greater confidence in the analytical predictions.



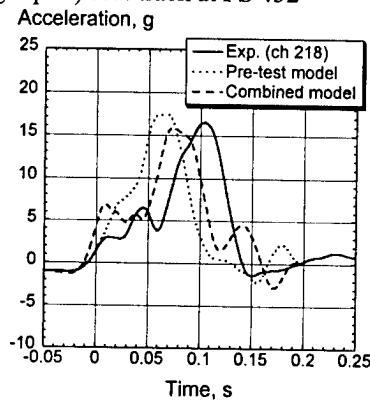
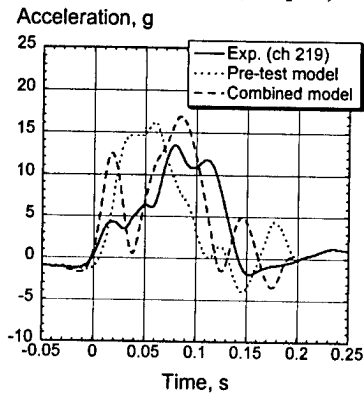
(a) Left inner seat track at FS 380



(b) Left inner (left plot) and outer (right plot) seat track at FS 418

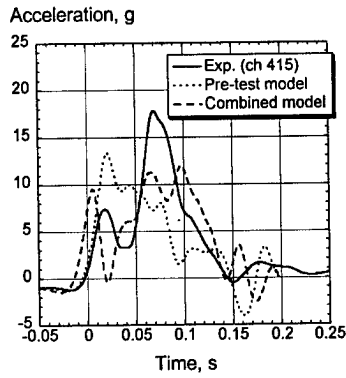


(c) Left inner (left plot) and outer (right plot) seat track at FS 452

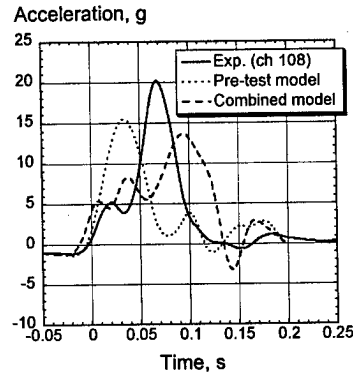
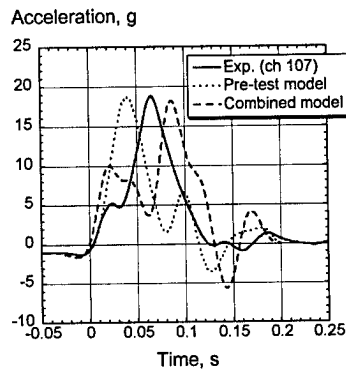


(d) Left inner (left plot) and outer (right plot) seat track at FS 484

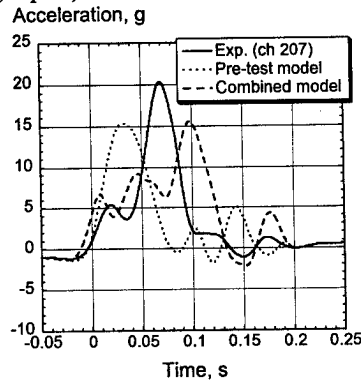
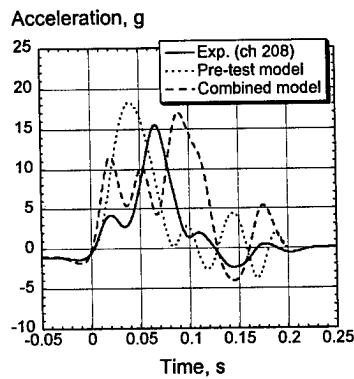
FIGURE 83. MEASURED VERTICAL ACCELERATION RESPONSES PLOTTED WITH THE PRETEST AND THE COMBINED LUGGAGE AND CARGO DOOR MODEL PREDICTIONS FOR THE LEFT SIDE SEAT TRACK AT FOUR LOCATIONS



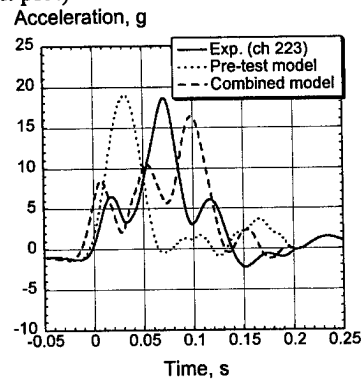
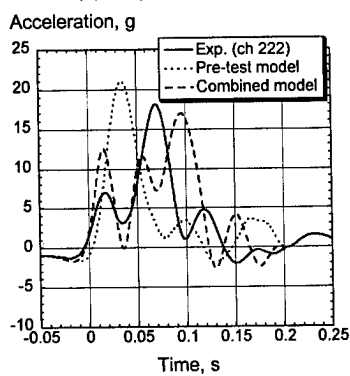
(a) Right inner seat track at FS 380



(b) Right inner (left plot) and outer (right plot) seat track at FS 418



(c) Right inner (left plot) and outer (right plot) seat track at FS 452



(d) Right inner (left plot) and outer (right plot) seat track at FS 484

FIGURE 84. MEASURED VERTICAL ACCELERATION RESPONSES PLOTTED WITH THE PRETEST AND THE COMBINED LUGGAGE AND CARGO DOOR MODEL PREDICTIONS FOR THE RIGHT SIDE SEAT TRACK AT FOUR LOCATIONS

## CONCLUDING REMARKS

The FAA has conducted 30-ft/s vertical drop tests of two 10-ft-long B737 fuselage sections, one with an auxiliary fuel tank mounted beneath the floor in October of 1999 and one with two different overhead bins and luggage in November of 2000. These tests provide an invaluable opportunity to evaluate the capabilities of computational tools for crash simulation through analytical and experimental correlation. To perform this evaluation, a full-scale three-dimensional finite element model of the fuselage section was developed using the nonlinear explicit transient dynamic finite element code, MSC.Dytran. Crash simulations were performed for both drop test configurations to generate analytical predictions of fuselage dynamic response and structural deformation.

The comparison of the crash simulation predictions and the experimental results from the vertical drop test of a B737 fuselage section with an auxiliary fuel tank shows that the simulation properly predicted the time sequence of events including the contact times between the fuel tank and the cargo and passenger floors. The predicted velocity responses of the left and right sides of the floor closely matched the experimental responses. The predicted buckling of the left side of the fuselage and the failures of the fuselage frames in the center and on the right side were nearly identical to the observed deformations and failures. Also, the predicted peak values of floor accelerations were typically within 10 to 20 percent of the experimentally measured values. Considering the complexity of this problem due to the presence of the fuel tank and the number of approximations made in the model development, the simulation exceeded expectations in predicting the outcome of the test. With more accurate material properties, failure criteria, and fuselage geometry, improved correlation may be obtained. However, the degree of analytical and experimental correlation obtained for this simulation illustrates the potential of nonlinear transient dynamic modeling as a design tool for aircraft crashworthiness.

The MSC.Dytran model of the B737 fuselage section was modified to represent the second test configuration by adding the overhead stowage bins and the luggage placed in the cargo hold. The assumptions and approximations used in the development of the model are important in that the level of accuracy of the correlation will determine, in some respects, whether the approximations used were valid. Pretest predictions of seat track and sidewall acceleration time histories and overhead bin responses were obtained from the simulation and were compared with the test data.

The predicted seat rail acceleration responses matched the overall shape and duration of the experimental acceleration pulses reasonably well. Also, the peak acceleration values were well predicted, i.e., within 25% with one exception. However, a phase shift in the time of occurrence of the peak acceleration was typically seen. For the fuselage sidewall locations, the correlation with test data varied according to position. For the accelerometers located on the left side of the fuselage, the simulation predicted the overall shape, duration, and peak g's of the acceleration pulses quite well. However, the correlation for channels located on the right side of the fuselage section was not as good. The peak accelerations of the Heath Tecna bin were predicted to be between 15 and 20 g's, with no failure of the vertical support struts. For the Hitco bin, the peak accelerations were predicted to be between 15 and 40 g's, depending upon location. Also, even though the axial loads in the support linkages of the Hitco bin were significantly higher than those of the Heath Tecna bin, the analysis indicates no failure of any of the support struts or

linkages. No failures of the Heath Tecna bin vertical struts or Hitco bin support linkages were observed during the test.

Finally, a study was performed to evaluate several model revisions and to determine the influence of the changes on model accuracy. These modifications included (1) changes in the contact definition between the lower fuselage structure and the wooden platform, (2) changes in model features including material and inertial properties, and (3) changes in the model to achieve a more accurate physical representation of the problem. The contact modifications include adjustments in the contact force penalty factor and the addition of friction. The changes in model features include a 25 percent reduction in yield stress for the 2024-T3 and 7075-T6 aluminum and a correction in the inertial properties of the model. To gain a better physical representation of the impact problem, a more accurate representation of the lower cargo door and surrounding structure was developed and a physical model of the luggage was added, as well as a platform model. Each of the modifications was performed independently of one another, thus allowing an understanding of the influence of the change on the results. Also, the same initial model was used which was the one used to generate the pretest predictions.

The two modifications that had the most influence on the accuracy of the simulation predictions were the addition of a physical model of the luggage and a more accurate representation of the lower cargo door and surrounding structure. Independently, these modifications showed improvement in the prediction of floor-level acceleration peak values and the time of occurrence of the peak. However, no one modification was able to correct all of the model inaccuracies. Consequently, a final model was used in which both the luggage and cargo door revisions were incorporated. The model results showed improved correlation with the floor-level velocity and acceleration responses, as well as better prediction of the deformation pattern of the actual fuselage structure.

#### REFERENCES

1. "Computational Methods for Crashworthiness," NASA Conference Publication 3223, October 1993.
2. Gamon, M., Wittlin, G., and LaBarge, B., "KRASH 85 User's Guide- Input/Output Format," DOT/FAA/CT-85/10, FAA Technical Center, Atlantic City Airport, NJ, May 1985.
3. Anon., "LS-DYNA3D User's Manual," Livermore Software Technology Company, Livermore, CA, 1997.
4. MSC.Dytran User's Manual Version 4.7, The MacNeal-Schwendler Corporation, Los Angeles, CA, 1999.
5. PAM-CRASH, Engineering Systems International SA, F-94588 Rungis, France.

6. Abramowitz, A., Smith, T.G, and Vu, T., "Vertical Drop Test of a Narrow-Body Transport Section With a Conformable Auxiliary Fuel Tank Onboard," DOT/FAA/AR-00/56, FAA William J. Hughes Technical Center, Atlantic City International Airport, NJ, October 2000.
7. Abramowitz, A., Smith, T.G., Vu, T., and Zvanya, J.R., "Vertical Drop Test of a Narrow-Body Transport Fuselage Section with Overhead Stowage Bins Onboard," DOT/FAA/AR-01/100, September 2002.
8. Hallquist, John O., "DYN3D User's Manual: Nonlinear Dynamic Analysis of Structures in Three Dimensions," University of California, Lawrence Livermore Laboratory, Report UCID-1592, Rev. 4, April 1988.
9. MSC/PISCES-2DELK User's Manual, The MacNeal-Schwendler Corporation.
10. Lahey, R.S., Miller, M.P., and Reymond, M., "MSC/NASTRAN Reference Manual, Version 68," The MacNeal-Schwendler Corporation, 1994.
11. Anon., "MSC.PATRAN, DYTRAN Preference Guide," Publication No. 903077, Version 6, The MacNeal-Schwendler Corporation, 1996.
12. Fasanella, E.L., Widmayer, E., and Robinson, M.P., "Structural Analysis of the Controlled Impact Demonstration of a Jet Transport Airplane," *Journal of Aircraft*, Volume 24, April 1987, pp. 274-280.

## APPENDIX A—FILTERING AND DATA QUALITY EVALUATION

### TEST DATA EVALUATION AND FILTERING.

Acceleration data is often difficult to interpret. Typically, an experimental structural acceleration pulse is composed of a large spectrum of frequencies superimposed together. The structure has many components, each with its own fundamental mode of oscillation, plus many harmonics. In crash dynamics, one is often concerned with the magnitude and duration of the fundamental large-body (aircraft) acceleration pulse that will be input into the passenger. Consequently, the high-frequency ringing of the structural components is of little interest. For example, when a sled test of a seat and dummy is performed, one generally does not have to worry with the spectrum of very high frequencies because the sled has been designed to eliminate them. However, the "raw" acceleration data from a full-scale aircraft crash can have so many high frequencies that the acceleration plot is almost impossible to interpret. In addition to the actual physical data, there can be electrical "noise" superimposed on the acceleration data. Such noise may be generated by electromagnetic interference, cross-talk between channels, inadvertent over-ranging of the accelerometer itself, accelerometer nonlinearities caused by exciting the resonance frequency of the accelerometer, over-ranging of the instrumentation caused by setting the voltage limits too low, etc. Today, most data is gathered digitally. This process complicates data acquisition as serious aliasing errors can also be introduced unless the data is prefiltered properly. Since this appendix is concerned with posttest filtering, errors in data collection will not be discussed further.

The fundamental acceleration pulse is input through the structure from the floor, to the seat, and then into the occupant. From its definition, the average acceleration is simply the change in velocity divided by the time interval and is given by the expression:

$$A_{\text{avg}} = (V_f - V_i) / (T_f - T_i)$$

where  $V_f$  is the final velocity,  $V_i$  is the initial velocity,  $T_f$  is the final time, and  $T_i$  is the initial time.

The instantaneous acceleration is obtained by making the time interval very small. From calculus, the above formula implies that one can differentiate the velocity to obtain the acceleration. Conversely, one can integrate the acceleration trace to get the velocity. The initial impact velocity is known in a drop test to be the square root of twice the drop height times the acceleration of gravity ( $V^2 = 2gh$ ). Therefore, as a quality check and to more accurately determine the fundamental acceleration pulse duration and rebound velocity, an integration to obtain velocity should always be performed on selected channels. If the integrated acceleration does not produce the impact velocity plus rebound, several checks must be performed. Typical questions are:

- was the accelerometer zeroed properly,
- did the acceleration trace come back to zero after impact,
- were the proper calibration factors used,
- did the accelerometer rotate or break loose in the impact,
- was the accelerometer hit by a flying object,

- was the accelerometer over ranged,
- was there an electrical problem?

The filtering frequency used to postprocess acceleration data is typically obtained from a standard such as SAE J211/1, see reference A-1. Appendix C of SAE J211/1 presents a general algorithm that can be used to generate a low-pass Butterworth phaseless digital filter. SAE has defined a set of channel frequency classes (CFC) for impacts of vehicles, which originally were designed for automobile impacts. These CFC's are 60, 180, 600, and 1000. However, all standards are general and cannot be applied to specific cases without detailed knowledge of their basis. From physics, the correct low-pass filtering frequency can only be determined from measuring the basic acceleration pulse duration. Thus, an event that occurs in a millisecond should not be filtered with the same low-pass filter frequency as an event that occurs in 100 millisecond. For extremely short duration impacts, the SAE CFC 1000 can be too low, likewise, for long pulse durations the CFC of 60 can be too high to extract the underlying fundamental pulse shape.

By integrating the acceleration pulse, not only can a quality check of the data be obtained, but the pulse duration of the fundamental mode can also be determined. The acceleration data from the B737 drop test conducted at the FAA in November 2000 was clean with few of the anomalies described previously. However, several data channels on the floor from the earlier drop test of the B737 section with the auxiliary fuel tank were not useable for correlation due to over ranging of some of the acceleration peaks. These channels were intended to record the time the floor impacted with the auxiliary fuel tank. Channel 103, an accelerometer located on the left inner seat track in the November 2000 test, was used to illustrate posttest quality checking and filtering.

The raw acceleration data from channel 103 is plotted in figure A-1 (note that positive acceleration is up). From this plot, it is extremely difficult to determine the pulse duration. Is it 0.15 second, or perhaps is it 0.175 second? What is the peak acceleration? Based on the plot of figure A-1, one might suggest that it is obviously about 85 g's. However, 85-g is the absolute peak of the high-frequency oscillatory response, not of the basic fundamental pulse. Also, note that the initial peak acceleration occurs in the negative direction. This behavior may seem strange at first, but it likely occurs due to a modal vibration that is setup at impact for this location. The modal vibration at time zero can be accelerating either up or down, depending on the exact physical location.

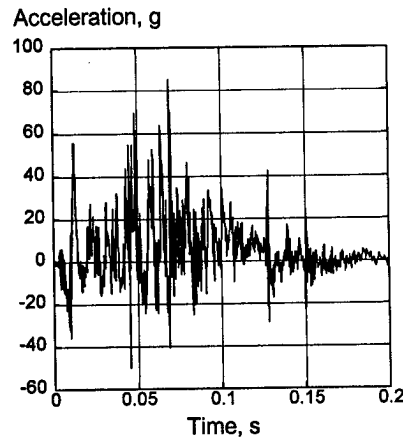


FIGURE A-1. PLOT OF RAW ACCELERATION DATA FROM CHANNEL 103, VERTICAL DIRECTION

The integration of the raw acceleration data was then performed to produce the velocity curve, as shown in figure A-2. The initial condition was applied, i.e., the velocity at time zero is -30 ft/s (downward). Unlike the complex acceleration curve shown in figure A-1, the velocity curve in figure A-2 is relatively simple. The velocity goes to zero at a time of 0.12 second, and by approximately 0.125 second it has gone positive to approximately 2 ft/s, which is the rebound velocity. Thus, the total velocity change including rebound is 32 ft/s. The duration of the fundamental pulse is about 0.125 second. Thus, the fundamental frequency is about  $1/T$  or 8 Hz. To extract the fundamental acceleration pulse, one should use a low-pass filter that has very low attenuation at a minimum of 8 Hz. Also, the approximate maximum acceleration of the fundamental pulse can be obtained by simply computing the maximum slope of the velocity curve from between 0.05 and 0.1 second by drawing in a straight line between the two points.

$$A_{\max} = (V_f - V_i) / (T_f - T_i) = (-5 - (-23)) / (0.1 - 0.05) = 18 \text{ ft/s} / 0.05 \text{ s} = 340 \text{ ft/s}^2 \text{ or } 11.2 \text{ g's}$$

Thus, without filtering, one can approximately obtain the maximum acceleration of the fundamental response of about 11.2 g's.

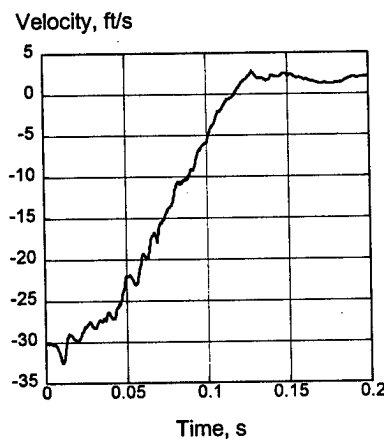


FIGURE A-2. VELOCITY OBTAINED FROM INTEGRATING THE RAW ACCELERATION TRACE IN FIGURE A-1  
(The initial velocity condition (-30 ft/s) was applied as the constant of integration.)

An SAE CFC 60 low-pass digital filter is applied to the channel 103 data and is plotted in figure A-3. The digital filter algorithm is for a two-pole Butterworth filter. To avoid phase shifts, the filter is applied forward and then backward in time. The SAE specifies the resulting filter as a four-pole filter. Note that the cutoff frequency for a CFC 60 is actually about 100 Hz (cutoff equals about 1.667 times CFC). Also, the formula found in appendix C for the SAE digital filter specifies that the filter frequency equals 2.0775 times the CFC. Therefore, the frequency input for the SAE CFC 60 low-pass filter must be 60 times 2.0775 = 124.65 Hz. Since the digital filter is first applied forward in time and then backward in time, the cutoff frequency is reduced from 124.65 Hz on the forward pass to approximately 1.667\*CFC or 100 Hz on the backward pass. The frequency used to describe a digital filter in the body of this report corresponds to the four-pole filter's cutoff frequency.

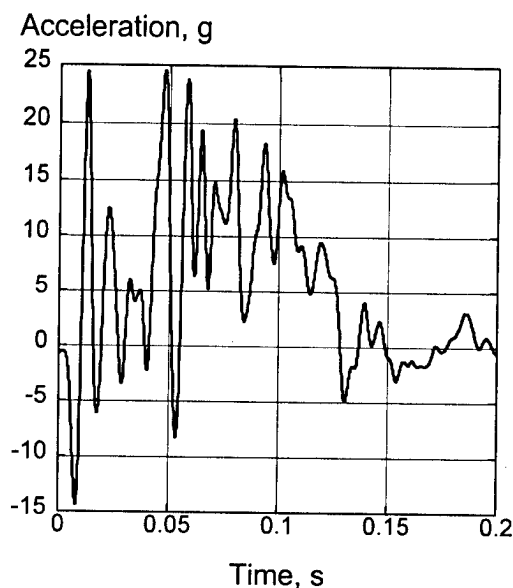


FIGURE A-3. CHANNEL 103 DATA FILTERED WITH SAE CFC 60 FILTER

The filtered response shown in figure A-3 still contains high-frequency oscillations that mask the underlying fundamental acceleration pulse. As shown in figure A-3, the peak accelerations of the filtered data are about 25 g's. Notice that the frequency of an adjacent maximum and minimum acceleration is about 100 Hz. If an adjacent maximum and minimum acceleration are averaged at the approximate center of the pulse (approximately 0.075 second), an average acceleration of  $(+ 17.5 \text{ g} + 2.5 \text{ g})/2 = 10 \text{ g}'\text{s}$  is obtained. The 10-g value is close to the value of 11.2 g's that was obtained earlier.

The acceleration data from channel 103 is filtered using a two-pole Butterworth low-pass digital filter from 10 Hz to a maximum of 80 Hz. Since the filter is applied forward and backward in time, the corresponding cutoff frequencies are 8 and 64 Hz. The family of filtered acceleration curves is shown in figure A-4. Each curve is labeled with the two-pole Butterworth cutoff frequency. For example, f10 represents a 10-Hz, two-pole Butterworth filter applied twice, which effectively yields an 8 Hz cutoff frequency.

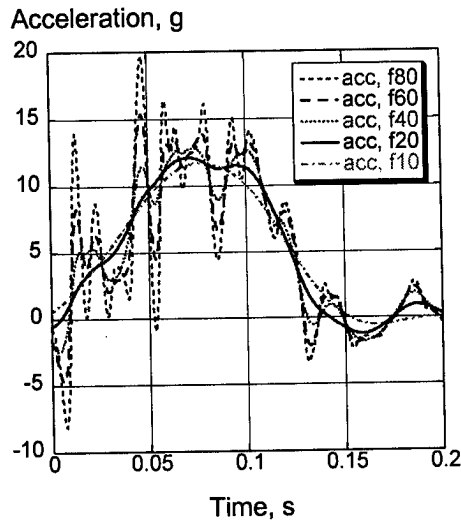


FIGURE A-4. CHANNEL 103 ACCELERATION DATA FILTERED WITH TWO-POLE BUTTERWORTH LOW-PASS DIGITAL FILTERS WITH FREQUENCIES RANGING FROM 10 TO 80 Hz

Note that the 10- and 20-Hz filters only show one basic pulse, and that the maximum acceleration is about 12 g's, again very close to the value calculated from the slope of the velocity curve. The rise time of the basic pulse can be used to calculate the onset rate, which is approximately  $10 \text{ g}/0.05 \text{ sec} = 200 \text{ g/second}$ . Next, to demonstrate the effect of "over filtering" for this specific example, a low-pass filter with a frequency below 10 Hz will be used. In figure A-5, the raw acceleration data from channel 103 is filtered using a 5-Hz, two-pole Butterworth low-pass digital filter.

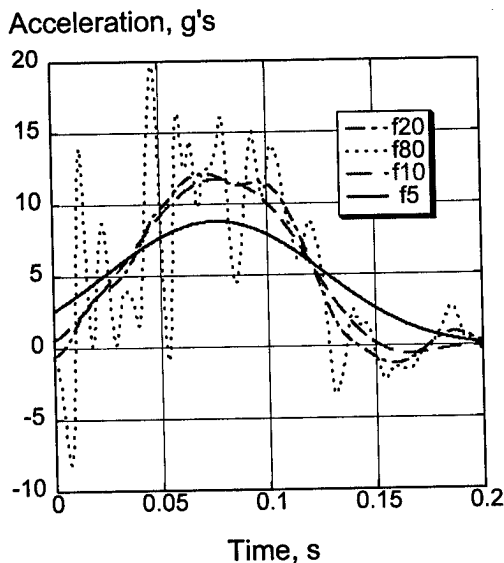


FIGURE A-5. CHANNEL 103 ACCELERATION DATA FILTERED WITH TWO-POLE BUTTERWORTH LOW-PASS DIGITAL FILTERS WITH FREQUENCIES OF 5, 10, 20, AND 80 Hz (Note that the 5-Hz filter distorts the pulse shape)

The pulse shape obtained when the raw acceleration data from channel 103 is filtered with the 5 Hz, low-pass filter is obviously distorted and spread out in time. This result confirms that the lowest filter frequency should be above 8 Hz. From figure A-5, both the 10- and the 20-Hz filters appear to extract the fundamental pulse. However, to be conservative, the 20-Hz filter is recommended for this acceleration. The 20-Hz filter provides the least distortion at time zero and does not spread the pulse duration. Note that the cutoff frequency for the 20-Hz digital filter is 16 Hz.

Each of the filtered acceleration responses, shown in figure A-5, is integrated to obtain the corresponding velocity responses, plotted in figure A-6. The question to answer is, "Does filtering distort the velocity trace?" The velocity response obtained by integrating the 10-Hz filtered acceleration follows the velocity response obtained from the raw acceleration data quite well. Obviously, each higher low-pass filtered acceleration, when integrated, (such as the 20 Hz, which is recommended for this pulse) will produce a velocity curve even closer to the raw data. However, it is evident that the velocity response obtained by integrating the 5-Hz filtered acceleration distorts the original velocity data.

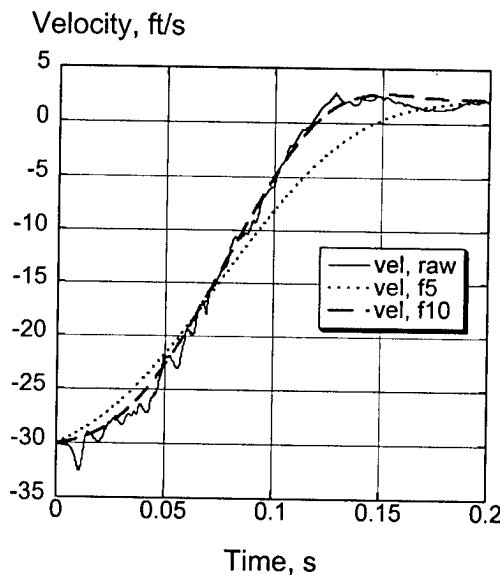


FIGURE A-6. A COMPARISON OF THE VELOCITY RESPONSES OBTAINED FROM INTEGRATING THE RAW DATA, AND INTEGRATING THE FILTERED 10- AND 5-Hz ACCELERATION DATA

#### FILTERING OF ANALYTICAL DATA.

The analytical results shown in this report have been filtered using either a 60- or 20-Hz, two-pole Butterworth digital low-pass filter applied forward and backward in time. The choice of filter frequency is important, especially for analytical results containing high-frequency oscillations where it must be set low enough to capture the underlying crash pulse. In addition, for finite element models, the amount of mass assigned to a node can influence the choice of filter frequency. As an illustration of the effect of the filter frequency and the effect of whether concentrated mass is applied to the node or not, the filtered acceleration time histories of two

nodal positions on the floor of the fuselage section are plotted in figures A-7 through A-9. In these figures, the acceleration responses were filtered using three different frequencies corresponding to 200, 125, and 40 Hz, respectively. The two nodes, node 3572 and node 3596, are located on the floor at the left inner seat track positions FS 380 and FS 400, respectively. Node 3572 is located on the front edge of the floor and has no concentrated mass associated with it. Node 3596 is located 20 in. from the front edge along the same seat track as node 3572; however, node 3596 has 122.8 lbs of concentrated mass assigned to it representing a portion of the seat and occupant mass on the floor.

Note that the acceleration responses are extremely noisy when filtered using a 200-Hz frequency, as shown in figure A-7. However, the response curve for node 3596 is much less noisy and has a lower magnitude than that of node 3572 because it has mass associated with it. The same observation is true for the acceleration responses filtered using a 125-Hz frequency, as shown in figure A-8. However, when the two acceleration responses are filtered using a 40-Hz frequency, the curves are smooth and provide the underlying crash pulse at both locations, as shown in figure A-9. It is important to note that many of the filtered data plots do not begin at the origin, i.e., zero acceleration at time equal 0.0 second. This phenomena is an artifact of the filtering process and can be minimized to a certain extent by adding many points before the actual data having negative time and 0 or -1 g acceleration, whichever value is appropriate.

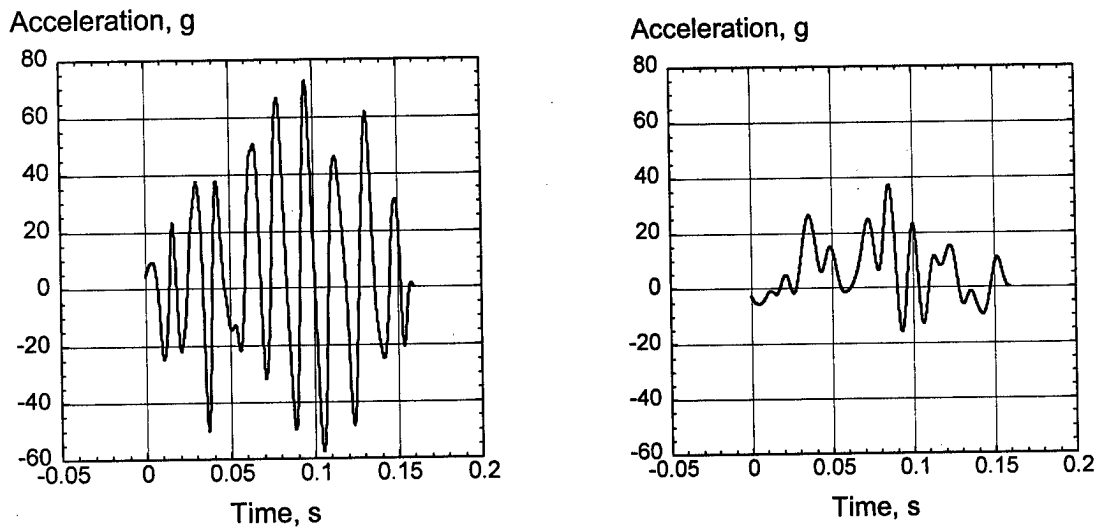


FIGURE A-7. 200-HZ FILTERED ACCELERATION RESPONSES OF NODE 3572 (LEFT PLOT) AND NODE 3596 (RIGHT PLOT)

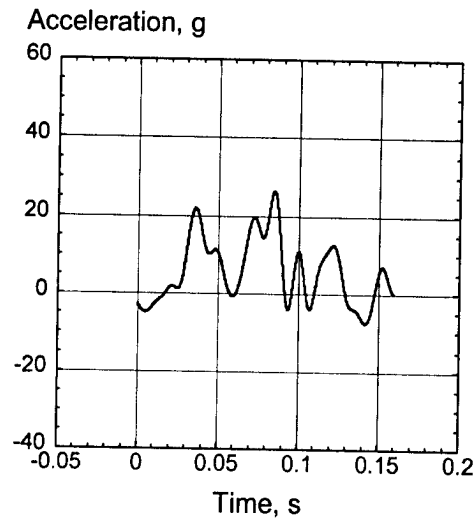
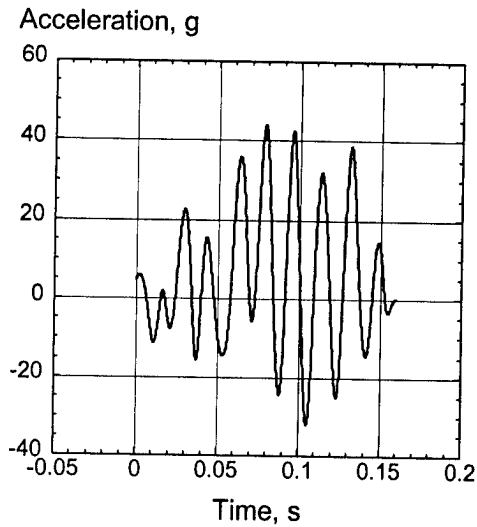


FIGURE A-8. 125-HZ FILTERED ACCELERATION RESPONSES OF NODE 3572 (LEFT PLOT) AND NODE 3596 (RIGHT PLOT)

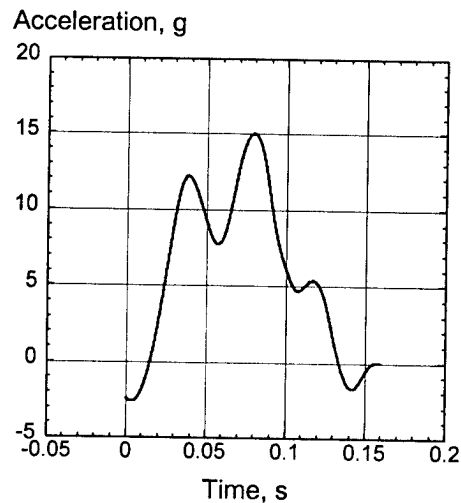
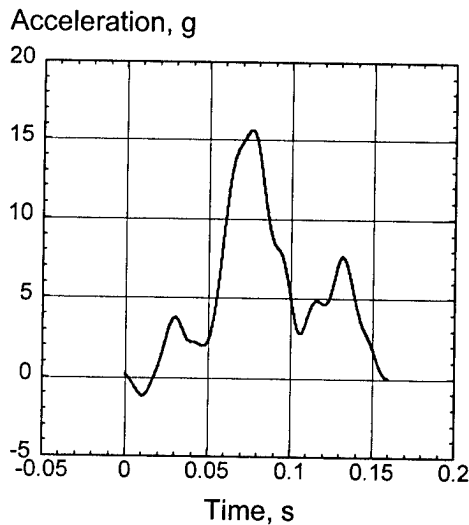


FIGURE A-9. 40-HZ FILTERED ACCELERATION RESPONSES OF NODE 3572 (LEFT PLOT) AND NODE 3596 (RIGHT PLOT)

RECOMMENDED PRACTICES.

In summary, the data evaluation and low-pass digital filtering techniques outlined in this appendix to extract the basic crash pulse can be very useful when comparing seat design pulses and sled test pulses with actual aircraft crash test data. The following practices are recommended:

1. Always examine the raw acceleration first and look for over-ranged data, electrical drop-outs, electrical noise, and other anomalies. Document any broken or cut electrical cables, any rotated or dislodged accelerometers. Determine that the free fall acceleration is

approximately -1 g, within experimental error. The acceleration should return to zero a second or two after impact. If an offset is determined, the data should be corrected.

2. Integrate several of the vertical acceleration traces as a sanity check to determine if the data is valid. Apply the initial velocity condition and determine if the calculated rebound velocity is reasonable when compared with motion picture of high-speed video analysis. Some rebound almost always occurs since stored elastic energy will be converted into rebound kinetic energy. Determine the total pulse duration, which is defined as the time from zero until the time of maximum rebound velocity. The duration of the pulse will determine the lowest frequency filter that should be used. Draw a straight line near the center of the velocity response to determine the fundamental pulse acceleration. The acceleration will be the slope of the straight line, which can be converted to g's by dividing by the proper conversion factor.
3. For a test other than a vertical drop test, the acceleration pulse must be examined for each direction.
4. Filter the structural accelerometer data initially with the SAE CFC 60 low-pass filter. This filter will pass a considerable amount of high-frequency ringing near 100 Hz that may mask the fundamental pulse. Seated occupants in a typical survivable crash do not respond to the high-frequency ringing. Use the pulse duration obtained in step 2 to develop a low-pass filter to extract the fundamental crash pulse. For many cases, a 20-Hz low-pass filter will produce good results.
5. For analytical results, recognize that the amount of mass applied to a node in a finite element model can greatly influence the amount of high-frequency ringing in the acceleration response. One method of reducing the oscillatory response of a node is to apply a small concentrated mass to the node. Another method is to average the acceleration responses of two adjacent nodes that are reasonably close together. Be careful to extract time history data at sufficiently high frequencies such that aliasing errors do not occur.

#### REFERENCE

- A-1. Society of Automotive Engineers, Recommended Practice: Instrumentation for Impact Test—Part 1, Electronic Instrumentation, SAE J211/1, March 1995.